INTERFACE STRUCTURE AND INTERDIFFUSION IN Mo/Si MULTILAYERS

Cover

A cross-sectional transmission electron microscope image of a Mo/Si multilayer with B_4C interlayers (light color). No B_4C layer is present at the first Mo-on-Si interface (bottom).

Interface structure and interdiffusion in Mo/Si multilayers
I. Nedelcu
Thesis, University of Twente, Enschede – Illustrated.
With references – With summary in Dutch, English and Romanian
ISBN 978-90-365-2550-3
Printed by: Universal Press

INTERFACE STRUCTURE AND INTERDIFFUSION IN Mo/Si MULTILAYERS

DISSERTATION

to obtain
the degree of doctor at the University of Twente,
on the authority of the rector magnificus,
prof. dr. W. H. M. Zijm,
on account of the decision of the graduation committee,
to be publicly defended
on Friday, 7th September 2007 at 13.15

by

Ileana Nedelcu

born on 26th April 1974

in Sibiu, Romania

This thesis has been approved by:

Promotor: Prof. Dr. F. Bijkerk

“Suavis est memoria laborum praeteritorum ”
Latin saying, meaning:
The memory of the passed efforts is always pleasant.

This thesis is based on the following publications:

Chapter 2: I. Nedelcu, R. W. E. van de Kruijs, A. E. Yakshin, F. D. Tichelaar, E. Zoethout, E. Louis, H. Enkisch, S. Müllender, F. Bijkerk, *"Interface roughness in Mo/Si multilayers"*, Thin Solid Films 515 (2), pp. 434-438 (2006)

Chapter 3: I. Nedelcu, R. W. E. van de Kruijs, A. E. Yakshin, F. Bijkerk, *Temperature dependent nano-crystal formation in Mo/Si multilayers*, Phys. Rev. B, accepted for publication.

Chapter 4: I. Nedelcu, R. W. E. van de Kruijs, A. E. Yakshin and F. Bijkerk, *Thermally enhanced interdiffusion in Mo/Si multilayers*, submitted to Journal of Appl. Phys.

Chapter 5: I. Nedelcu, R. W. E. van de Kruijs, A. E. Yakshin, E. Louis, F. Bijkerk, S. Müllender, *Substrate recovery layers for EUVL optics: effects on multilayer reflectivity and surface roughness,* Proceedings SPIE 6517-110, (2007)

Chapter 6: I. Nedelcu, R. W.E van de Kruijs, A. E. Yakshin, F. Bijkerk, *Microstructure of Mo/Si multilayers with B_4C as barrier layers*, submitted to Applied Optics

The author was also co-author of the following publications and patent:

A. E. Yakshin, R. W. E. van de Kruijs, F. Bijkerk, E. Louis, I. Nedelcu, *Reflektives optisches element für EUV lithographievorrichtungen*, 06184PUSPRO, US 60/888,144, US, EU, Priority date 05/02/2007

A. E. Yakshin, R. W. E. van de Kruijs, E. Zoethout, I. Nedelcu, E. Louis, F. Bijkerk, H. Enkisch, and S. Müllender, *Enhanced reflectance interface engineered Mo/Si multilayers using thermal particle deposition*, Proceedings SPIE 6517, 651701 (15/03/2007)

A.E. Yakshin, R.W.E. van de Kruijs, I. Nedelcu, E. Zoethout, E. Louis, H. Enkisch, S. Müllender, and F. Bijkerk, *Interface engineering of Mo/Si multilayers for enhanced reflectance in EUVL applications*, presented at the 2006 International Extreme Ultra-Violet Lithography (EUVL) Symposium, Barcelona, Proc. Vol. CD 7870, (2006)

E. Louis, E. Zoethout, R.W.E. van de Kruijs, I. Nedelcu, A.E. Yakshin, F. Bijkerk, H. Enkisch, S. Müllender, G. Sipos, D. Ehm, and P. Kürz, *EUVL multilayer coating development",* presented at the Fourth International Extreme Ultra-Violet Lithography (EUVL) Symposium, San Diego, Proc. Vol. CD (2006)

R.W.E van de Kruijs, E. Zoethout, A.E. Yakshin, I. Nedelcu, E. Louis, F. Tichelaar, H. Enkisch, G. Sipos, S. Müllender, F. Bijkerk, *Nano-size crystallites in Mo/Si multilayers optics*, Thin Solid Films 515 (2), pp. 430-433 (2006)

E. Louis, E. Zoethout, R.W.E. van de Kruijs, I. Nedelcu, A.E. Yakshin, S. Alonso van der Westen, T. Tsarfati, F. Bijkerk, H. Enkisch, and S. Müllender, *Multilayer coatings for the EUVL process development tool*, Emerging Lithographic Technologies IX, San José, SPIE 5751, pp. 1170-1177 (2005)

E. Louis, A.E. Yakshin, E. Zoethout, R.W.E. van de Kruijs, I. Nedelcu, S. Alonso van der Westen, T. Tsarfati, , F. Bijkerk, H. Enkisch, S. Müllender, B. Wolschrijn and B. Mertens, *Enhanced performance of EUV multilayer coatings,* SPIE Optics & Photonics, San Diego, Proceedings SPIE 5900-02 (2005)

E. Louis, E. Zoethout, R.W.E. van de Kruijs, I. Nedelcu, A.E. Yakshin, F. Bijkerk, H. Enkisch, S. Müllender, G. Sipos, D. Ehm, and P. Kürz, *EUVL multilayer coating development*, presented at the Third International Extreme Ultra-Violet Lithography (EUVL) Symposium, Miyazaki, Vol CD (2004)

This work is part of the FOM Industrial Partnership Programme I10 (‘XMO’) which is carried out under contract with Carl Zeiss SMT AG, Oberkochen and the ‘Stichting voor Fundamenteel Onderzoek der Materie (FOM)’, the latter being financially supported by the ‘Nederlandse Organisatie voor Wetenschappelijk Onderzoek (NWO)’.

Table of contents

1. Introduction..... 13
1.1. Motivation 13
1.2. Theory of the multilayers mirrors 16
1.3. Properties of ultra-thin Mo and Si films 19
1.3.1. Multilayer roughness 20
1.3.1.1. Ion beam smoothening of surface roughness 20
1.3.1.2. Roughness dependence on interlayer formation and Mo crystallinity 21
1.3.2. Silicide interfaces 21
1.3.3. Preventing silicide interface formation 22
1.4. Thermal stability 24
1.4.1. Diffusion at interfaces 25
1.4.2. Silicide formation upon annealing 26
1.4.2.1. Mo/Si multilayers 26
1.4.2.2. Mo/Si multilayers with B_4C at interfaces 27
1.5. Substrate recovery layers 27
1.6. Producing Mo/Si multilayers 29
1.6.1. Deposition method 29
1.6.2. Layer control 30
1.7. Analysis methods 31
1.7.1. XES, XPS, AFM 33
1.7.2. X-ray measurements 33
1.7.3. Thermal annealing treatment 34
1.8. Multilayer optics applications 36
1.9. Outlook- in this thesis 39
1.10. References 39
2. Interface roughness in Mo/Si multilayers…….....45
2.1. Abstract 45
2.2. Introduction 46

2.3. Experimental details 46
2.4. Results and discussions 47
2.4.1. Roughness dependence as a function of ion energy 47
2.4.1.1. Ion treatment during layer growth 47
2.4.1.2. Ion treatment applied after layer deposition 49
2.4.2. Roughness dependence as a function of the Mo ratio 51
2.5. Summary and conclusions 53
2.6. Acknowledgments 54
2.7. References 54
3. Temperature dependent nano-crystal formation in Mo/Si multilayers....57
3.1. Abstract 57
3.2. Introduction 58
3.3. Experimental 59
3.4. Experimental results and discussion 60
3.4.1. Nano-crystallinity of as-deposited multilayers 60
3.4.2. Multilayer structure at enhanced temperatures 64
3.4.2.1. State up to *h*-$MoSi_2$ crystallization (T = 20 - 300 °C) 67
3.4.2.2. State after *h*-$MoSi_2$ crystallization (T = 300 - 400 °C) 68
3.4.2.3. Quasi - equilibrium state (T = 800 °C) 70
3.4.3. Model of silicide formation at enhanced temperatures 71
3.5. Summary 73
3.6. Acknowledgments 74
3.7. References 74
4. Thermally enhanced interdiffusion in Mo/Si multilayers …….....77
4.1. Abstract 77
4.2. Introduction 78
4.3. Experimental 78
4.4. Results and discussion 80
4.4.1. Diffusion through Mo-Si transition zones at enhanced temperatures 80
4.4.2. Abrupt phase transition to *h*-$MoSi_2$ 83
4.5. Impurities effect on the abrupt phase transformation to *h*-$MoSi_2$ 85
4.6. Conclusions 88

4.7. Acknowledgments 88
4.8. References 89
5. Substrate recovery layers for EUVL optics: effects on multilayer reflectivity and surface roughness …….....93
5.1. Abstract 93
5.2. Introduction 94
5.3. Sample preparation and analysis 95
5.4. Results and discussion 97
5.4.1. AFM analysis 97
5.4.2. Hard X-ray scattering 99
5.4.3. EUV reflectivity 101
5.5. Summary and conclusions 102
5.6. Acknowledgments 103
5.7. References 103
6. Microstructure of Mo/Si multilayers with B_4C as barrier layers 105
6.1. Abstract 105
6.2. Introduction 106
6.3. Experimental 106
6.4. Results and discussion 108
6.4.1. Optical response 108
6.4.2. Layered structure 110
6.4.3. B_4C barrier quality against thermally induced diffusion 113
6.5. Summary and conclusions 116
6.6. Acknowledgments 116
6.7. References 117
7. Summary.....119
8. Samenvatting.....121
9. Rezumat.....123
10. Acknowledgments.....127
11. Curriculum vitae.....129

1. Introduction

1.1. MOTIVATION

From the entire spectrum of electromagnetic radiation, the human eye is only able to detect a very small part, the so-called "visible light" region, ranging from wavelengths of 380 to 780 nm. In addition, the resolving power of the eye is limited, typically approximately 1 mm at a distance of 1 m, prohibiting the detection of "invisible" details. To extend the human limits and observe small structures, mankind has developed many tools varying from simple magnifying glasses to state-of-the-art X-ray and electron microscopes. Visible light microscopes already extend the detectable feature size down to several hundred nanometers using *magnifying* optics (lenses). To resolve details below the wavelength of visible light, it is necessary to use special microscopes that can use light with a wavelength down to several tenths of a nanometer, as well as optics, which are designed for such wavelengths.

By reversing the optical direction, it is straightforward to state that large features can be reduced in size by making use of *demagnifying* optics. Projection lithography used in semiconductor manufacturing for the fabrication of integrated circuits (IC's), currently uses near-visible light (193 nm) and demagnifying lenses and mirrors to project a pattern onto a photo-resist layer [1, 2], see also Figure 1. In this way, IC's are nowadays being produced with smallest features below 100 nm.

The industrial demand to reduce the feature size is governed by Moore's law. According to Moore's law, the complexity of chip designs increases such that the number of transistors in a chip doubles every 18 months. As a result, transistor feature dimensions have to be reduced continuously. Since the minimum feature size that can actually be printed using projection lithography is typically proportional to the wavelength of the light that is used, the introduction of sub-50 nm feature size projection lithography calls for the use of wavelengths well below the current industry standard of 193 nm. For such short wavelengths, the illuminating light will be absorbed for a large fraction in the lens system, reducing the throughput of a chip-manufacturing machine.

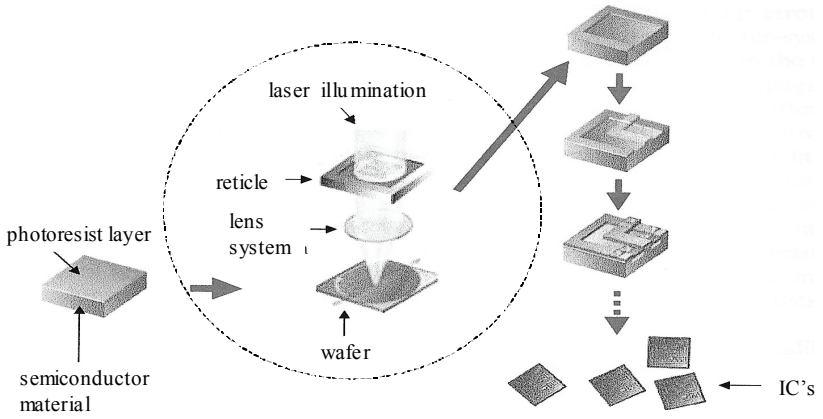

Figure 1. The principle of projection lithography: a reticle pattern is imaged onto a photo resist using demagnifying optics.

To retain high throughput, a solution can be found in the use of reflecting optics, instead of transmitting optics. Due to the low reflectivity of single film coatings, the practical solution is to design multilayer coatings consisting of stacked reflective layers, constructively adding up partial reflections that enable high throughput optics for implementing lithography at the sub-50 nm node.

Next generation lithography tools, expected to be introduced commercially around 2010, will make use of reflecting multilayer optics, and is schematically shown in Figure 2. The operational wavelength of such a tool is governed by the availability of a stable, high intensity illumination source, as well as the availability of highly reflective multilayer coatings. Both criteria are met by the wavelength of 13.5 nm (Extreme Ultra Violet, or EUV). Due to the high absorption cross-sections in EUV range, a limited range of materials is suitable for designing a multilayer with high peak reflectance.

The mirrors used to demagnify the image consist of alternative Mo/Si layers with thicknesses of several nanometers. Such ultra-thin films often exhibit microscopic properties (e.g. density, crystallinity, and roughness) that can be quite different from those of bulk materials. This uncertainty leads to severe difficulties in designing the optical column in EUV tools. For example, the uncertainty in silicide composition at the Mo/Si interfaces could lead to an unacceptable loss of image quality at the resist level.

Additional challenges are found in the requirement that multilayer coatings should remain stable at high photon fluxes under severe operational conditions including high temperatures, surface plasma formation, ion sputtering damage, and surface contamination.

This thesis focuses on developing a comprehensive understanding of the physics that occur in "classic" Mo/Si multilayers, i.e. multilayers without diffusion barriers. The knowledge obtained from this work had led to improved multilayer optics that incorporate diffusion barriers, enabling multilayers that can function in high-temperature applications, as well as leading to the current world record in EUV peak reflectance. The next sections will focus on describing the basic multilayer design that is used to reflect nanometer wavelength radiation. The current understanding of multilayer physics is presented as a reference for the work described in this thesis. In addition, the multilayer fabrication technique that was used to produce the investigated samples will be discussed. The main content of this thesis focuses on the experimental work on EUV multilayers that has been carried out at FOM Rijnhuizen, within the framework of the Industrial Partnership Programme "XMO", in collaboration with Carl Zeiss SMT AG.

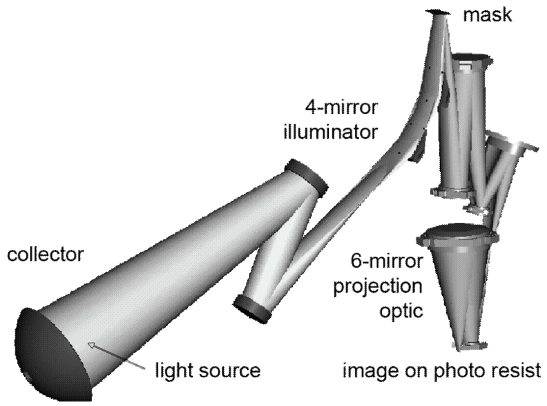

Figure 2. Typical design of an EUVL optical layout.

1.2. THEORY OF MULTILAYER MIRRORS

Any material used to reflect radiation in the X-ray or EUV regime will reflect only a few percent because the refractive index n is close to unity. The refractive index n is defined as: $n = 1 - \delta + i\beta$, where δ is the real part and β the imaginary part of n. For several materials δ and β are plotted in Figure 3 for a wavelength of 13.5 nm.

To achieve a high mirror reflectivity, a multilayer system is considered, composed of two alternative materials, one with low δ (low Z material) and another one with high δ (high Z). To obtain constructive interference of all partial reflections presented in Figure 4, basically all reflected radiation at these interfaces should be added in phase. Ignoring absorption, and incorporating a phase-shift of 180° from low δ / high δ interfaces, all reflections are in-phase by choosing low δ and high δ layer thicknesses which are equal. Due to high absorption in the high δ material, the thickness of this layer should be reduced to maximize the reflectivity and in practice the optimum is achieved at a high δ fraction slightly below 50% of the multilayer period.

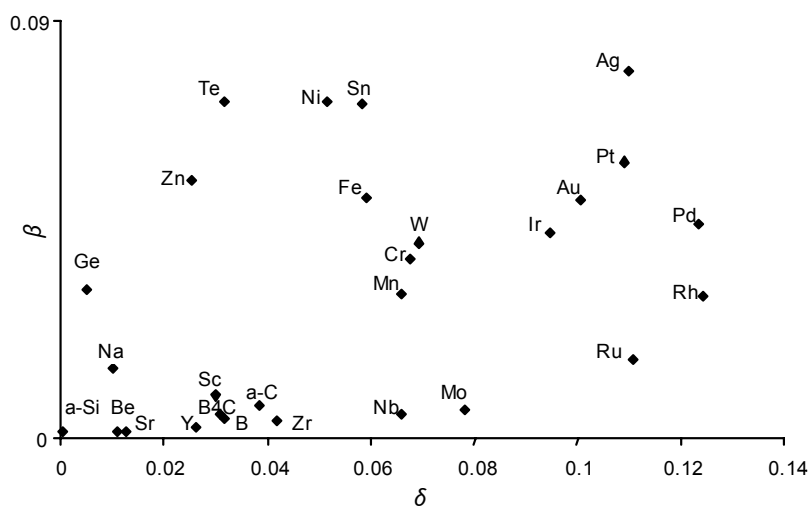

Figure 3. The real and imaginary parts of the refractive index $n = 1 - \delta - i\beta$ of the elements at the wavelength of 13.5 nm.

To reflect radiation with λ exactly matching 13.5 nm, the thickness d of each period (consecutive two layers) has to be designed to satisfy Bragg's law,

$$n\lambda = 2d \sin \theta, \qquad (1)$$

where n is an integer number representing the Bragg order, and θ is the incident angle of the radiation. From this, using λ = 13.5 nm, it follows that the period thickness should be $d \sim 6.9$ nm, resulting in low δ and high δ layer thicknesses of ~4 nm and ~3 nm, respectively.

Apart from choosing the right materials to build the multilayer, it is also important that the interdiffusion zones at the interfaces of the deposited materials and the added surface roughness during deposition are as low as possible. As a result, it is not sufficient to use only information from Figure 3 when designing a multilayer for a practical application. Figure 5 presents the best reflectivity results obtained in practice, for multilayers consisting of different materials combinations that reflect radiation with soft X-ray radiation (below carbon K-absorption edge at 4.37 nm), obtained by the Institute of Physics on Microstructure, (IPM) from Russia and EUV wavelengths (above 4.37 nm), obtained by Lawrence Livermore National Laboratory (LLNL) in collaboration with Lawrence Berkeley Laboratory (LBL) from USA and the Foundation for Fundamental Research on Matter (FOM) from the Netherlands. The highest reflectivity at 13.5 nm is obtained for Mo/Si multilayers. Mo/Be shows also good values at 10 nm, but due to the poisonous nature of Be, research on EUVL mirrors has been focused on Mo/Si multilayers.

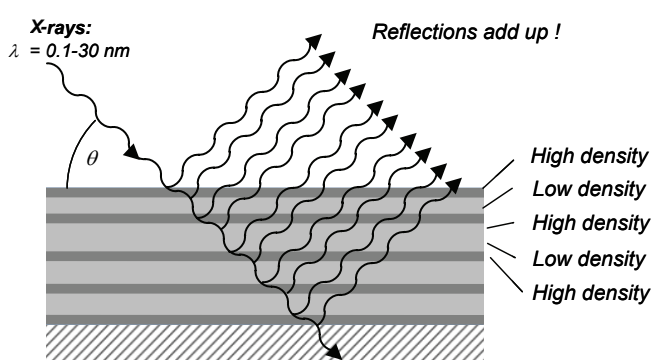

Figure 4. Representation of the constructive interference principle of a multilayer.

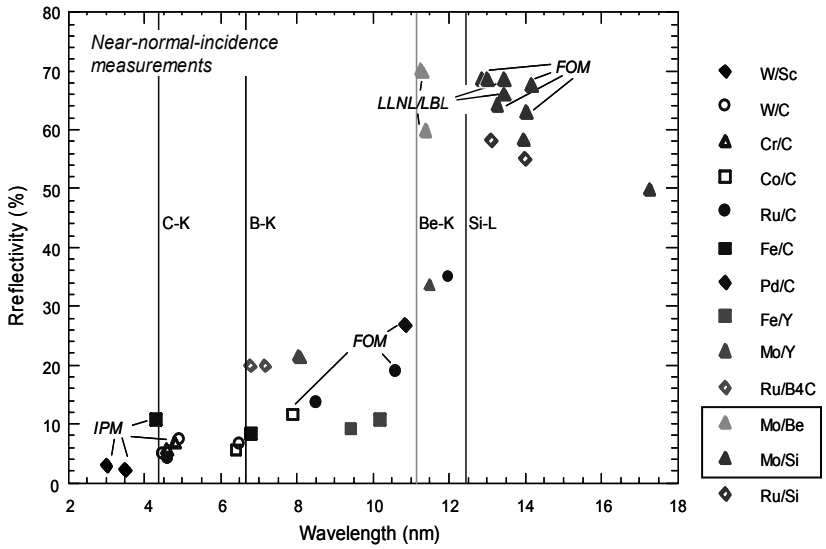

Figure 5. Reflectivity as a function of wavelength for multilayers consisting of different material pairs.

A transmission electron microscope (TEM) image of a Mo/Si multilayer is presented in Figure 6. The picture illustrates the need for very precise deposition control of layer thicknesses, a principal requirement for achieving a high reflectivity of the multilayer. However, in the zoomed region it can be observed that very thin interlayers (sub-nanometer thickness) are formed at the layers interfaces. The Mo/Si multilayer in reality consists of 4 layers, instead of two. This reduces the multilayer optical contrast, reducing the reflectivity at 13.5 nm. More details about this are discussed in sections 1.3.2 and 1.3.3.

The basic physics that plays a role in layer growth and subsequent compound formation, as well as the interdiffusion processes that are expected to take place under illumination, are not yet understood to the degree that will be required to ensure commercial viability of EUVL optics. This thesis aims at contributing in the understanding of such physics processes, focusing on the interdiffusion and roughness development at the interfaces. In the next sections, these processes and their influence on the multilayer reflectivity at 13.5 nm and on the thermal stability will be discussed in detail.

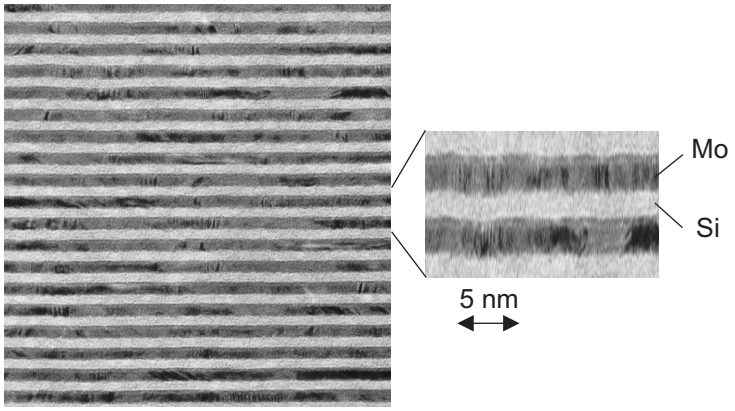

Figure 6. Cross-section TEM picture of a Mo/Si multilayer.

1.3. Properties of ultra-thin Mo and Si films

The improvement of the reflectivity of multilayer mirrors has always been a priority for EUVL research because a gain in reflectivity directly translates into a higher throughput for chip manufacturing. Although theoretically a reflectivity of 74 % can be achieved, in practice less than 70 % is realized due to silicide formation at the Mo/Si interfaces as well as a high surface roughness of EUVL substrates and added roughness during layer growth. The highest reflectivity reported in literature on Mo/Si multilayers was recently obtained in our group with a novel composition of interlayer design, resulting in 70.15 % at 13.5 nm [3], a significant increase over the ~69 % reflectance reported on a standard Mo/Si system [4].

During multilayer fabrication, the substrate roughness develops throughout the multilayer, resulting in significant reflectivity loss. Based on our earlier work [5] the reflectivity can be increased if the multilayer roughness is reduced by applying Kr ion treatment after each Si layer deposition. A more detailed discussion will be presented in section 1.3.1. In sections 1.3.2 and 1.3.3 we will present a survey of previous investigations into the process of silicide formation. A full understanding of silicide stoichiometry and crystallinity seems essential to further improve the reflectivity of Mo/Si multilayers. In addition to this, we will discuss the replacement of the naturally formed silicides by other materials by which multilayer reflectivity can be increased.

1.3.1. Multilayer roughness

1.3.1.1. Ion beam smoothening of surface roughness

In Mo/Si multilayer systems deposited by electron beam evaporation, Puik et al [6] showed that ion bombardment of Mo layers causes a reflectivity gain (monitored by in-situ soft X-rays) due to surface smoothening. Reflectivity increases up to a threshold thickness of removed Mo, followed by a reflectivity loss due to intermixing at the Mo-on-Si interface. In Mo/Si multilayers, Schlatmann et al [7] showed that by using H ion beam bombardment, the atomic density of Si could be increased and roughness can be decreased. Voorma et al [8] investigated the effect of ion bombardment as a function of angle of incidence and ion energy, for ion smoothening after deposition of each Si layer. It was found that roughness decreases with increasing angle and ion energy due to the smoothening effect by viscous flow, which dominates intermixing, and atoms removal by ion bombardment. As a result of these studies the ion-gun angle was 50° while the Si removal amount and the ion energy were optimized for the best reflectivity results. In this thesis, these conditions are referenced as the "standard" multilayer fabrication settings.

The previous studies focused on post-deposition ion-bombardment, especially on the influence of ion bombardment of Si surfaces. In chapter 2 we present a study of multilayer smoothening using Kr ion bombardment during as well as after Si layer deposition. Surface roughness is characterized using off-specular scattering of hard X-ray. The results are discussed and compared with the multilayer reflectivities obtained at 13.5 nm.

1.3.1.2. Roughness dependence on interlayer formation and Mo crystallinity

Roughness in W/Si systems, studied by Jergel et al [9], was found to develop as a function of annealing temperature, in addition to increased interdiffusion and displacement at the interfaces. A similar effect at enhanced temperatures was observed in Mo/Si multilayers by Voorma et al [10]. The interface roughness of Mo/Si multilayers was analyzed as a function of substrate temperature during deposition and was found to exhibit a minimum value at 215 °C, attributed to a balance in two competing processes:

vacancies in the Si layer in which Mo atoms can diffuse (at lower temperatures) and high diffusion of Mo into Si layer (at higher temperatures). In this study, the structure of both Mo and Si was amorphous. An extensive study of Mo/Si multilayers deposited by electron beam evaporation was reported by Stearns et al [11], where the interface roughness was found to be connected to the texture of crystalline Mo layers and the variation in thickness of the interlayers upon annealing.

The Mo/Si multilayers investigated in literature have so far been produced with a fixed Mo fraction Γ close to 0.4, equivalent to 40 % of the period, which is suitable for high reflectance multilayers in EUVL applications. However, for other applications (e.g. narrow band EUV diagnostics [4,12]) multilayers with much lower Mo ratios are needed. In addition, stress-compensation layers in EUV optics or parts of broad band multilayer mirrors [13] consist of multilayers with high Mo ratios. In spite of the known interface roughness dependence by the thickness of crystalline Mo layers, and the various applications of multilayers with different Mo fractions, the roughness development through stacks with different Mo fractions has so far not been investigated. In this thesis, in chapter 2 we investigate the dependence of multilayer roughness on the Mo layer thickness, a process which is suggested to be correlated to the crystalline Mo layer growth.

1.3.2. Silicide interfaces

Literature is rich in reporting on silicide formation at metal-Si interfaces. In Mo/Si systems, ion beam induced intermixing was studied by Kessels et al [14] and the silicide formation at interfaces affected by ion bombardment was explained based on the formation enthalpies of different compounds.

A large part of the work reported in literature has been performed on magnetron sputtered Mo/Si multilayers. Yulin et al [15] reported for magnetron sputtered multilayers the existence of symmetric Mo-Si interfaces when Mo is amorphous, while asymmetric interfaces were reported when Mo is crystalline. For multilayers deposited with the same technique, Bajt et al [16] investigated the amorphous-to-crystalline transition of the Mo layer as a function of its thickness. It was found that for less than 2 nm, the Mo structure is amorphous and for larger than 2 nm, the Mo structure is polycrystalline. These results were obtained for Mo/Si multilayers that were ion beam sputtered and magnetron sputtered.

So far, only few results [11] have been reported on the crystallographic structure of multilayers deposited by electron beam evaporation with different thicknesses of the Mo layers. We will show in chapter 3 that also for Mo/Si deposited by electron beam evaporation a sharp transition occurs in the crystallographic state of Mo at a thickness layer of 2.3 nm, similar to that observed in magnetron sputtered samples. In chapter 3 we will present details on the crystalline silicide that appears to form for Mo thicknesses lower than 2.3 nm, in contrast to the amorphous nature reported for magnetron sputtering. The silicides formed at Mo-Si interfaces are investigated for a large range of Mo fractions. The type of silicides and their crystallographic states are presented in detail in chapter 3.

1.3.3. Preventing silicide interface formation

The replacement of naturally formed silicides at Mo-Si interfaces by other materials is expected to enhance the multilayer reflectivity. The PXRMS Multilayer Survey Results illustrates the progress in Mo/Si multilayer reflectivity due to B_4C and C barrier layers deposited at interfaces, and it is presented in Table 1:

d(nm)	N	Grazing Angle (°)	λ (nm)	R (%)	Deposition	Contact	Reference
6.885	60	67.51	12.52	71.4	Magnetron Sputtering	S. Braun, H Mai, M.Moss, A.Leson	The multilayer contains B_4C and C barrier layers. The reflectivity was measured at PTB/BESSY2 in January 2002.
6.89	60	70	12.73	71.05	Magnetron Sputtering	S. Bajt	Measured in July 2001, Presented at SPIE conference (Soft X-ray and EUV Imaging Systems) in San Diego, SPIE Vol. 4506
6.89	50	85	12.75	70.9	Magnetron Sputtering	S. Bajt	Multilayer contains B_4C diffusion barriers. The measurement was done at the ALS beamline in summer 2001.
6.97	60	70	12.8	70.6	Magnetron Sputtering	S. Bajt	Measured at CXRO/ALS June 2001. The multilayer contains diffusion barrier layers.
6.65	50	88.5	13	69.5	Evaporate Ion Polish	E.Louis, A.Yakshin, P.Gőrts, F. Bijkerk	E. Louis et al. Progress in Mo/Si multilayer coating technology for EUVL optics SPIE 3997 (Micro Lithography) Santa Clara 2000

Table 1. PXRMS Multilayer survey displays multilayer reflectivity progress with B_4C or C barriers

In this table, N is the multilayer number of periods. Note that, when comparing reflectivity values in Table 1, it should be taken into account that reflectivity depends on the X-ray angle of incidence, as well as on the wavelength. When the grazing angle decreases, the wavelength decreases and the reflectivity increases. Simulations with the program IMD [17] present in Figure 7 the reflectivity and wavelength variation with the grazing angle.

Multilayer simulations with the software package IMD were carried out to determine which Mo/Si interface is more sensitive to the multilayer optical contrast. The amplitude of the electric field generated by a standing wave for 13.5 nm is maximum (anti-node) at the Si-on-Mo interface and minimum (node) at the Mo-on-Si interface. First we consider the Mo-on-Si interface. To increase reflectance, the optical properties of the interface on Si are actually less important than the thickness of the interface, due to the presence of a node. A reflectivity gain can therefore be obtained when the silicide that is naturally formed at Mo-on-Si interfaces is replaced by another material that acts as diffusion barrier, and has a thickness less than the naturally formed silicide thickness.

At the other interface, there are two possibilities for increasing the reflectance: to deposit a diffusion barrier with lower thickness than the naturally formed silicide or to deposit a material with better optical contrast. For the first case, success has been reported in literature [18,19] when applying thin C and B_4C barrier layers. In Figure 8 we simulated with IMD [17] the reflectivity of a Mo/Si multilayer with B_4C and $MoSi_2$ at its interfaces. We used $MoSi_2$ as a reference interface in these simulations because it was previously identified as the naturally formed silicide at Mo-on-Si interfaces [16, 20]. By using transmission electron microscopy, the naturally formed $MoSi_2$ thicknesses were determined to be 0.5 nm at the Si-on-Mo interface and 1 nm at the Mo-on-Si interface [16, 21]. If B_4C layers of 0.2-0.3 nm could be deposited, a reflectivity gain of maximum 1.5% could be obtained by depositing thin B_4C layers at Mo-Si interfaces. Such an increase was reported by Bajt et al [19], from 68.8% at 13.4 nm for magnetron sputtered Mo/Si multilayers, to 70% at 13.5 nm by using B_4C at both interfaces.

Although there are many reports on the reflectivity gain when depositing B_4C interlayers, the exact stoichiometry of the B_4C formed on Mo and on Si has never been investigated. In chapter 6 we investigate the growth of B_4C barrier layers on both Mo and Si surfaces, as a function of B_4C layer thicknesses. We discuss the different B:C stoichiometries that are formed at the interfaces, and the impact on the optical and thermal response of the multilayers.

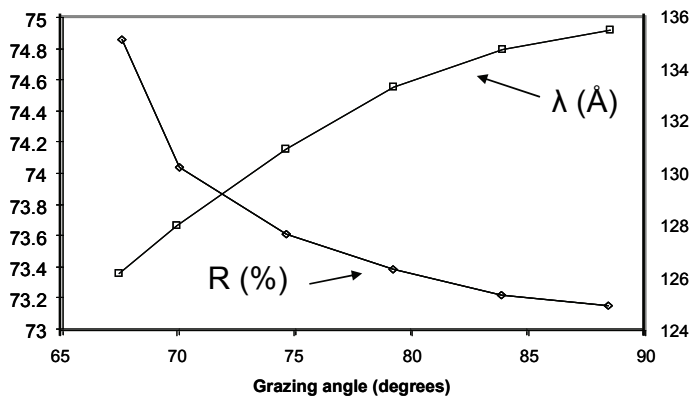

Figure 7. The simulated reflectivity and wavelength as a function of the grazing angle.

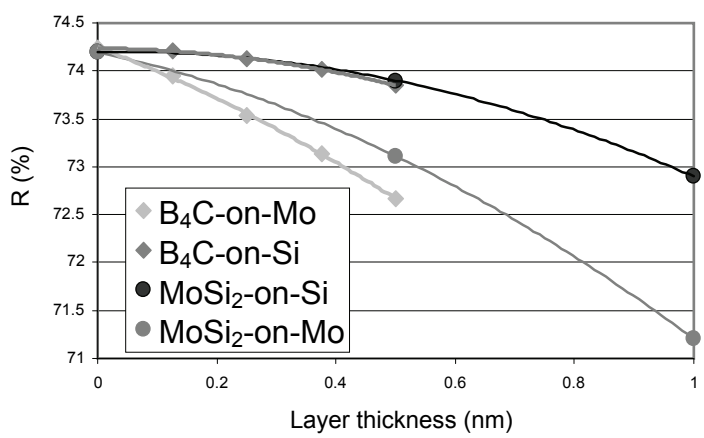

Figure 8. The IMD simulation of the reflectivity as a function of B_4C and $MoSi_2$ layer on Mo and on Si.

1.4. THERMAL STABILITY

The most important issue for application of Mo/Si multilayers in EUVL optics is not just to increase the multilayer reflectivity, but actually to ensure the optics lifetime, since the optics should be able to resist changes under high photon loads for up to 30000

hours. Standard Mo/Si multilayers are expected to rapidly degrade in time under EUV exposure. The reason for this is the diffusion of different species (mainly oxygen) from the multilayer surface into the stack which causes a decrease in the multilayer optical contrast and additional absorption, reducing the multilayer reflectivity as a function of time.

To insure a good lifetime for EUVL optics, the properties of the protective layer applied in top of the Mo/Si multilayer are currently intensive studied [22]. However, even with a perfect protective layer, the multilayer stability over time is not solved. In addition to influencing the surface chemistry, the high photon flux also enhances interdiffusion between Mo and Si at the interfaces. As a result, the silicide layers that are naturally formed at the interfaces during fabrication may continue to expand in time.

1.4.1. Diffusion at interfaces

Rosen et al [23] showed that the interdiffusion coefficient in a Mo/Si system can be calculated as

$$D = [w^2(t)-w^2(0)]/2t, \qquad (2)$$

where w(t) is the interlayer width after annealing time t, and $w(0)$ is the initial interlayer width. The interdiffusion constant can be used to calculate activation energies using Arrhenius law,

$$D = D_0\exp(-E_a/kT), \qquad (3)$$

where D_0 is a pre-exponential coefficient, independent of temperature T, and E_a is the activation energy of interdiffusion.

Rosen et al for the first time observed that upon annealing as a function of time, diffusion takes place preferentially at the Mo-on-Si interfaces. To explain the observed phenomena we study in chapter 4 the diffusion processes at Mo/Si interfaces as a function of annealing temperature. For this we extend a diffusion model for the formation of asymmetric interfaces at room temperature, first proposed by Yulin et al [15], towards temperatures in the range of 150 – 400 °C. According to the model, the thick silicide formed at Mo-on-Si interface was formed by the surface diffusion of Si atoms on growing Mo surface. In contrast, the thin silicide formed at the Si-on-Mo interface was formed by the bulk Si diffusion into textured Mo grains. The diffusion in annealed Mo-Si multilayers was investigated separately at each Mo-Si interface and from this study the cause of complete multilayer re-crystallization into h-$MoSi_2$ (for temperatures higher than 300 °C) is presented in detail in chapter 4. In the same chapter, a model is proposed to

explain the connection between diffusion and multilayer re-crystallization upon annealing.

1.4.2. Silicide formation upon annealing

1.4.2.1. Mo/Si multilayers

The silicides formed during annealing are of particular interest for the stability of multilayer for application in EUVL. Many previous studies report on silicide formation upon annealing Mo/Si multilayers. The formation of Mo-Si silicides as a function of temperature up to 1000 K was investigated by Kondratenko et al [24] who showed that the final silicide formed upon annealing is *t*-$MoSi_2$. However, no clear explanation is given for the preference regarding the formation of *t*-$MoSi_2$, over other existing silicides such as Mo_3Si, Mo_5Si_3 and $MoSi_2$, Actually, Liang and Chen [25] produced multilayers with different Mo:Si ratio and they obtained different silicides upon annealing. They attributed this result to many competing processes like Si crystallization, intermixing of constituent atoms and silicide formation. Chi et al [26] discuss the phase diagram for the Mo/Si binary system and explain silicide formation by nucleation as the rate-controlling mechanism for *h*-$MoSi_2$ formation, followed by *t*-$MoSi_2$ formation at a higher temperature. *h*-$MoSi_2$ and *t*-$MoSi_2$ formation are governed by activation energies of 1.5 eV and 7.8 eV, respectively. The importance of activation energies was analyzed by Johnson et al [27], who explained silicide formation based on the correlation between the nucleation and the stoichiometry of the surrounding amorphous phase.

Most studies reported on in literature have in common that they are focused on Mo-Si multilayers with the Mo:Si ratios optimized for the formation of Mo_3Si, Mo_5Si_3 and $MoSi_2$. No other Mo:Si ratios were considered for identifying and explaining silicide formation upon annealing in Mo/Si multilayers. In this thesis, to identify all major phase transformations in Mo/Si systems we perform an extensive study by sequentially annealing of multilayers with the same period thickness but a large range of Mo fractions (0.1 - 0.8) up to 800 °C, when the final silicides are formed before ultimately resulting in complete multilayer defoliation. The phase transformations identified via X-ray diffraction method will be explained in chapter 3 by using a thermodynamic model that is based on minimization of the total free energy.

1.4.2.2. Mo/Si multilayers with B_4C at interfaces

At the Mo/Si interfaces, many materials have been applied to enhance multilayer stability. For example, Alink et al [28] used CH^+ ions to implant C into Si layers and reported thermal stability of both reflectivity and multilayer period up to 150 °C. Feigl et al [29] deposited Mo_2C at Mo-Si interfaces and increased the thermal stability of the multilayer reflectivity with 200 °C. To increase multilayer stability, also Mo and Si surface passivation by materials like N, reported here in chapter 4, was considered and research is carried on this direction. These results show that by deposition of other materials at Mo-Si interfaces, stable compounds can be formed that significantly decrease Mo-Si diffusion. However, most of these compounds will only increase the multilayer stability at the cost of EUV reflectivity.

The addition of sub-nanometer thick films of B_4C at the interfaces has been shown to be quite successful, not only to enhance the reflectivity, but also to enhance the stability of multilayers [18]. Bottger et al [30] investigated the period compaction of multilayers with B_4C on Mo and B_4C on Si and deduced an asymmetry of Mo-Si interfaces formed after deposition. They also investigated the Mo crystalline structure in the presence of B_4C deposited on Mo or on Si. From this, they concluded that diffusion takes place preferentially at Mo-on-Si interfaces, in agreement with Rosen [23], and that upon annealing *h*-$MoSi_2$ nucleates at the Mo-on-Si interfaces.

As a general rule, B_4C barriers do slow down diffusion, but the addition of B_4C on Si works less well then expected. In chapter 6, the thermal behaviour of multilayers with B_4C deposited on Mo and on Si is analyzed and explained based on the material growth properties and minimization of the formation enthalpies.

1.5. SUBSTRATE RECOVERY LAYERS

In this thesis we treat the issue of the re-utilization of the expensive substrates that are used in coating iterations to optimize multilayer deposition parameters. Also, EUVL optics may need replacement due to build-up of contamination [22] during tool operation and due to thermally enhanced interdiffusion at the Mo/Si interfaces. The

ability to do removal of a multilayer coating and re-coating of the cleaned substrate would significantly reduce cost-of-ownership of commercial EUVL tools.

Several methods exist to remove the multilayer from the substrate. The main problem encountered when using most substrate recovery methods (e.g. wet chemical etching), is an unacceptable increase in substrate surface roughness upon multilayer removal and a corresponding EUV reflectivity loss after re-coating of the recovered substrate.

A better method to recover the substrates proposes the use of a substrate recovery layer, which can be removed together with the multilayer to recuperate the original substrate. Gaines et al [31] proposed a thick protective layer of 30 nm SiO_2, followed by a 100 nm Al layer on top of which the Mo/Si multilayer was deposited. A solution of hydrochloric acid and cupric sulfate was used to etch the Al layer and released the multilayer. The multilayer reflectivity was reduced by the presence of the Al layer. Early et al [32] used an amorphous carbon layer between the substrate and the multilayer which was removed by wet-chemical etching. Also in this case, the EUV reflectivity was reduced.

We propose in chapter 5 another material, a polyimide, to be used as a separation layer in the substrate recovery process. The polyimide choice is motivated by previous studies on its property of reducing substrate roughness. When applying polyimide on a substrate, R. Souffli reported surface smoothening for an aspheric substrate [33], as well as a roughness reduction from 1.76 nm to 0.27 nm in the high-spatial frequency domain for a diamond substrate [34].

In this thesis, experiments were performed successfully on Si substrates. In chapter 5 EUV reflectivity and surface roughness are compared for substrates in all recovery process stages. The same polyimide was applied on Zerodur substrates that are normally used in EUVL process. For this case, EUV multilayer reflectivity is also reported.

1.6. PRODUCING Mo/Si MULTILAYERS

1.6.1. Deposition method

All multilayer samples on which results are presented in this thesis have been created using the deposition setup presented in Figure 9 an electron beam is used to melt a solid target, resulting in a flux of thermalized (<1 eV) particles. In contrast with deposition techniques that deposit particles with kinetic energies of tens of electron volts, the low kinetic energy of electron beam evaporated particles enables layer growth with relatively sharp interfaces. The slightly different layer growth and Mo-Si interlayer formation may actually be favorable for achieving higher multilayer reflectivity.

The deposition system, developed in the early 1990's [35] consists of two vacuum vessels separated by a valve and shutter. The lower vessel contains the target materials and electron beam evaporator. The upper vessel holds the substrate and various in-situ analysis equipment. The base pressure in the upper chamber was below 2×10^{-8} mbar. A Residual Gas Analyzer (RGA) provides information on the partial pressures in the system. The relation between background pressure and multilayer quality has previously been discussed in ref. [24].

The sample is mounted in the upper vacuum vessel on a holder that rotates to assure homogeneous deposition. In the lower vessel, Mo and Si are alternatively evaporated from the multi-target holder by an electron beam which is swept by magnetic coils to ensure a homogenous melt. To obtain a desirable flux gradient over a large surface area, particle flux masking can be applied for specific materials. Finally, to suppress roughness development during multilayer growth, ion beam smoothening is applied to each deposited Si layer, using Kr ions supplied by a Kauffmann type ion gun which is oriented under a 50° angle to the substrate.

Recently, the schematic deposition setup presented here was modified to also allow deposition of multilayers by magnetron sputtering. The biggest advantage of this method is the very stable deposition rates. On the other hand, good uniformity over large area is obtainable by the electron beam evaporation method. So far, no significant differences were apparent in the Mo/Si multilayer quality produced by these two methods. All the results further presented in this thesis were obtained on multilayers that were prepared using electron beam evaporation.

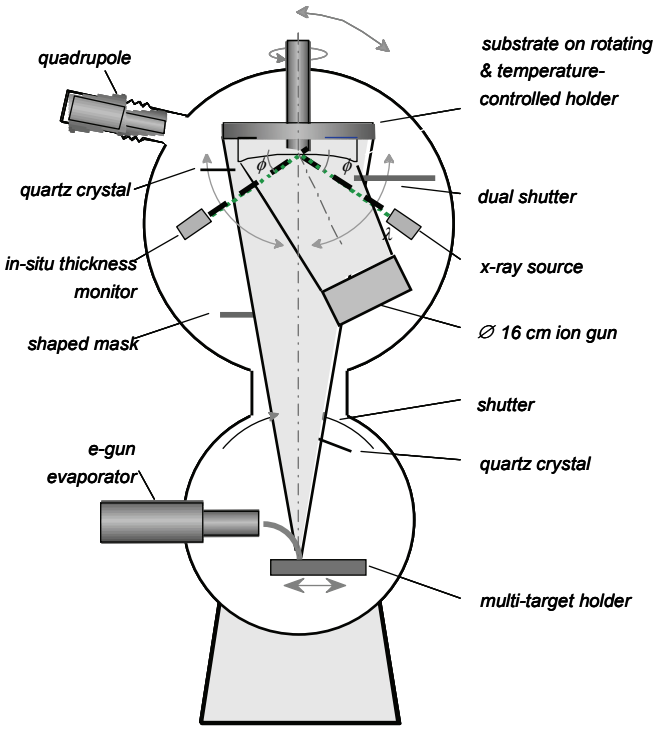

Figure 9. Schematic view of an UHV electron beam deposition setup.

1.6.2. Layer control

The layer thickness control needs to be very precise to match the period of the deposited multilayers to the incident radiation from EUV sources. For this purpose, layer control is achieved through in-situ monitoring of X-rays reflecting from the growing film. The X-ray monitoring system exhibits oscillations in the reflected intensity, depending on the exact phase relation between the surface reflection and reflections from buried interfaces. During deposition, the reflectivity is continuously being monitored, and when a predetermined position on this curve is reached, the shutter between the two vessels is closed to stop deposition. To obtain different multilayer period thicknesses according to Bragg's law (Eq. (1)), the angle of the incoming X-ray radiation and its detection can modified by moving the X-ray source and detector on a circular holder. Apart of the in–

situ X-ray monitoring system, 4 quartz oscillators can be used to control layer thicknesses, one in the lower vessel and 3 in the upper vessel around the sample holder.

The whole deposition process is controlled by a script which dictates the successive steps in the deposition process. The script runs under a computer program written in LabView which is designed to operate each physical device (electron gun, ion gun, shutter, etc) during the deposition. Feedback from the layer control monitoring system is immediately coupled back to the layer deposition and treatment sources to ensure multilayer periodicity.

1.7. ANALYSIS METHODS

To understand the behaviour of macroscopic multilayer properties such as d-spacing or layer periodicity, reflected intensity, and multilayer stress induced substrate deformation, it is necessary to analyze the effects of the structural and chemical processes at atomic resolution. Table 2 displays the most common techniques used to investigate the surface and in-depth composition and structure of thin films.

A combination of TEM and Cu-K calibration was successfully used by Kessels et al [36] to analyze Mo/Si multilayers that were exposed to ion bombardment. Therefore, additional intermixing occurs at Mo-Si interfaces and the resulting silicide thicknesses of 1.1 and 1.2 nm were sufficient to allow silicide identification. In the case of 0.5 and 1 nm silicides formed at Mo/Si interfaces directly after deposition, analyzed in this thesis, silicide identification was possible with this method, although in similar systems a gradient in Mo-on-Si interlayer composition was reported by Slaughter et al [20]. To further investigate silicide composition, the silicide thickness could be increased by sample thermal treatment (chapter 1.4).

Technique	Principle	Disadvantage	Advantage
TEM	Transmitted energetic electrons are imaged	Intensity scale has no calibration	High in-depth resolution (best resolution)
HAADF	Measures diffraction angle of the forward scattered electrons	Limited to high Z materials	Non-destructive, elemental quantitative analysis
XPS	Photons excite electrons, that emit an inner-shell electron	Average information over 1 nm, in-depth information by sputtering	Elemental specific, non destructive
XES	Electrons excite electrons, that emit a photon	Average information over 1 nm, in-depth information by sputtering	Elemental specific, non destructive
WAXRD	X-ray diffract from the crystalline structures	Average information over the whole multilayer	Non-destructive, good resolution
XRF	Photons excite atoms that emit an e-ray photon	No in-depth information	Non-destructive, elemental specific
(L/M/H)EIS and RBS	Energetic ions scatter at structure, structure can be determined from energy loss	May destroy structure during measurement	Elemental specific
SIMS	Ions sputter and ionize material from surface, with mass measured using mass spectrometer	Limited in-depth information	High material selectivity
EELS	Measurement of loss of energy of transmitted electrons	Resolution less than TEM	Elemental specific, non destructive
AES	Electrons excite atoms, which emit an electron	Only surface, no lateral resolution	Sensitive for chemical compositions
EDX	Electrons excite atoms, which emit a photon	Averages over large depth scales, limited lateral resolution	High material selectivity
SEM	Electrons excite atoms, emitted atoms are imaged	Averages over large depth scales	Works well for 3D structures, high lateral resolution
AFM	Scans surface with needle, measures forces	No in-depth information, material independent	High lateral resolution
STM	Scans surface with needle, measures tunnel current	No in-depth information, needs conducting surface	Very high lateral resolution, can distinguish materials

Table 2. Analysis techniques most commonly used for multilayer surface and in-depth investigation.

1.7.1. XES, XPS, AFM

To determine the atomic composition of barrier materials at Mo-Si interfaces, in chapter 6 in-depth XPS profiling was used by sputtering the material using an Ar gun. To identify silicide stoichiometries in annealed multilayers, in chapter 4 XES was used to compare the Si 3p spectral density states to reference $MoSi_2$, Mo_5Si_3 and Mo_3Si spectra. In addition to the qualitative information on compound composition that XES and XPS provide, TEM was used to quantify interface silicide thicknesses (chapter 2 and 4).

In chapter 5, AFM measurements were used to characterize multilayer high-spatial frequency roughness (HSFR) when a substrate recovery layer is deposited between the multilayer and the substrate. In this case, AFM data seemed to show the same roughness, although EUV reflectivity indicated clear differences, supported by off-specular X-ray scattering measurements. This might be caused by the AFM tip limitation to probe only the relatively smooth SiO_2 top layer of the multilayer. Power Spectral Density (PSD) curves extracted from AFM measurements do show differences in HSFR, which are in agreement with EUV reflectivity measurements.

1.7.2. X-ray measurements

The physical properties of Mo/Si multilayers (diffusion at interfaces, crystallinity, roughness) were mostly studied using hard X-ray measurements using a Philips X'Pert double crystal X-ray diffractometer using Cu-Kα line radiation (0.154 nm). The source contains a 4-bounce Ge monochromator and the detector is automatically protected against overload intensity by a Ni beam attenuator situated in front of it.

Two X-ray methods (GIXR) and (WAXRD) were used to determine period thickness and the crystalline structure of Mo and its silicides upon multilayer annealing. During the grazing incidence X-ray (GIXR) measurement, the source is fixed and the sample moves together with the detector in the θ - 2θ geometry, such that the reflected intensity from the sample is collected by the detector. In the case of Wide Angle X-ray Diffraction, the source and the sample are fixed and the detector registers the diffracted

intensity while moving using 2θ geometry. The average crystallite size was determined from Scherrer equation:

$$X = \frac{0.94\lambda}{L\cos(\theta)}, \quad (4)$$

where L is the full width at half maximum determined for every peak in the spectrum, and 2θ is the diffraction angle between the source and the detector.

To analyze multilayer roughness, specular and off-specular X-ray measurements were performed. Although specular reflectivity is sensitive to roughness, it also depends on many other factors such as optical contrast, thickness errors in the stack, silicide formation at the interfaces, etc. An additional method to analyze the roughness is diffuse scattering (rocking curves), which was used to study Mo/Si multilayer roughness in chapters 2 and 5.

The multilayer reflected intensity at incident radiation around 13.5 nm was measured near normal incidence at the Physikalisch-Technische Bundesanstalt (PTB) [37] at the BESSY II storage ring in Berlin.

1.7.3. Thermal annealing treatment

A large part of the work carried out in this thesis involves the behaviour of multilayers at high temperatures, enabling the study of thermally enhanced diffusion and intermixing. The multilayers were successively annealed for 48 h from 20 °C to 350 °C using a halogen lamp in a vacuum chamber (base pressure 10^{-7} mbar). Figure 10 displays the aluminum annealing holder which was used to mount mono-crystalline Si substrates. Two thermocouples enable the temperature reading from the holder and at the surface of the Si substrates. The thermocouple inside the holder was used to regulate the temperature during annealing. The temperature fluctuation around the set value was ±2 °C and the reproducibility of the average temperature value for the same set value was ±1 °C.

Several multilayers were annealed in successive runs at increasingly higher temperatures and compared to multilayers annealed directly to the highest temperature to check if there is any effect of annealing history. No significant differences were observed between the two methods, and only successively annealed samples will be reported on here. After each annealing cycle the multilayer was analyzed using hard X-rays (GIXR

and WAXRD for λ = 0.154 nm) and soft X-rays (GIXR for λ = 13.5 nm). However, initial annealing effects during temperature rising to the set value were not possible to analyze using this set-up. Therefore, an annealing stage mounted in the Cu-K reflectometer is currently being explored.

Sequential annealing at temperatures in the range 350 – 800 °C was performed into an oven using a W filament (pressure 10^{-7} mbar). Damage of the multilayers occurred upon annealing at temperatures higher than 800 °C.

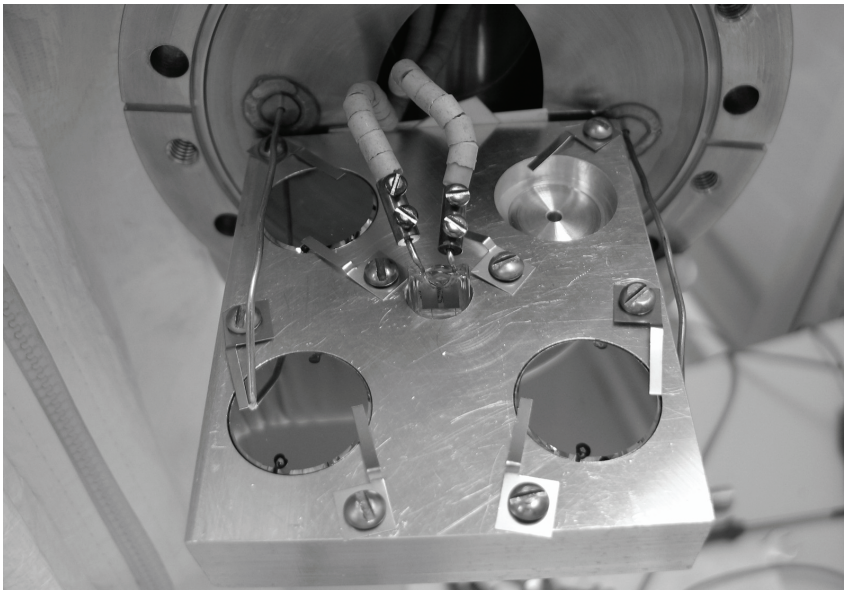

Figure 10. Photograph of the annealing system used to perform thermal treatment on samples with mono-crystalline Si substrates. The halogen lamp is in the center of the Al holder. The holder can accommodate 4 samples (3 are present in the photo). Two thermocouples measure the temperature on the sample surface and in the aluminum holder.

1.8. MULTILAYER OPTICS APPLICATIONS

Mo/Si multilayers have multiple applications apart of EUV lithography, mostly due to the fact that they can be deposited on curved substrates. Therefore they can be used in many imaging applications like microscopes and telescopes.

One such application is EUV photoemission microscopy for surface science. In this case, Mo/Si multilayers are used to build a so named Schwarzschild objective which receives photons of 91.8 eV (13.5 nm wavelength) and focuses them on the sample. The sample emits photoelectrons that, when further analyzed, reveal elemental composition and chemical bonding of elements at the surface.

Another application is EUV astronomy. An EUV image of the sun (Figure 11, [38]) is obtained in the wavelength range from 17.1 nm to 17.5 nm, and is dominated by line emission from highly ionized Fe (Fe^{+8} and Fe^{+9}) that is present in coronal plasma regions where the temperature is $1.2x10^6$ K.

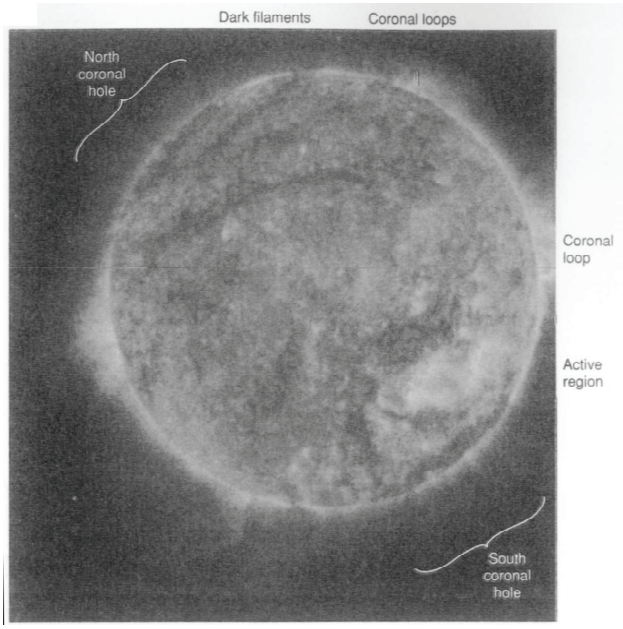

Figure 11. EUV image of the sun obtained with a rocket launched Cassegrain telescope employing multilayer coated normal incidence optics.

To obtain images in this wavelength range (bandpass), Mo/Si mirrors (concave and convex) are used with a multilayer period of 8.55 nm and Γ = 0.43, yielding peak reflectivities of 35 % at 17.2 nm. The bandpass is further narrowed to the needed range by an Al L-edge filter (17.1 nm).

As in astronomy, multilayer mirrors are convenient to isolate certain spectral lines. An application for this is the development of the EUV or X-ray lasers, where one lasing line has to be isolated from the background. Another example is plasma diagnostics. Here, different mirrors can be used to select characteristic emission from different areas in the plasma. Multilayer mirrors are also used for magnetic material studies. In this case, the mirrors are designed for use at the Brewster's angle (laterally graded multilayer design), where the reflectivity for s-polarized radiation at a Bragg peak can be orders of magnitude higher than the reflectivity for p-polarized radiation.

Another application of multilayer mirrors is X-ray microscopy, where analog to optical microscopes, optics are needed to collimate the radiation of a light source onto a sample, but at much shorter wavelengths. The advantage is a much higher resolution than for visible light, due to the smaller wavelength of X-rays, as given by Rayleigh's resolution criterion,

$$\Delta x = 1.22\lambda/NA, \qquad (5)$$

where Δx is the smallest center-to-center distance of two resolvable objects and NA is the numerical aperture. In addition, to form a high quality image of the sample, a high optical contrast between different parts of the sample and a sufficient transmission of radiation through the sample are needed. For biological samples containing carbon and water, only two wavelength ranges yield enough optical contrast between these two materials: visible light and the so called water window (2.4 - 4.4 nm). Due to a low penetration depth (10 μm) of radiation into water, the image of a complete cell is obtained with some difficulty. Still, compared to electron microscopy, which can perform very high resolution images but requires the cut of the cell in slices, X-ray spectroscopy enables high-resolution images of complete cells.

Multilayer mirrors can also be used in X-ray fluorescence spectroscopy which is a non-destructive method used to determine the concentration of elements present in solid, powdered or liquid samples. Incident photons create core-level vacancies in sample atoms through photoemission. The characteristic line emission (fluorescence) is detected by an energy selective detector that allows elemental identification. The role of multilayer mirrors is to focus the hard X-ray radiation coming from a synchrotron source.

Finally, the multilayer design can be improved by etching regions from the multilayer, using electron beam lithography together with reactive ion etching as shown

in Figure 12. Such a Mo/B_4C multilayer, called lamellar multilayer amplitude grating enables a significantly improved B-K, Si-K and Cu-L emission in terms of bandwidth and peak reflectivity when recorded by such monochromator with respect to the standard multilayers [39].

A challenging future application of multilayer optics is in the field of X-ray Free Electron Lasers. In these devices, electrons are accelerated to extreme energy levels and are used to generate X-ray radiation at high intensity. Multilayer mirrors are explored as optical elements to focus and isolate the EUV and X-ray radiation. The challenge is to provide a high long-term stability of these elements, essential due to the degradable influence of the ultra-short and intense X-ray radiation pulses.

Also, by etching in depth a standard multilayer to obtain in plane a Fresnel zone plate, new 3-D nanostructure optical devices can be built. These new devices would enable wavelength selectivity, focusing, and imaging of unprecedented high quality. For example, the biophysics of DNA and other C- and O- containing molecular structures might ultimately be imaged with resolutions of few tenths of nanometers.

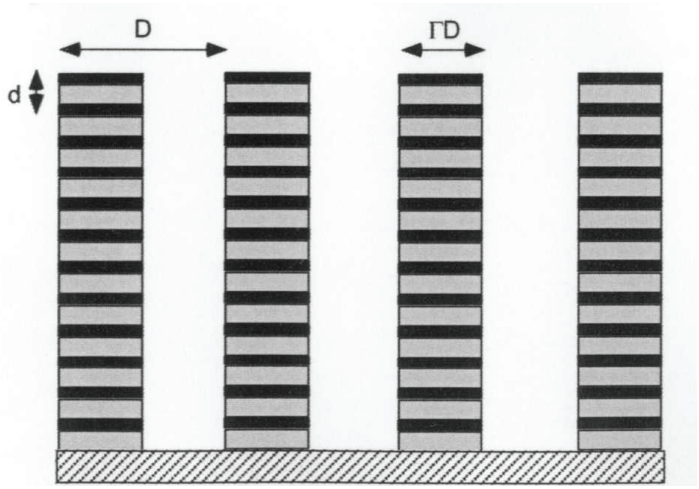

Figure 12. Scheme of a lamellar multilayer amplitude grating.

1.9. OUTLOOK – IN THIS THESIS

To maximize the reflectivity of multilayer optics, the multilayer surface roughness should be reduced as much as possible. The work presented in chapter 2 enables a better understanding of the layer smoothening when different types of Kr ion treatment during and after Si layer deposition are applied.

In chapters 3 and 4 we present the characteristics of silicides formed at Mo-Si interlayers at room temperature and upon multilayer annealing. In chapter 3 silicide formation and evolution during annealing is investigated as a function of the Mo fraction. Chapter 4 describes the diffusion at Mo-Si interfaces during annealing. The preferential diffusion at Mo-on-Si interface is explained based on thin film growth properties.

The production of EUVL optics currently requires many expensive smooth substrates (< 0.2 nm) to be used in the iterative manufacturing process. A polyimide layer, used as a separation layer between substrate and multilayer, proves to be a good solution for expensive substrate recovery. The effect of a polyimide buffer layer on the properties of the added multilayer is investigated in chapter 5. Multilayer roughness and reflectivity are considered, as well as the effect of polyimide on the applicability for EUV coatings.

Finally, to improve the performance of EUVL optics, B_4C is currently investigated as an added material at Mo-Si interfaces to increase reflectivity and thermal stability. In chapter 6 we study the formation of B_4C at Mo-Si interfaces and explain observed behaviour in optical response as well as thermal stability.

1.10. REFERENCES

1 H. Meiling, H. Meijer, V. Banine, R. Moors, R. Groeneveld, H. Voorma, U. Mickan, B. Wolschrijn, B. Mertens, G. van Baars, P. Kürz, N. Harned, "First performance results of the ASML alpha demo tool", Proceedings SPIE Conference, **6151**, 615108-12, Santa Clara, (2006)

2 M. van den Brink, www.sematech.org/meetings/archives.htm, International EUVL Symposium, Barcelona (2006)

3 A.E. Yakshin, R.W.E. van de Kruijs, E. Zoethout, I. Nedelcu, E. Louis, F. Bijkerk, H. Enkisch, S. Müllender, 'Interface engineering of Mo/Si multilayers for enhanced reflectance in EUVL applications', International EUVL Symposium, Barcelona, www.sematech.org/meetings/archives.htm. (2006)

4 E. Louis, A. E. Yakshin, P. C. Gőrts, S. Oestreich, R. Stuik, E. L. Maas, M. J. Kessels, F. Bijkerk, M. Haidl, S. Müllender, M. Mertin, D. Schmitz, F. Scholze, G. Ulm, "Progress in Mo/Si multilayer coating technology for EUVL optics" SPIE **3997,** art. No. 406 (Micro Lithography), Santa Clara (2000)

5 E. Louis, H.-J. Voorma, N. B. Koster, L. Shmaenok, F. Bijkerk, R. Schlatmann, J. Verhoeven, Yu. Ya. Platonov, G. E. van Dorssen and H. A. Padmore, "Enhancement of reflectivity of multilayer mirrors for soft x-ray projection lithography by temperature optimization and ion bombardment", Microelectronic Engineering **23** (1-4), pp. 215-218 (1994)

6 E. J. Puik, M.J. van der Wiel, H. Zeijlemaker and J. Verhoeven, "Ion-bombardment of thin-layers - the effect on the interface roughness and its x-ray reflectivity", Review of Scientific Instruments **63** (1), pp. 1415-1419 (1992)

7 R. Schlatmann, A. Keppel, Y. Xue, J. Verhoeven and M. J. van der Wiel, "Enhanced reflectivity of soft x-ray multilayer mirrors by reduction of Si atomic density", Applied Physics Letters **63** (24), pp. 3297-3299 (1993)

8 H. -J. Voorma, E. Louis, F. Bijkerk and S. Abdali, "Angular and energy dependence of ion bombardment of Mo/Si multilayers", Journal of Applied Physics, **82** (4), pp. 1876-1881, (1997)

9 M. Jergel, E. Majkova and S. Luby, "X-ray reflectivity and non-specular scattering investigation of amorphous W/Si multilayers after rapid thermal annealing", Journal de Physique IV, Colloque C8, supplement au Journal de Physiqye **I**, 3, pp. 337-340 (1993)

10 H. -J. Voorma, E. Louis, N. B. Koster, F. Bijkerk, "Temperature induced diffusion in Mo/Si multilayer mirrors", Journal of Applied Physics, **83** (9), pp. 4700-4708 (1998)

11 M. B. Stearns, C-H Chang, D. G. Stearns, "Optimization of growth conditions of vapor deposited Mo/Si multilayers", Journal of Applied Physics, **71** (1), pp. 187-195 (1992)

12 E. Yakshin, R.W.E van de Kruijs, I. Nedelcu, E. Zoethout, E. Louis, F. Bijkerk, I. Kozhevnikov, C. Bruineman, H. Enkisch, S. Müllender, presentation at 7th International Conference on Physics of X-Ray Multilayer Structures (Sapporo, 2004)

13 E. Zoethout, G. Sipos, R. van de Kruijs, A. Yakshin, E. Louis, S. Müllender, F. Bijkerk, "Stress mitigation in Mo/Si multilayers for EUV lithography", Proceedings SPIE **5037**-106, Santa Clara (2003)

14 M.J.H. Kessels, J. Verhoeven, A. E. Yakshin, F. D. Tichelaar, F. Bijkerk, "Ion beam induced intermixing of interface structures in W/Si multilayers", Nuclear Instruments and Methods in Physics Research B **222**, pp. 484-490 (2004)

15 S. Yulin, T. Feigl, T. Kuhlmann, N. Kaiser, A.I. Fedorenko, V. V. Kondratenko, O. V. Poltseva, V. A. Sevryukova, A. Yu. Zolotaryov, E. N. Zubarev, "Interlayer transition zones in Mo/Si superlattices", Journal of Applied Physics, **92** (3), pp. 1216-1220 (2002)

16 S. Bajt, D. G. Stearns, P. A. Kearney, "Investigation of the amorphous-to-crystalline transition in Mo/Si multilayers", Journal of Applied Physics, **90**, 2, pp. 1017-1025 (2001)

17 IMD, version 4.1.1, written by David L. Windt (2000)

18 S. Braun, H. Mai, M. Moss, R. Scolz, A. Leson, "Mo/Si Multilayers with Different Barrier Layers for Applications as Extreme Ultraviolet Mirrors", Japanese Journal of Applied Physics, **41**, pp. 4074-4081 (2002)

19 S. Bajt, J. Alameda, T. Barbee, W.M. Clift, J.A. Folta, B. Kaufmann, E. Spiller, "Improved Reflectance and Stability of Mo/Si Multilayers", Optical Engineering **41** (8), pp. 1797-1804 (2002)

20 J. M. Slaughter, A. Shapiro, P. A. Kearney, and C. M. Falco, "Growth of molybdenum on silicon: Structure and interface formation", Physical Review B **44 (8)**, pp. 3854-3863 (1991)

21 D. G. Stearns, R. S. Rosen, and S. P. Vernon, "Fabrication of high-reflectance Mo-Si multilayer mirrors by planar-magnetron sputtering", Journal of Vacuum Science and Technology A **9 (**5**)**, pp. 2662-2669 (1991)

22 B. Mertens, M. Weiss, H. Meiling, R. Klein, E. Louis, R. Kurt, M. Wedowski, H. Trenkler, B. Wolschrijn, R. Jansen, A. van de Runstraat, R. Moors, K. Spee, S. Plőger, R. van de Kruijs, "Progress in EUV optics lifetime expectations", Microelectronic Engineering **73-74,** pp. 16-22 (2004)

23 R. S. Rosen, D. G. Stearns, M. A. Viliardos, M. E. Kassner, S. P. Vernon, Y. Cheng, "Silicide layer growth rates in Mo/Si multilayers", Applied Optics, **32**, no. 34, pp. 6975-6980 (1993)

24 V. V. Kondratenko, Yu. P. Perschin, O.V. Poltseva, A. I. Fedorenko, E. N. Zubarev, S. A. Yulin, I. V. Kozhevnikov, S. I. Sagitov, V. A. Chirkov, V. E.

Levashov, A. V. Vinogradov, "Thermal stability of soft Mo-Si and $MoSi_2$-Si multilayer mirrors", Applied Optics, **32**, no.10, pp. 1811-1816 (1993)

25 J. M. Liang, L. J. Chen, "Interfacial reactions and thermal stability of ultrahigh vacuum deposited multilayered Mo/Si structures", Journal of Applied Physics, **79** (8), pp. 4072-4077 (1996)

26 E. Chi, J. Shim, J. Kwak, H. Baik, " Silicide formation by solid-state diffusion in Mo/Si multilayer thin films", Journal of Materials Science **31**, pp. 3567-3572 (1996)

27 C. Johnson, K. Anderson, A. Gromko, D. Johnson, "Variation of the Nucleation Energy of Molybdenum Silicides as a Function of the Composition of an Amorphous Precursor", Journal of the American Chemical Society **120**, pp. 5226-5232 (1998)

28 L. G. A. M. Alink, R. W. E. van de Kruijs, E. Louis, F. Bijkerk, J. Verhoeven, "Improved temperature stability of Mo/Si multilayers by carbide based diffusion through implantation of low energy CH^+_x ions", Thin Solid Films **510**, pp. 26-31 (2006)

29 T. Feigl, H. Lauth, S. Yulin, N. Kaiser, "Heat resistance of EUV multilayer mirrors for long-time applications", Microelectronic Engineering **57-58**, pp. 3-8 (2001)

30 T. Bottger, D. C. Meyer, S. Braun, M. Moss, H. Mai, E. Beyer, "Thermal stability of Mo/Si multilayers with boron carbide interlayers", Thin Solid Films **444**, pp. 165-173 (2003)

31 D. P. Gaines, N. M. Ceglio, S. P. Vernon, M. Krumrey, and P. Muller, "Repair of high performance multilayer coatings", in *Multilayer Optics for Advanced X-Ray Applications*, N.M. Ceglio, ed. Proceedings SPIE **1547**, pp. 228-238 (1991)

32 K. Early, D. L. Windt, W. K. Waskiewicz, O. R. Wood II, and D. M. Tennant, "Repair of soft x-ray optical elements by stripping and re-deposition of Mo/Si reflective coatings", Journal of Vacuum Science and Technologies **B 11**, pp. 2926-2929 (1993)

33 R. Soufli, "Polyimide smooths surface of EUV aspheric condenser", Laser Focus World **41** (2) (2005)

34 R. Soufli, E. Spiller, M.A. Schmidt, J. C. Robinson, S. L. Baker, S. Ratti, M. A. Johnson, E. M. Gullikson, "Smoothing of diamond-turned substrates for extreme ultraviolet illuminators", Optical Engineering **43** (12), pp. 3089-3095 (2004)

35 E. Louis, H. –J. Voorma, N.B. Koster, F. Bijkerk, Yu. Ya. Platomov, S. Yu. Zuev, S.S. Andreev, E. A. Shamov, N. N. Salashchenko, "Multilayer coated

reflective optics for Extreme UV lithography", Microelectronic Engineering **27 (**1-4**),** pp. 235-238 (1995)

36 M. J. H. Kessels, F. Bijkerk, F. D. Tichelaar and J. Verhoeven, "Determination of in-depth density profiles of multilayer structures", Journal of Applied Physics, **97** (9), art. No. 093513 (2005)

37 J. Tümmler, H. Blume, G. Brandt, J. Eden, B. Meyer, H. Scherr, F. Scholz, G. Ulm, „Characterization of the PTB EUV reflectometry facility for large EUVL optical components", Proceedings SPIE **5037**-265 (2003)

38 D. Atwood, *"Soft x-rays and extreme ultraviolet radiation: Principles and Applications"*, Cambridge University Press (2000)

39 R. Benbalagh, J-M. Andre, R. Barchewitz, P. Jonnard, G. Julie, L. Mollard, G. Rolland, C. Remond, P. Troussel, R. Marmoret, E. O. Filatova, "Lamellar multilayer amplitude grating as soft-X-ray Bragg monochromator", Nuclear Instruments and Methods in Physics Research A **541**, pp. 590-597 (2005)

2. Interface roughness in Mo/Si multilayers

2.1. ABSTRACT

In this chapter we present a study of surface roughness development at the molybdenum-on-silicon and silicon-on-molybdenum interfaces in Mo/Si multilayers as employed in Extreme UV lithography. Thin Mo/Si multilayers, with layer thicknesses of 3-5 nm, were deposited using electron beam evaporation. The effect of ion treatment on the surface roughness was studied by X-ray reflectometry and transmission electron microscopy. Without ion treatment we observed built up of correlated roughness. The roughness development is shown here to depend strongly on the thickness of the crystalline Mo layer. Independent of the Mo ratio in a period, we show that a minimal amount of ion treatment is required to smoothen the multilayer roughness, which is also confirmed by EUV reflectivity measurements. At high ion energies the layers become smoother due to a larger ion penetration depth. The higher penetration depth is also shown to initiate additional interdiffusion and structural changes at buried interfaces.

2.2. INTRODUCTION

For Extreme Ultra Violet (EUV) lithography projection equipment for future chip manufacture, Mo/Si multilayers are being developed as reflecting coatings for illuminator and projection optics. A critical property of such multilayers is a high near-normal incidence reflectance for 13.5 nm radiation, requiring a low surface roughness at Mo-Si interfaces [1]. The surface roughness that develops during a low particle energy deposition process, used for the fabrication of the multilayer structures, can for a large part be attributed to the crystalline nature of the Mo layers [2]. To reduce roughness, the film surface can be bombarded with ions during and/or after every layer deposited [3,4,5]. Due to preferential ion sputtering expected along preferred Mo crystallite orientations and ion-induced changes in the Mo crystallite lattice strain [6], ion treatment of Si layers is generally preferred as a means to reduce surface roughness. The optimization of the EUV reflectivity with respect to the applied ion energy after deposition and the ion angle to the substrate was described in detail by Voorma et al [7]. However, a full analysis of the ensemble of mechanisms at play in the formation of the multilayer structures requires detailed experimental information on the system's properties.

In this work, we analyze the influence of the ion energy and the material volume where ions are applied during layer growth on the interface morphology. Interface roughness and width were analyzed using X-ray reflectometry and transmission electron microscopy (TEM). We present data on multilayer growth using low energy ion treatment, where, below the ion sputtering threshold, smoothening takes place without material removal. This allows us to specifically investigate the growth process avoiding materials sputtering. Additional experiments were carried out at higher ion energies where physical sputtering of deposited materials becomes significant. We investigate changes in the structure of buried interfaces due to ions penetrating below the growth surface. Experimental results are validated by comparison with reflectivity calculations [8], correlating reflectivity changes to the changes in roughness and interface width.

2.3. EXPERIMENTAL DETAILS

Multilayers of typically 50 bilayers of Mo and Si were deposited by electron beam evaporation onto 25x25 mm^2 super-polished silicon substrates. The multilayer period was chosen to be approximately 7 nm, optimal for reflecting 13.5 nm wavelength

radiation. Samples were produced with different ion-surface interactions (energy, treatment volume) under an angle of 50° with respect to the deposited layer surface and different Mo ratios $\Gamma = d_{Mo}/(d_{Mo}+d_{Si})$, where d_{Mo} and d_{Si} are the thickness of molybdenum and silicon, respectively. The pressure during deposition was in the range $1.5 - 4 \times 10^{-8}$ mbar. Quartz mass balances and an in-situ X-ray reflectometer were used for layer thickness control. The deposition process is described in detail elsewhere [3].

The multilayer roughness and period thickness were analyzed by grazing incidence X-ray reflectivity (GIXR) and diffuse scattering measurements, with a Philips X'Pert diffractometer at the Cu-K_α wavelength λ = 0.154 nm. EUVL reflectivity was measured at λ = 13.5 nm wavelength and 1.5 degree off normal. Interface roughness and layer crystallinity was determined with Transmission Electron Microscopy (TEM) in both bright field mode (Philips CM30T) and lattice imaging mode (Philips CM300UT-FEG) at 300 kV. Only bright field images are shown in this paper. Specimens for TEM were prepared by Ar ion milling cross sections of the multilayers glued on a copper grid.

2.4. RESULTS AND DISCUSSIONS

2.4.1. Roughness dependence as a function of ion energy

2.4.1.1. Ion treatment during layer growth

In general, for low ion energies, typically below 50 - 100 eV, layer smoothening takes place without significant material removal due to the low ion sputtering yield. Figure 13 shows GIXR measurements for multilayers deposited using ion assistance during layer growth. Kr ions of 60 eV were applied in the final 25 %, 50 %, 75 % and 100 % of the Si layer deposition. Reflectivity simulations show that an increase of the reflected intensity of the high order Bragg peaks indicates a decreasing roughness.

Figure 13 therefore shows that the roughness continuously decreases when a larger part of Si is treated with ions. However, the EUV reflectivity (insert Figure 13) does not show the continuous increase that would be expected from a continuously

decreasing roughness. For 75 % and 100 % of the Si layer treated with Kr ions, the EUV reflectivity actually decreases. This can only be explained by the fact that, when ions are applied at the first part of the layer deposition, they also affect the underlying Si-on-Mo interface. This assumption is validated by a detailed analysis of the 1st order Bragg peak [9] which shows that the thickness of the interfaces increases. The combination of surface smoothening and additional intermixing causes the maximum observed in the EUV reflectivity.

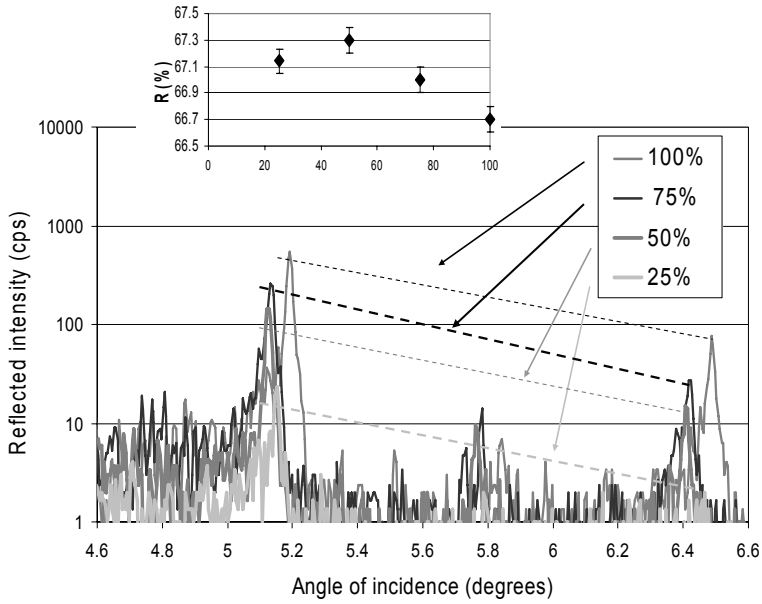

Figure 13. GIXR measurements at Cu-K wavelength for different fractions of the Si layer smoothened by Kr ions of 60 eV. The reflected intensity shows that the roughness decreases with the amount of the Si layer treated by ions. The EUV reflected intensity shows that the highest value is met when 50 % of the Si layer is treated by ions.

2.4.1.2. Ion treatment applied after layer deposition

At higher ion energies, additional layer smoothening takes place due to the larger interaction penetration depth (i.e. larger interaction volume, see also Sect. 2.4.1.1.). Although this should result in higher EUV reflectivities, additional intermixing should

also take place, limiting or even negating the reflectivity gain. In addition, deposited material removal takes place due to the increasing sputtering yields. To reduce effects of intermixing and material removal during deposition, at high energies ions should preferably be applied at the last part of the layer and/or after layer deposition has finished. To investigate the effect of ion energy on the multilayer roughness, a fixed amount of 0.5 nm was removed by ion polishing after each deposited Si layer with ion energies in the range 100 eV - 2000 eV. To determine the effect of high ion energy treatment on layer roughness, we analyzed higher order Bragg peaks in the Cu-K reflectometry spectrum. For energies of 100 - 150 eV, no significant difference is noticed in high order Bragg peak reflected intensity, see also Figure 14. Although the ion energy is sufficient to efficiently remove the deposited material, no significant additional smoothening is observed.

By further increasing the ion energy, a reduction of the high orders Bragg peak intensities suggests that the roughness actually increases. Figure 15 shows a TEM analysis of Mo/Si multilayers polished with Kr ions of 130 eV and 2000 eV. We observe that different amounts of silicide are formed at the Si-on-Mo interfaces: 0.8 nm at an ion energy of 130 eV and 1.6 nm at 2000 eV. The increased amount of silicide formed in the multilayer where 2000 eV ion energy was applied shows that the ions are passing through the Si layer and through intermixing create additional silicide at the Si-on-Mo interface.

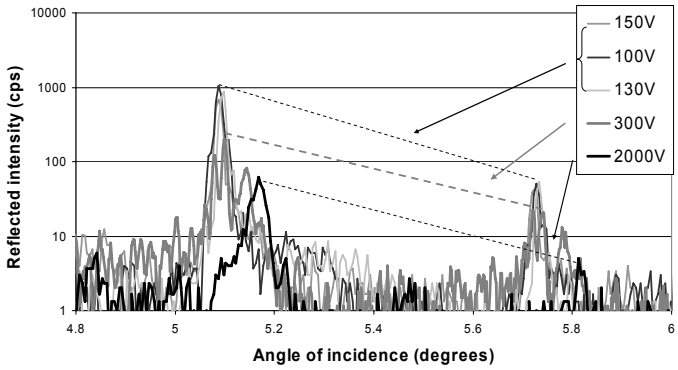

Figure 14. GIXR measurements for different ion energies applied after Si deposition for removing 0.5 nm of material. The reflected intensity decreases with ion energy, indicating an increase of the roughness.

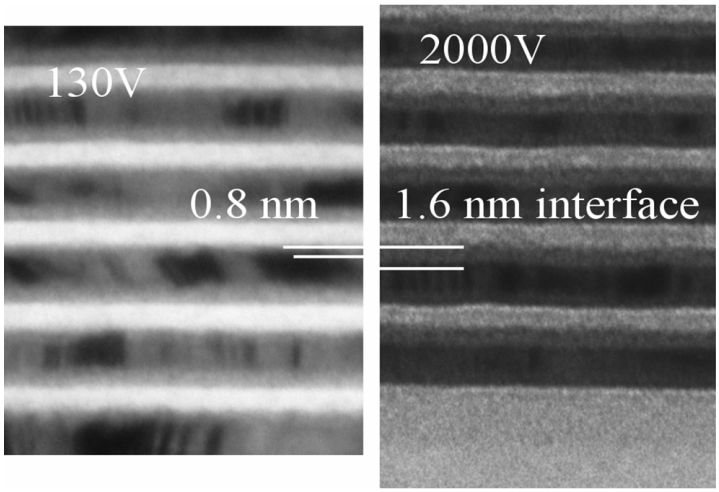

Figure 15. Cross sectional bright field TEM image of two Mo/Si multilayer, smoothened using Kr ions of 130 eV and 2000 eV. The Si-on-Mo interface thickness is increasing from 0.8 nm to 1.6 nm towards high energy.

These results are confirmed by TRIM calculations. A more detailed analysis of the TEM line profiles clearly shows Mo, Si and separate Mo_xSi_y phases present in the multilayer. The TEM intensity profile was converted to a density profile by iteratively changing the density scale, calculating the corresponding Cu-K reflectivity, and comparison with experimental results. From the resulting density profile, the Si-on-Mo interface was identified as $MoSi_2$ [10]. The presence of a low formation enthalpy compound can be explained by the additional energy that is provided by 2000 eV ions during deposition. At lower ion energies, or without bombardment (Mo-on-Si), Mo_3Si is formed at the interfaces [2]. From TEM it is estimated that the roughness increases from 0.45 nm at 130 eV to 0.9 nm at 2000 eV. Reflectivity simulations show that this increase would result in a 5 % lower reflectivity. Simulations also show that by increasing the silicide at the Si-on-Mo interface from 0.8 nm Mo_3Si to 1.6 nm $MoSi_2$, the reflectivity should decrease by another 3%. Combined, both effects explain the experimentally observed 8 % reflectivity decrease of the 2000 eV treated multilayer samples.

2.4.2. Roughness dependence as a function of the Mo ratio

Due to the direct influence of the Mo ratio Γ on the intensity of Bragg peaks and EUV reflectivity, it is complicated to evaluate interface roughness for different Mo ratios from changes in reflectivities alone. As an alternative, roughness can be estimated from diffuse X-ray scattering experiments [11]. Figure 16 shows diffuse X-ray scattering from Mo/Si high reflectance multilayers (HRML) with Mo ratio of 0.4, and stress compensation multilayers (SCML) with Mo ratio of 0.7, as well as a combined stack of Γ = 0.4 and Γ = 0.7, for a fixed amount of 0.5 nm Si removal after each deposited layer. The increased diffuse scattering indicates increased roughness for higher Mo ratios. This is confirmed by TEM analysis of the combined multilayer, where the average top-valley roughness was found to be lower for Γ = 0.4 than for Γ = 0.7. It is apparent that for thick Mo layers, surface ion treatment of Si does not suffice to completely smoothen the additional roughness that builds up due to low adatom mobility during the growth of crystalline Mo grains [2]. If this additional roughness that builds up during deposition of a high Mo ratio multilayer can not be smoothened during deposition of a subsequent low Mo ratio multilayer, this could negatively affect EUV reflective elements, where underlying high Mo ratio multilayers are used for stress compensation purposes [6].

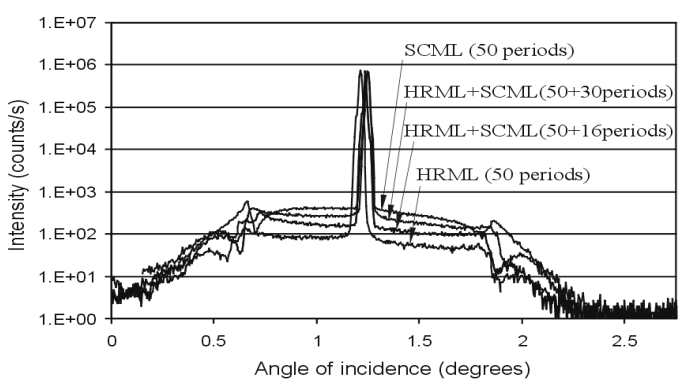

Figure 16. Diffuse scattering from single and combined Mo/Si multilayers with Γ = 0.4 and Γ = 0.7. The increased intensity indicates that the roughness increases with the Mo amount per period.

From Figure 16 it can be shown that the off-specular scattering from combinations of high reflectance multilayers (Γ = 0.4) and stress compensation multilayers (Γ = 0.7) with different numbers of periods is given by the weighted average of the contributing multilayers. This fact shows that the top multilayer does not have increased roughness, compared to the case when it was deposited directly on a substrate. This suggests that the additional roughness that develops during high Mo ratio multilayer deposition is efficiently smoothened during the first part of the low Mo ratio multilayer growth. The recovery of the in-situ X-ray reflectivity signal during deposition of the first periods of low Mo ratio multilayer confirms this process.

To further investigate the smoothening process after layer deposition, multilayers were prepared with different amounts of Si removal, at a fixed ion energy of 130 eV. The removed amount of Si was controlled by the X-ray in-situ system, calibrated by quartz mass balances. From the diffuse scattering curves presented in Figure 17 (Mo ratio 0.7), a threshold value for Si removal is observed below which ion smoothening does not suffice to prevent build-up of interface roughness. Figure 18 shows the roughness increase as a function of the amount of removed material, calculated from changes in the diffuse scattering patterns for Mo ratios 0.4 and 0.7.

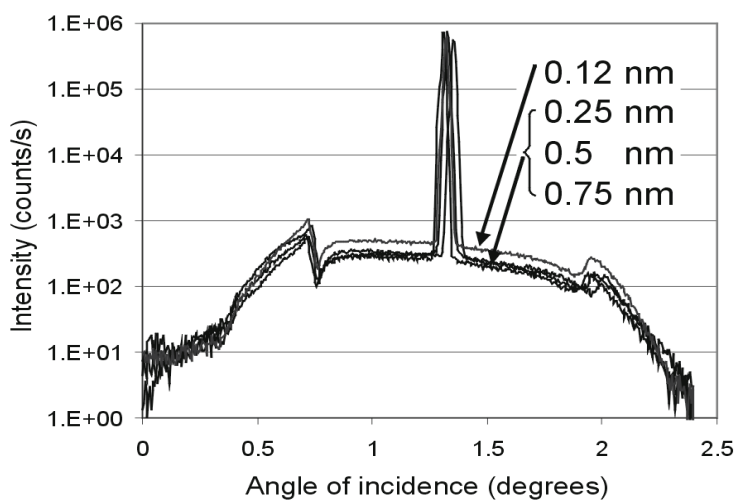

Figure 17. Diffuse scattering from a Mo/Si multilayer with Γ = 0.7 for different amounts removed of Si. The scattered intensity is significantly higher when 25 % of the standard 0.5 nm Si amount is removed.

The presence of such a threshold could be explained by a roughness development model where only the top surface builds up roughness, and can be efficiently smoothened using 130 eV ions, while additional roughness/intermixing below this surface cannot be smoothened but does contribute to diffuse scattering. This interpretation is confirmed by the presence of the same threshold for both low and high roughness (low and high Mo ratio) multilayers. The dependence of the smoothening threshold on the ion energy is currently under investigation.

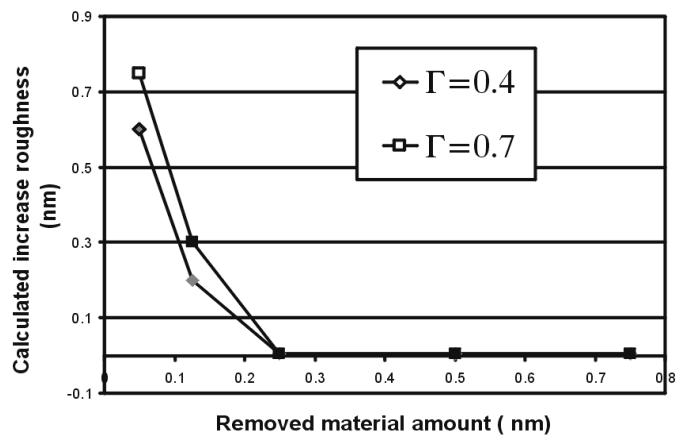

Figure 18. Calculated roughness increase as a function of the removed amount of Si for multilayers with $\Gamma = 0.4$ and $\Gamma = 0.7$. In both cases the roughness increases when the amount of removed material is smaller than 0.25 nm.

2.5. SUMMARY AND CONCLUSIONS

We investigated the interface roughness of Mo/Si multilayers as a function of ion treatment during and after Si layer deposition. Ion smoothening during layer deposition works efficiently when applied at low energies and during the latter part of the layer deposition. For higher energies and/or additional treatment of the initial part of Si, the smoothening process becomes more efficient. However, it was found that in those cases additional intermixing will occur at buried interfaces. For low energy ions applied after layer deposition, the roughness increases with increasing Mo ratio, a process which may be correlated to the crystalline Mo layer growth. Independent of the absolute

roughness value (Mo ratio), smoothening of the Si surface prevents build-up of roughness, as long as a minimal surface treatment process is performed. Furthermore, under high ion energy bombardment, the Si-on-Mo interface stoichiometry changes from Mo_3Si to $MoSi_2$. Model simulations that take into account all changes in interface widths, stoichiometry and roughness are shown to accurately explain the observed reflectivity changes at 13.5 nm wavelength.

2.6. ACKNOWLEDGMENTS

This work is carried out in the frame of FOM research programme I10/XMO, the Industrial Partnership Programme 'eXtreme UV Multilayer Optics' carried out under contract with Carl Zeiss SMT AG, Oberkochen, and the 'Stichting voor Fundamenteel Onderzoek der Materie (FOM)'. The latter is financially supported by the 'Nederlandse Organisatie voor Wetenschappelijk Onderzoek (NWO)'. The HRTEM measurements were performed at Delft University of Technology. The EUV reflectivity was measured at the Physikalisch-Technische Bundesanstalt (PTB) using the electron storage ring BESSY II, Berlin, Germany.

2.7. REFERENCES

1. E. Spiller, D. Stearns, and M. Krumrey, "Multilayer x-ray mirrors: interfacial roughness, scattering, and image quality", Journal of Applied Physics **74** (1), pp. 107- 118 (1993)

2. R.W.E van de Kruijs, E. Zoethout, A.E. Yakshin, I. Nedelcu, E. Louis, F. Tichelaar, H. Enkisch, G. Sipos, S. Müllender, F. Bijkerk, "Nano-size crystallites in Mo/Si multilayers optics", Thin Solid Films **515** (2), pp. 430-433 (2006)

3. E. Louis, H.-J. Voorma, N.B. Koster, F. Bijkerk, Yu.Ya. Platonov, S.Yu. Zuev, S.S. Andreev, E.A. Shamov, N.N. Salashchenko, "Multilayer coated reflective

optics for extreme UV lithography", Microelectronic Engineering **27**, pp. 235-238 (1995)

4. E. J. Puik, M.J. van der Wiel, H. Zeijlemaker and J. Verhoeven, "Ion-bombardment of thin-layers - the effect on the interface roughness and its x-ray reflectivity", Review of Scientific Instruments **63** (1), pp. 1415-1419 (1992)

5. D.K. Brice, J.Y. Tsao and S.T. Picraux, "Partitioning of ion-induced surface and bulk displacements", Nuclear Instruments & Methods in Physics Research Section B-Beam Interactions with Materials and Atoms, **44 (3)**, pp. 68-78 (1989)

6. E. Zoethout, G. Sipos, R. van de Kruijs, A. Yakshin, E. Louis, S. Müllender, F. Bijkerk, "Stress mitigation in Mo/Si multilayers for EUV lithography", Proceedings SPIE **5037**-106, Santa Clara (2003)

7. H. J. Voorma, E. Louis, F. Bijkerk and S. Abdali, "Angular and energy dependence of ion bombardment of Mo/Si multilayers", Journal of Applied Physics, **82** (4), pp. 1876-1881, (1997)

8. IMD, version 4.1.1, written by David L. Windt, (2000)

9. A.E. Yakshin, E. Louis, P.C. Gőrts, E.L.G. Maas and F. Bijkerk, "Determination of the layered structure in Mo/Si multilayers by grazing incidence X-ray reflectometry", Physica B, **283**, pp. 134-148 (2000)

10. M.J.H. Kessels, J. Verhoeven, A.E. Yakshin, F.D. Tichelaar and F. Bijkerk, "Ion beam induced intermixing of interface structures in W/Si multilayers", Nuclear Instruments & Methods in Physics Research Section B-Beam Interactions with Materials and Atoms, **222** (3-4), pp. 484-490, (2004)

11. D. E. Savage, J. Kleiner, N. Schimke, Y. H. Phang, T. Jankowski, J. Jacobs, R. Kariotis and M. G. Lagally, "Determination of roughness correlations in multilayer films for x-ray mirrors", Journal of Applied Physics, **69**, 3, pp. 1411-1424 (1991)

3. Temperature dependent nano-crystal formation in Mo/Si multilayers

3.1. ABSTRACT

We investigated the nano-crystallinity of Mo/Si multilayers as a function of Mo:Si ratio in the period using grazing incidence and wide angle X-ray diffraction, both for as-deposited samples and after thermal annealing up to 800 ºC under UHV conditions. The research was performed on EUV multilayers with period thickness of approximately 7 nm. The as-deposited multilayer nanostructure was found to depend on the Mo to Si layer thickness ratio. For intermediate Mo fractions in the multilayer period, a four layer system is formed, with amorphous Si and polycrystalline Mo layers separated by silicide interfaces, while for low and high Mo fractions a two component system is formed, respectively consisting of a pure Mo layer (in the case of a high Mo fraction) or pure Si layer (low Mo fraction) separated by a single silicide interface. Using the crystallographic properties of the multilayer during annealing, we describe the continuous development of the multilayer structure and growth of the silicide interfaces. Our study has led to an explanatory model which is based on the total free energy minimization of the multilayer system. Finally, a phase transition to a crystalline silicide is observed at $T > 300$ ºC. This phase transition can also explained by minimization of the total free energy.

3.2. INTRODUCTION

For next generation Extreme Ultra Violet Lithography (EUVL) systems [1], Mo/Si multilayers will be used as reflective coatings for different optics. To achieve a high multilayer reflectivity, a good optical contrast of the materials can be obtained if the Mo/Si interfaces are abrupt after multilayer deposition.

It is generally known that the layer interfaces in Mo/Si multilayers are not abrupt, since intermixing and/or compound formation occurs. These naturally formed interfaces are typically several atomic layers thick and reduce the optical contrast between Mo and Si and decrease the reflectivity. Furthermore, intermixing continues at increased temperatures, an effect that can easily occur at the high EUV illumination powers that are foreseen for EUVL at so-called HVM (high volume manufacturing) conditions in the ultimate industrial lithography process. In addition, a non-homogeneous distribution of temperatures will result in non-homogeneous changes in the layered structure, creating e.g. optical path differences which reduce the image quality. Although it has been shown that diffusion barriers can suppress the intermixing and compound formation [2], a full understanding of the as-deposited layered structure and its behaviour at enhanced temperatures is required for proper choice of barrier layer materials and thicknesses.

In this paper we study the Mo/Si multilayer composition as a function of the annealing temperature in order to reveal their nano-structural composition. The Mo fraction in the multilayer is varied from a low value (application e.g. for narrow band EUV diagnostics [3]) through intermediate value (application for high reflectance EUV optics) to high value (application e.g. for stress-compensation layers in EUV optics or broad band multilayer reflectors [4]). Besides being interesting from the application point of view, such a systematic study of the multilayer structure as a function of the Mo fraction enables more detailed understanding of the multilayer composition and structure, including its interfacial layers. For low and high Mo fractions, the layered structure and interface composition has been uniquely determined in our study by grazing incidence X-ray reflectivity (GIXR) measurements. In addition, GIXR was used to determine the evolution of the multilayer period, yielding information on the process of interface silicide formation. The change of crystallographic parameters during annealing was characterized by wide angle X-ray diffraction (WAXRD) and compared with the layered structures obtained by GIXR. Based on these measurements, a model is developed that

explains the silicide formation during annealing by the availability of bulk material components and a tendency of the multilayer system to minimize its free energy. This behaviour has only become obvious in this study by systematically investigating all Mo fraction ranges.

3.3. EXPERIMENTAL

Multilayers, consisting of 50 bilayers of Mo and Si were deposited by UHV electron-beam evaporation onto 25×25 mm^2 super polished silicon substrates. A series of multilayers with a period thickness of 6.9 nm was produced for a large range (between 0.1 and 0.8) of the Mo fraction, defined by $\Gamma = d_{Mo}/(d_{Mo}+d_{Si})$, where d_{Mo} and d_{Si} are the thicknesses of molybdenum and silicon, respectively. The base pressure during deposition was better than 2×10^{-8} mbar, the deposition system being described elsewhere [5]. Kr ions were applied during layer growth to suppress roughness development within the multilayer. As a result of this, a reflectivity of 69 % is routinely achieved at 13.5 nm at near-normal incidence [4,6], with a best value [3] of over 70%.

The multilayers were successively annealed for 48 h from 20 °C to 800 °C using a halogen lamp in a vacuum chamber (base pressure 10^{-7} mbar) and analyzed by grazing incidence X-ray (GIXR) and wide angle X-ray diffraction (WAXRD) with a Philips X'Pert double crystal X-ray diffractometer using Cu-K_α line radiation (0.154 nm). During the WAXRD measurements, the sample was rotated by φ = 20° in the sample plane to suppress the diffraction peak from the mono-crystalline substrate and aligned with the incident beam at a fixed angle of ω = 1° to maximize the illuminated area and thereby the diffracted intensity. The Mo, Si and Mo_xSi_y patterns have been identified using reference spectra from the ICCD database [7]. Reference multilayers were annealed both in successive runs at increasingly higher temperatures, as well as directly to the highest temperature to check if there is any effect of annealing history. No significant difference was observed between the two methods, and only successively annealed samples will be reported on here. Transmission Electron Microscopy (TEM) was used in both bright field mode (Philips CM30T) and lattice imaging mode (Philips CM300UT-FEG) at 300 kV. Specimens for TEM were prepared by Ar ion milling of multilayer cross sections glued on a copper grid.

3.4. EXPERIMENTAL RESULTS AND DISCUSSION

3.4.1. Nano-crystallinity of as-deposited multilayers

In this section, the spontaneous formation of Mo silicides in multilayers just upon deposition is discussed, as a function of Γ with Γ in the range 0.1 - 0.8. For multilayers with $\Gamma < 0.33$, the entire Mo-layer is found to be converted into silicide in a reaction with Si so that the multilayer period consists of two layers. For $\Gamma > 0.33$ only a part of the Mo is consumed in that reaction to form four layers: pure Mo and Si layers, and two silicide interlayers between the pure components.

Figure 19a shows XRD curves from multilayers with $\Gamma = 0.1$ and $\Gamma = 0.28$ representative for the range $\Gamma < 0.33$. The crystallographic pattern is identified as cubic Mo_3Si [7,8]. The diffraction peaks are presented in Table 3. This is in contrast with previously published results [9,10], showing the formation of an amorphous interlayer which was suggested to be $MoSi_2$. The formation of Mo_3Si instead of $MoSi_2$, as reported here, could be connected to the deposition method used. In the case of the here applied deposition technique of electron beam evaporation, the energy of the particles is in the order of 0.1 eV, while for sputter deposition it is in the range of 1-10 eV and higher. Other parameters, like the quality of the vacuum could also influence the spontaneous formation of silicides after deposition. Experiments to determine the exact contribution of different parameters to different silicides after deposition are presently carried out.

Figure 19b shows an XRD spectrum from a multilayer with $\Gamma = 0.4$, representative for samples in the range 0.33 - 0.8, the pattern being characteristic for a Mo (bcc) polycrystalline structure. This is in agreement with previously published results for multilayers deposited by magnetron sputtering [2, 9,10,11].

Concerning the composition of the interlayers, Braun et al [11] suggested the formation of amorphous $MoSi_2$ at both interfaces based on its low enthalpy of formation. In our earlier studies of multilayers deposited by electron beam deposition, simulations of the GIXR reflectivity indicated that the interlayer stoichiometry depends on the energy of the Kr ions [12] applied after each Si layer to smoothen the surface. For example, for multilayers with $\Gamma = 0.4$ and an ion energy of 300 eV, a combination of two silicides, Mo_5Si_3 and $MoSi_2$, occurred, while for an ion energy of 2 keV only one silicide, namely

$MoSi_2$, was found at both interfaces. These results are in agreement with a TRIM calculation [13] which shows that 2 keV Kr ions can penetrate the entire Si layer (of 4.5 nm) and reach the buried Si-on-Mo interface, while 300 eV Kr ions can penetrate only the top 1.5 nm of the Si layer being ion polished.

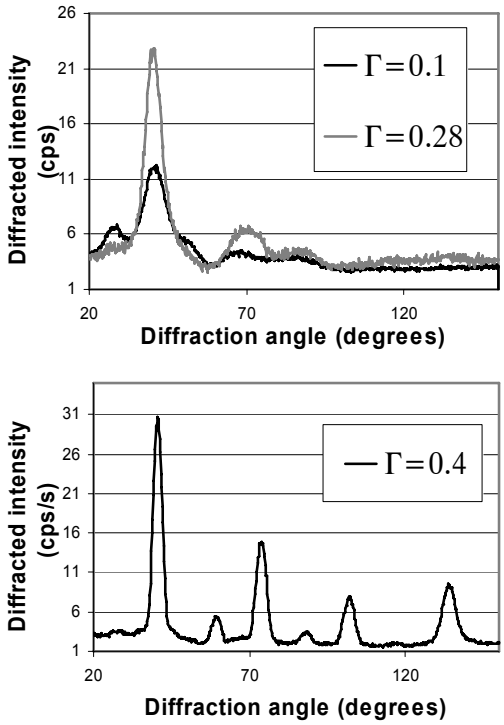

Figure 19. For $\Gamma < 0.33$ (a), a polycrystalline Mo_3Si diffraction pattern is observed. The high background at high Γ indicates amorphous Mo or Mo_XSi_Y growth. All the diffraction peaks are presented in Table 3. Wide angle X-ray diffraction data for $\Gamma = 0.4$ (b) indicates a typical polycrystalline bcc Mo structure, which is observed for all $\Gamma > 0.33$.

Structure name	hkl	Diffraction angle (degrees)	Normalized diffracted intensity	Structure name	hkl	Diffraction angle (degrees)	Normalized diffracted intensity
Mo	110	40.5	1	*c*-Mo_3Si	110	25.70	0.24
	200	58.61	0.19		210	41.18	1
	211	73.67	0.43		211	45.32	0.31
	220	98.62	0.15		222	66.03	0.12
	310	101.42	0.24		320	69.11	0.17
	222	115.96	0.07		321	72.16	0.27
	321	132.64	0.43		420	89.41	0.03
h-$MoSi_2$	101	26.43	0.5	*t*-$MoSi_2$	002	22.54	0.39
	111	41.6	1		101	29.93	0.66
	112	48.32	0.4		110	39.52	0.75
	211	63.29	0.2		103	44.45	1
	114	70.72	0.16		112	45.97	0.2
	301	72.8	0.16		200	57.13	0.2
	115	85.2	0.1		202	62.2	0.09
	223	98.47	0.2		211	65.83	0.1
	403	116.67	0.04		006	71.79	0.04
	411	126.98	0.12		213	75.13	0.29
	223	132.67	0.3		116	85.19	0.1
t-Mo_5Si_3	200	18.37	0.02				
	220	26.08	0.05				
	211	27.49	0.25				
	002	36.54	0.25				
	321	38.25	0.71				
	202	41.18	0.38				
	420	41.83	0.59				
	411	42.76	1				
	222	45.45	0.57				
	521	54.46	0.08				
	323	66.92	0.18				
	631	67.84	0.12				
	710	68.75	0.17				
	602	69.86	0.24				
	413	70.07	0.33				
	642	81.92	0.11				
	660	85.3	0.08				
	732	86.34	0.04				

Table 3. The diffraction peaks of Mo and Mo silicides used to identify the diffraction spectra.

We have analysed the crystallite size (both Mo and Mo_3Si) in the growth direction for $\Gamma = 0 - 0.28$ (Mo_3Si crystallites) and $\Gamma = 0.33 - 1$ (Mo crystallites). This size, shown in Figure 20, was determined from the width of the (110) diffraction peak (present in both Mo and Mo_3Si diffraction patterns), using Scherrer's formula [14],

$$X = \frac{0.94\lambda}{L\cos(\theta)} \quad , \qquad (4)$$

where $\lambda = 0.154$ nm, L is the full width at half maximum determined for every peak in the spectrum, and 2θ is the diffraction angle between the source and the detector. Since the diffracting planes giving rise to the (110) peak are oriented like the film plane (offset by 20°), the crystallite size in the film growth direction can be easily calculated by correcting for this offset angle. For comparison, the solid grey line in Figure 20 indicates the deposited amount of Mo, while the dashed line indicates the thickness of the pure part of the Mo, i.e. after consumption of a part of the Mo for the formation of silicide interlayers at the Si interfaces. It is directly apparent that there are two regions of crystallite formation, with full crystallisation occurring only for $\Gamma > 0.33$.

Shown in Figure 20 is the expected crystallite size of Mo_3Si for $\Gamma = 0.1 - 0.28$, based on calculations assuming that all deposited Mo forms crystalline Mo_3Si (dotted line). However, our experimental data shows that the increase in Mo_3Si crystallite size as a function of Γ is much smaller than these calculated values. This suggests that Mo_3Si grows crystalline only initially up to 1.5 nm while at larger thicknesses only amorphous growth of Mo or Mo-silicide occurs. This could be caused by the formation of crystalline Mo or Mo_3Si as a function of the as deposited Mo thickness when the Mo layer is covered by the next Si layer. This will be discussed in detail in reference 15.

In contrast with low Γ systems, for $\Gamma > 0.33$, corresponding to Mo amounts larger than 2.3 nm, the crystalline size in the growth direction seems to be comparable to the as deposited Mo layer thickness. The figure thus shows an abrupt onset of Mo crystallization above a Mo thickness of ~2.3 nm, in agreement with earlier data [9,10]. Since formation of interfaces directly after deposition will reduce the Mo amount available for crystallization (dashed curve in Figure 20) the observed crystallite size suggests that the Mo nano-crystals extend beyond the thickness of the pure Mo layer. It should however be noted that the Scherrer formula might not be fully correct to determine the size of our nano-sized crystals. We have therefore also performed ab-initio full pattern X-ray diffraction simulations for nano-sized crystallites [16]. By comparing these calculated spectra to the XRD data, we find crystal sizes which are slightly smaller

than the pure Mo thickness, a result which would leave space for the assumption of amorphous interfaces. High-resolution transmission electron microscopy also suggests that both Mo-Si interfaces are amorphous, although this technique may not detect sub-nanometer crystallites. More detailed simulations, as well as TEM studies (EDS and EELS), are being carried out to properly investigate size effects of nano-sized crystallites, and distinguish between the presence of crystalline and amorphous interfaces.

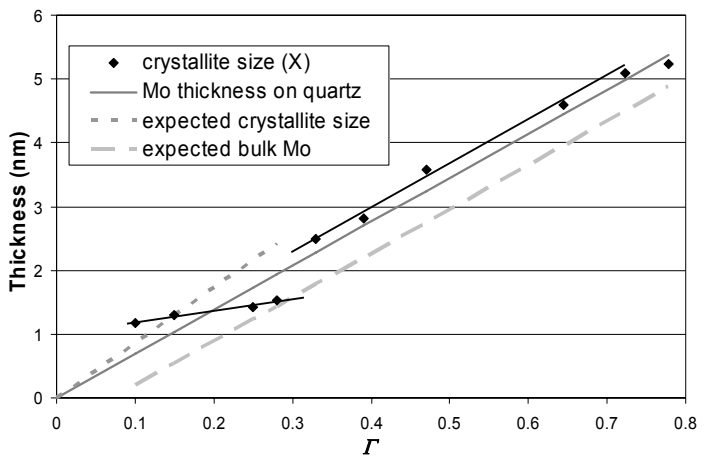

Figure 20. Crystallite size in the growth direction as a function of Mo fraction, compared to deposited Mo thickness on quartz. For $\Gamma < 0.33$, a crystalline Mo_3Si interface is initially formed, with predominantly amorphous growth of added Mo. For $\Gamma > 0.33$ the crystallite size of the period is comparable to the deposited Mo, suggesting (partly) crystalline silicide interfaces. The absence of any silicide peaks actually suggests amorphous interface growth.

3.4.2. Multilayer structure at enhanced temperatures

We will discuss the multilayer behaviour upon thermal treatment as a function of Γ. We have subdivided our temperature range based on major changes in the composition of multilayers considering the h-$MoSi_2$ crystallization for $T > 300$ °C. Table 4 presents the silicide composition for multilayers with $\Gamma = 0.1$ - 0.8 in all temperature ranges.

<table>
<tr><th></th><th>0.1 – 0.28</th><th>0.33 – 0.35</th><th>0.4 - 0.5</th><th>0.6 – 0.65</th><th>0.7</th><th>0.8</th></tr>
<tr><td>T = 20 °C</td><td>Crystalline Mo_3Si</td><td colspan="4">Amorphous silicides (Mo_5Si_3 + $MoSi_2$)*</td><td>Amorphous $MoSi_2$</td></tr>
<tr><td>T = 300 °C</td><td>Crystalline Mo_3Si</td><td colspan="4">Amorphous silicides (Mo_5Si_3 + $MoSi_2$)* + Amorphous $MoSi_2$</td><td>Amorphous $MoSi_2$</td></tr>
<tr><td>T = 400 °C</td><td colspan="3">Crystalline h – $MoSi_2$</td><td colspan="2">Amorphous Mo_5Si_3</td><td>Amorphous silicide**</td></tr>
<tr><td>T = 800 °C</td><td colspan="2">Crystalline t – $MoSi_2$</td><td colspan="2">Crystalline Mo_5Si_3</td><td colspan="2">Crystalline Mo_3Si</td></tr>
</table>

* Amorphous silicides in the range Γ = 0.33 - 0.7 before annealing have been suggested in an earlier study [12] to be a mixture of two silicides Mo_5Si_3 and $MoSi_2$. We also suggest that apart of these initial silicides, additional amorphous $MoSi_2$ is grown upon annealing at T = 300 °C.

** The nature of amorphous silicide for Γ = 0.8 at T = 400 °C could not be uniquely identified.

Table 4. Overview of silicide formation before and after annealing at 800 °C, as a function of the Mo fraction. Note, that "amorphous silicides" in the range Γ = 0.33 - 0.7 before annealing have been suggested in an earlier study [12] to be a mixture of two silicides Mo_5Si_3 and $MoSi_2$. We also suggest that this part does not change at T = 300 °C, with additional amorphous $MoSi_2$ being grown upon annealing. The crystallographic structure of "amorphous silicide" for Γ = 0.8 at T = 400 °C could not be uniquely identified.

Figure 21 shows an overview of the multilayer crystallinity as a function of the Mo fraction (Γ = 0.1, 0.35, 0.65, 0.8) for different temperatures (20 °C, 300 °C, 400 °C and 800 °C). The spectra corresponding to all these temperatures are presented in the same graph for a better comparison, for each Mo fraction, by applying the same offset. For temperatures up to 400°C it is convenient to distinguish three different types of multilayer structures: low Γ (0.1 - 0.28), intermediate Γ (0.33 - 0.78) and high Γ (0.8). All the crystallographic structures of Mo and Mo silicides from this article were identified using reference powder diffraction spectra [7], for the diffraction spectra displayed in Figure 19 and Figure 21 and listed in Table 3. Note that the crystallographic spectrum of Mo_3Si for Γ = 0.8 at T = 800°C from Table 4 was identified as a mixture of Mo and Mo_3Si.

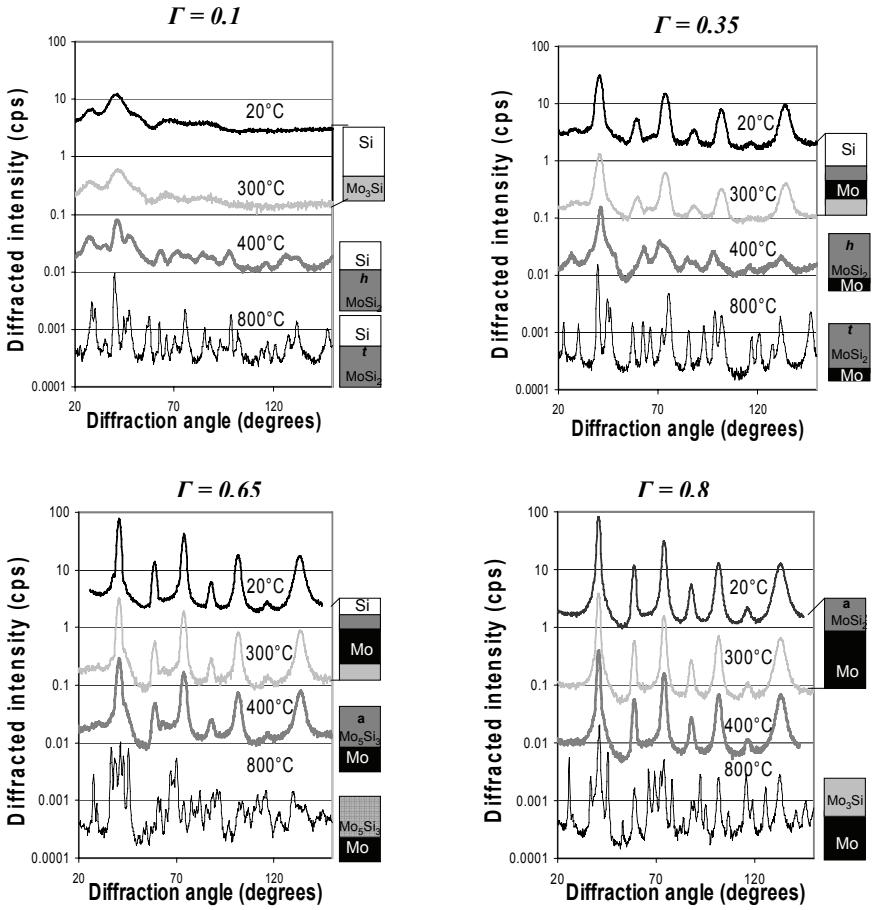

Figure 21. Overview of wide angle X-ray diffraction data as a function of temperature (a). The spectra corresponding to all these temperatures are presented in the same graph for a better comparison, for each Mo fraction, by applying the same offset. For $\Gamma < 0.33$, Mo_3Si shows a phase transformation to $MoSi_2$ at 400 °C. For $\Gamma = 0.35$ a slow decrease of the Mo crystallite size (growth of the Mo_XSi_Y interfaces) is followed by a phase transformation to *h*-$MoSi_2$ (b). For $\Gamma = 0.65$ only a slow decrease of Mo crystallite size occurs up to 400 °C suggesting amorphous silicide formation, but no change in the multilayer crystallographic structure. For $\Gamma = 0.8$, there is no phase transformation of the bulk Mo nor of the amorphous silicide formed after deposition. Formation of different crystalline silicides occurs at 800°C for the investigated multilayers with $\Gamma = 0.35$, 0.65 and 0.8, respectively.

3.4.2.1. State up to h-$MoSi_2$ crystallization (T = 20 - 300°C)

Annealing up 300 °C shows the following processes as a function of the Mo fraction. For the multilayers with Γ = 0.1 - 0.28, the initial microcrystalline structure formed at room temperature does not change. For Γ = 0.33 - 0.78 a gradual decrease of peak intensities and increase of peak widths is observed indicating a decreasing Mo crystallite size. This would suggest a gradual growth of the amorphous silicide interfaces upon annealing. This result is confirmed by TEM measurements, where the Mo-on-Si interface did increase upon annealing, with the amount of additional silicide formed being equal to the consumed Si amount (though the thickness of the Si-on-Mo interface did not change). The only compound that would show this behaviour is $MoSi_2$ based on the molecular volumes calculated from bulk atomic masses (A) and tabulated density values (ρ) for each of the compounds [17] (see Table 5).

	A [g/mol]	ρ [g/cm^3]	V [cm^3/mol]	V_{Mo} [cm^3/mol]	V_{Si} [cm^3/mol]	V_{Mo}/ $V_{silicide}$	V_{Si}/ $V_{silicide}$	$\Gamma_{stoichiometric}$ V_{Mo}/ (V_{Mo}+V_{Si})
Mo	95.9	10.2	9.40					
Si	28.08	2.3	12.21					
Mo_3Si	315.78	8.97	35.21	28.21	12.21	0.80	0.35	0.70
Mo_5Si_3	563.74	8.2	68.75	47.01	36.63	0.68	0.53	0.56
$MoSi_2$	152.06	6.24	24.37	9.401	24.42	0.39	1.00	0.28

Table 5. Molecular volumes of Mo and Si calculated from bulk atomic masses (A) and tabulated density values (ρ) existing in all MoxSiy compounds are used to calculate $\Gamma_{stoichiometric}$ which is the Mo fraction corresponding to the silicide formation by total consumption of bulk components.

It is shown in Table 5 that 1 nm Si and 0.4 nm Mo is consumed while forming 1 nm of $MoSi_2$, and therefore the maximum amount of $MoSi_2$ will be formed for $\Gamma_{stoichiometric}$ = 0.28. For Γ = 0.8, the WAXRD patterns are identical for all temperatures up to and including 400 °C. It is difficult to obtain information about the crystallinity of interfaces because the crystalline Mo is occupying around 80 vol% of the period and

dominates the WAXRD spectra. However, no change of the diffraction pattern upon annealing would suggest no crystallization of the compound formed during deposition. The GIXR measurements on as deposited multilayers were uniquely fitted with a two layer system consisting of Mo/$MoSi_2$, which suggests that amorphous $MoSi_2$ is formed directly after deposition e.g. as a result of Kr ions penetration through the entire 1.5 nm Si layer, in agreement with TRIM calculation [13].

3.4.2.2. State after h-$MoSi_2$ crystallization (T = 300 – 400 °C)

Annealing in the range 300 °C to 400 °C shows more pronounced processes. A clear phase transformation occurs for Γ = 0.1 - 0.5. For Γ = 0.1 - 0.28 the crystallographic pattern of Mo_3Si transforms into *h*-$MoSi_2$. For Γ = 0.33 - 0.5 the crystallographic pattern of *h*-$MoSi_2$ also appears. The formation of *h*-$MoSi_2$, which was also previously reported [18], could be linked to crystallization of the silicide interlayers [9, 18,19,20]. For Γ = 0.6 – 0.78 the small decrease of Mo crystallite size observed in the range 20 – 300 °C continues up to 400 °C suggesting continuous amorphous silicide interface formation without exhibiting the phase transformation to *h*-$MoSi_2$. The silicides formed can not be identified from the diffraction pattern because they do not appear in the crystalline phase [19]. To determine the silicide formed upon annealing, we investigate the period compaction upon annealing as a function of the period thickness for three samples with Γ = 0.6 in the period range 5 - 10.3 nm. Figure 22 shows the measured period compaction d - d_0, as a function of the initial d-spacing, where d_0 and d are the multilayer period directly after deposition and after annealing at 400 °C, as determined from Bragg's law,

$$m\lambda = 2d\sin\theta\sqrt{1-\frac{2\delta}{\sin^2\theta}}\,, \qquad (6)$$

where m = 1,2,3,…, δ = 1- n is the real part of the refractive index, λ = 0.154 nm is the Cu-K_α wavelength and θ is the angle between the incident X-ray beam and the multilayer surface.

Figure 22 shows experimentally measured data (open points) and the calculated period compaction, assuming a full transformation of all available Mo and Si into three different silicides: either Mo_3Si, Mo_5Si_3 or $MoSi_2$ (solid lines). Best match of the calculations to the experimental data is clearly obtained for Mo_5Si_3. Formation of silicides in case of Γ = 0.8 could not be uniquely identified because within the

experimental errors no significant changes were observed in the multilayer structure (Figure 19).

Figure 23 displays a summary of the crystallite size in the growth direction determined from the width of the (110) diffraction peak for both Mo and *h*-$MoSi_2$ as a function of the annealing temperature up to 400 °C for all investigated Mo fractions. In the temperature range 150 – 300 °C, only a small decrease in crystallite size for all range of Γ occurs, suggesting no change in the multilayer nanocrystallinity. For Γ = 0.1 - 0.5 at temperatures higher than 300 °C the crystallite size in the growth direction increases significantly (Figure 23a). This increase is proportional to the available Mo amount, with a maximum at $\Gamma_{stoichiometric}$ = 0.28, due to the full consumption of all available Mo and Si into $MoSi_2$ as shown in Table 5. For a Mo fraction higher than 0.28, less $MoSi_2$ is formed due to a deficiency of Si in the multilayer period, and the increase in crystallite size is therefore smaller. For Γ = 0.6 - 0.8 the crystallite size is actually decreasing (Figure 23b). This is caused by a decrease in Mo crystallite size as a result of continuing silicide formation. Note that the silicide formed does not show up at the diffraction pattern being amorphous.

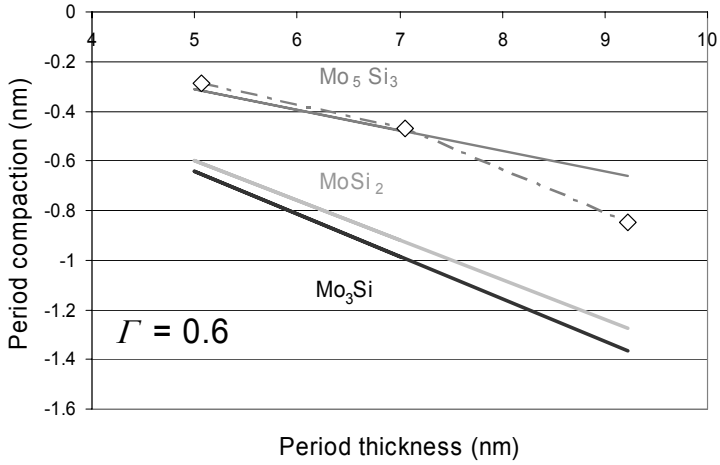

Figure 22. Period compaction after annealing at 400 °C as a function of period thickness. Calculations of the expected period compaction show a best fit to the experimental data for a transition to Mo_5Si_3.

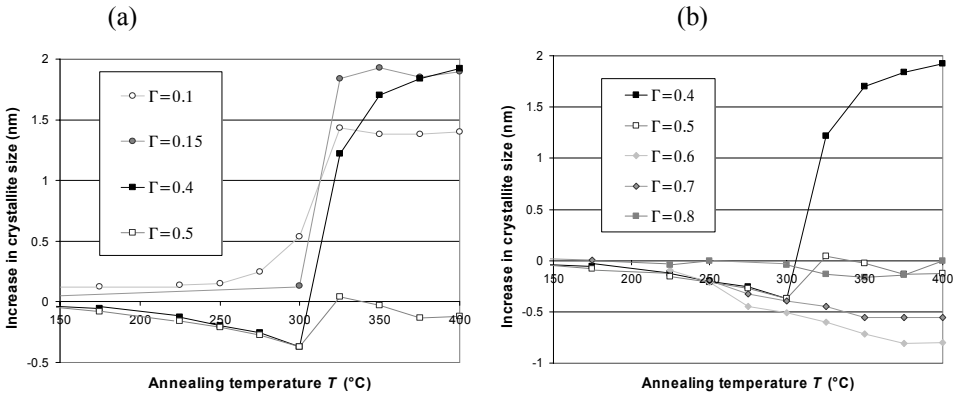

Figure 23. Change of crystallite size in the growth direction as a function of annealing temperature for multilayers with Γ in the range 0.1 – 0.8. A sudden crystallization of is observed for temperatures higher than 300 °C only for multilayers with Γ in the range 0.1 – 0.5. Note that the data for $\Gamma = 0.4$ is shown in both figures as a reference.

3.4.2.3. Quasi - equilibrium state (T = 800 °C)

Annealing at 800 °C is accompanied by strong diffusion processes in which all available material has reacted. This leads to formation of new silicides in the crystalline phase. In Figure 19a different crystalline silicides are identified using references from powder diffraction files of *t*-$MoSi_2$ (Γ = 0.1, 0.35), Mo_5Si_3 (Γ = 0.65) and Mo_3Si (Γ = 0.8), respectively. If the formation of these silicides occurs according to Table 5, this should lead to two types of two-layer systems: silicide/Si (Γ = 0.1) and silicide/Mo (Γ = 0.35, 0.65, 0.8), depending on the available material. Indeed, after annealing the presence of Si (Γ = 0.1) and Mo (Γ = 0.8) besides the silicides was clearly identified.

Using Eq.(4), crystallite sizes of 20-30 nm are calculated, showing that crystals are penetrating through 3 - 4 periods. This is confirmed by GIXR measurements which show that the periodic nature of the multilayer is severely affected. The silicide formation before and after annealing at 400 °C and 800 °C is summarized in Table 4 as a function of Γ. Interpretation of the process of compound formation at high temperatures is discussed in the next section.

3.4.3. Model of silicide formation at enhanced temperatures

To understand the formation of Mo silicides upon annealing, here we present a thermodynamic model based on calculation of the most favourable energetic state of the annealed multilayer considering the available amounts of Mo and Si. The free energy due to the formation of a silicide was calculated as $\Delta H*m$, where ΔH is the enthalpy as listed in Table 6 and m is the amount of formed silicide. In these calculations the entropy can be neglected [21], as shown in Table 6.

Figure 24 shows the total free energy as a function of the Mo fraction, for the three prevailing compounds. Note that we do not distinguish between different crystallographic structures (cubic, hexagonal, tetragonal) for Mo_5Si_3 or $MoSi_2$, because of their similar formation energies. Each curve has a minimum at the point where the available Mo and Si exactly match the amount of material required to form the compound stoichiometry. Table 5 displays the calculated Mo fractions ($\Gamma_{stoichiometric}$) for which all available bulk components are consumed in the formation of different silicides. From Figure 24 we can determine the compounds with which the system can reach the most energetically favourable state as a function of the Mo fraction. For $\Gamma < 0.4$ this state is $MoSi_2$, for Γ in the range 0.4 - 0.68 it is Mo_5Si_3, for $\Gamma > 0.68$ it is Mo_3Si or possibly a mixture of Mo_3Si and Mo_5Si_3.

Compound	ΔH (kJ/mole)	ΔS (kJ/mole)
$MoSi_2$	-44	-0.0015
Mo_5Si_3	-39	-0.0001
Mo_3Si	-28	0.0003

Table 6. Formation enthalpies and entropies, resp. of Mo_xSi_y compounds.

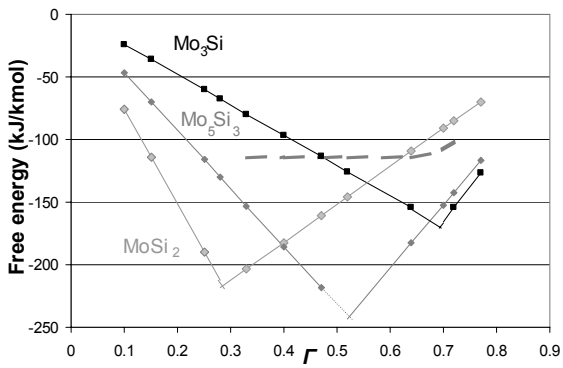

Figure 24. Total free energy as a function of Mo fraction for the different compounds that could be formed after annealing, assuming all available material is used. The dashed line represents the calculated free energy of the system upon annealing at 300 °C just before the crystallization into *h*-$MoSi_2$. For Γ > 0.6 energetically it is not favorable to form *h*-$MoSi_2$.

Annealing at the highest temperature applied in this work (800 °C) shows that the systems do ultimately form the predicted compounds, see Table 4. Experiments also show that in the period thickness range of 5 -10 nm the final silicide stoichiometry upon annealing does depend only on Γ and not on absolute Mo or Si layer thicknesses. This proves validity of the described model. Formation of Mo_3Si instead of a mixture of Mo_3Si and Mo_5Si_3 in case of $\Gamma = 0.8$ indicates that in spite of a small difference between the free energy of the system for the cases of Mo_3Si and Mo_5Si_3, the final, most favourable state is reached. Note that we still observed the surprising spontaneous formation of crystalline Mo_3Si at room temperature in low Γ systems, an effect which is not fully understood (section 3.4.1).

Results on annealing at lower temperatures (400 °C) can also be explained with the presented thermodynamic model, however at this temperature kinetics play a significant role. Some of the structures form silicides that correspond to stable states ($MoSi_2$ for $\Gamma < 0.4$ and Mo_5Si_3 for $\Gamma = 0.6$ - 0.65) or to metastable states ($MoSi_2$ for $\Gamma =$ 0.4 - 0.5 and Mo_5Si_3 for $\Gamma = 0.7$). From our thermodynamic model we understand why certain silicides are not formed in the metastable state. To show this, we calculate the free energy of the system at $T = 300$ °C (dashed line in Figure 24), where all the multilayers in the range $\Gamma = 0.33$ - 0.7 are proven to have the same structure (see section 3.4.2.1): for this calculation we considered 1 nm Mo_5Si_3 and 0.5 nm $MoSi_2$ interfaces that are initially formed during deposition as suggested by modeling of GIXR measurements [12]. As a

result, for $\Gamma < 0.45$, it is energetically favourable to convert the existing interfaces and all remaining Mo and Si into $MoSi_2$ or Mo_5Si_3, but not to Mo_3Si. At the same time, for $\Gamma >$ 0.6, it is energetically favourable to convert the existing interfaces and all remaining Mo and Si into Mo_3Si or Mo_5Si_3, but not to $MoSi_2$. In the range Γ = 0.45 - 0.6 all three silicides could form.

Finally, we note that our model is based on thermodynamic properties of bulk materials; possible deviations caused by ultra-thin film effects are not considered. Other effects, like Mo crystallization for thicknesses higher than 2.3 nm or Si densification due to Kr ion treatment at Γ = 0.8, should be further investigated.

3.5. SUMMARY

We have investigated the nano-crystallinity of Mo-Si multilayer reflecting structures of relevance for Extreme UV lithography. Mo-Si multilayers of 50 periods were deposited by electron beam evaporation with a Mo fraction Γ in the range 0.1 - 0.8 and annealed up to 800 °C. For as-deposited samples, we identified *c*-Mo_3Si nano-crystals at the interfaces for Γ = 0.1 - 0.25, amorphous interfaces for Γ = 0.33 - 0.7 and amorphous $MoSi_2$ for Γ = 0.8. Upon annealing, for multilayers with Γ = 0.1 - 0.25, a phase transformation to *h*-$MoSi_2$ occurs at temperatures higher than 300 °C. Up to 300 °C multilayers with a Mo fraction in the range 0.33 - 0.5 show an increase of the thickness of the naturally formed interfaces, and at higher temperatures again the phase transformation to *h*-$MoSi_2$ takes place. Finally, for multilayers with Γ = 0.6 - 0.8, amorphous Mo_5Si_3 and Mo_3Si is expected to form at low temperatures (based on experiments carried out at 400 °C), with a transformation to the crystalline phase observed at 800 °C.

In conclusion, we observe gradual growth of interfaces upon annealing to 300 degrees, with a phase transformation occurring at higher temperatures. The final phase after annealing at high temperatures is explained by a simple model that allows the determination of the final stoichiometry, based on minimization of the total free energy. This model predicts a dependence of the stoichiometry on the Mo fraction, with no dependence on the multilayer period in the studied range, in agreement with all experimental results.

3.6. ACKNOWLEDGMENTS

The authors wish to thank Frans Tichelaar for the TEM measurements at Delft University of Technology. This work is part of the FOM Industrial Partnership Programme I10 ('XMO') which is carried out under contract with Carl Zeiss SMT AG, Oberkochen and the 'Stichting voor Fundamenteel Onderzoek der Materie (FOM)', the latter being financially supported by the 'Nederlandse Organisatie voor Wetenschappelijk Onderzoek (NWO)'.

3.7. REFERENCES

1 H. Meiling, H. Meijer, V. Banine, R. Moors, R. Groeneveld, H. Voorma, U. Mickan, B. Wolschrijn, B. Mertens, G. van Baars, P. Kürz, N. Harned, "First performance results of the ASML alpha demo tool", Proceedings SPIE Conference, **6151**, 615108-12, Santa Clara, (2006)

2 S. Bajt, J. Alameda, T. Barbee, W.M. Clift, J.A. Folta, B. Kaufmann, E. Spiller, "Improved Reflectance and Stability of Mo/Si Multilayers", Optical Engineering **41** (8), pp. 1797-1804 (2002)

3 A.E. Yakshin, R.W.E. van de Kruijs, E. Zoethout, I. Nedelcu, E. Louis, F. Bijkerk, H. Enkisch, S. Müllender, 'Interface engineering of Mo/Si multilayers for enhanced reflectance in EUVL applications', International EUVL Symposium, Barcelona, www.sematech.org/meetings/archives.htm (2006)

4 E. Zoethout, G. Sipos, R. van de Kruijs, A. Yakshin, E. Louis, S. Müllender, F. Bijkerk, "Stress mitigation in Mo/Si multilayers for EUV lithography", Proceedings SPIE **5037**-106, Santa Clara (2003)

5 E. Louis, H.-J. Voorma, N.B. Koster, F. Bijkerk, Yu.Ya. Platonov, S.Yu. Zuev, S.S. Andreev, E.A. Shamov, N.N. Salashchenko, "Multilayer coated reflective optics for extreme UV lithography", Microelectronic Engineering **27**, pp. 235-238 (1995)

6 E. Zoethout, P. Suter, R.W.E. van de Kruijs, A.E. Yakshin, E. Louis, F. Bijkerk, H. Enkisch, S. Müllender, "Subatomic accuracy in EUVL multilayer coatings", Proceedings SPIE Conference, **5374**-140, Santa Clara, (2004)

7 ICCD database, http://www.iccd.com

8 R. W. E. Kruijs, E. Zoethout, A.E. Yakshin, I. Nedelcu, E. Louis, F. Tichelaar, H. Enkisch, G. Sipos, S. Müllender, F. Bijkerk, "Nano-size crystallites in Mo/Si multilayers optics", Thin Solid Films **515** (2), pp. 430-433 (2005)

9 S. Yulin, T. Feigl, T. Kuhlmann, N. Kaiser, A.I. Fedorenko, V. V. Kondratenko, O. V. Poltseva, V. A. Sevryukova, A. Yu. Zolotaryov, E. N. Zubarev, "Interlayer transition zones in Mo/Si superlattices", Journal of Applied Physics, **92** (3), pp. 1216-1220 (2002)

10 S. Bajt, D. G. Stearns, P. A. Kearney, "Investigation of the amorphous-to-crystalline transition in Mo/Si multilayers", Journal of Applied Physics, **90**, 2, pp. 1017-1025 (2001)

11 S. Braun, H. Mai, M. Moss, R. Scolz, A. Leson, "Mo/Si Multilayers with Different Barrier Layers for Applications as Extreme Ultraviolet Mirrors", Japanese Journal of Applied Physics, **41**, pp. 4074-4081 (2002)

12 A.E. Yakshin, E. Louis, P.C. Gőrts, E.L.G. Maas, F. Bijkerk, "Determination of the layered structure in Mo/Si multilayers by grazing incidence X-ray reflectometry", Physica B, **283**, pp. 143-148 (2000)

13 J. F. Ziegler, J. P. Biersack, http://www.srim.org, Annapolis, MD, (1984-2003)

14 B.E. Warren: *X-Ray diffraction* (Dover Publications, Inc., New York, 1999)

15 I. Nedelcu, R. W. E. van de Kruijs, A. E. Yakshin and F. Bijkerk, "Thermally enhanced interdiffusion in Mo/Si multilayers", submitted to Journal of Applied Physics

16 T. N., Nielsen, R.W.E. v.d. Kruijs, A. Yakshin, I. Nedelcu, E. Louis, F. Bijkerk, Annual meeting of the Danish Physics Society (2006)

17 S. P. Murarka, *SILICIDES FOR VLSI APPLICATIONS* (Academic Press, Orlando, 1983)

18 R. S. Rosen, D. G. Stearns, M. A. Viliardos, M. E. Kassner, S. P. Vernon, Y. Cheng, "Silicide layer growth rates in Mo/Si multilayers", Applied Optics, **32**, no. 34, pp. 6975-6980 (1993)

19 C. Johnson, K. Anderson, A. Gromko, D. Johnson, "Variation of the Nucleation Energy of Molybdenum Silicides as a Function of the Composition of an Amorphous Precursor", Journal of the American Chemical Society **120**, pp. 5226-5232 (1998)

20 V. V. Kondratenko, Yu. P. Perschin, O.V. Poltseva, A. I. Fedorenko, E. N. Zubarev, S. A. Yulin, I. V. Kozhevnikov, S. I. Sagitov, V. A. Chirkov, V. E. Levashov, A. V. Vinogradov, "Thermal stability of soft Mo-Si and $MoSi_2$-Si multilayer mirrors", Applied Optics, **32**, no.10, pp. 1811-1816 (1993)

21 F.R. de Boer, R. Boom, W.C.M. Mattens, A.R. Miedema, and A.K. Niessen, *Cohesion in Metals: Transition metal alloys* (North-Holland Physics Publishing, Amsterdam, 1988)

4. Thermally enhanced interdiffusion in Mo/Si multilayers

4.1. Abstract

The formation and development of Mo-Si interfaces in Mo/Si multilayers upon thermal annealing, including a transition to *h*-$MoSi_2$, has been investigated using high resolution transmission electron microscopy, X-ray reflectivity and X-ray diffraction measurements. The silicide layers naturally formed at Mo-Si interfaces, i.e. just upon and after the deposition, are amorphous and have different thicknesses for as deposited samples, with the Mo-on-Si interlayer being the largest. In addition, silicide growth at Mo-Si interfaces during annealing before the phase transformation predominantly takes place at the Mo-on-Si interface and a $MoSi_2$ interface layer is formed. Diffusion continues until a thick $MoSi_2$ layer is formed at the interface, at which point the interface crystallizes and diffusion speeds up, finally resulting in an abrupt intermixing and phase transition of the entire interface to *h*-$MoSi_2$. This model predicts an onset of the phase transition which does not depend primarily on the annealing temperature, but on a threshold thickness of the $MoSi_2$ interface before crystallization takes place. This crystallisation threshold is shown to exist not only in the Mo/Si system, but also occurs for Mo/Si multilayers where the natural interfaces are replaced by diffusion barriers composed of other elements than Mo and Si.

4.2. INTRODUCTION

Extreme ultraviolet lithography (EUVL) systems, utilizing Mo/Si reflective optics, are currently considered as next generation lithography systems for the semiconductor industry [1]. The principal requirement for an EUVL optical system, is to produce an image with near-diffraction limited resolution, requiring accurate control of the reflected wave, including its phase, along the optical path. Due to the high dose of EUV radiation incident on the optics during the lithography process, their temperature might easily reach a few hundreds degrees, which would influence properties such as the multilayer period thickness. Although a small change of the period thickness does not dramatically change the peak reflectance, the resulting small change in the reflected wavelength of a full EUVL system composed of 10 mirrors leads to phase errors that can add up to several percents, affecting the image quality.

Previous studies on thermally treated Mo/Si multilayers at temperatures in the range 20 - 800 °C already revealed the formation of different Mo silicides [2,3]. Elsewhere, we presented a model based of the minimization of the total free energy to explain the formation of preferred silicides as a function of the Mo/Si ratio in the multilayer [4]. In this work, we focus on the formation and growth upon annealing of the interdiffusion zones in Mo/Si multilayers, as previously reported [5,6]. We show that the reported behaviour upon annealing in Mo/Si interlayers can be linked to the asymmetry of interlayer transition zones that were formed directly after deposition. From combined grazing incidence (GIXR) and wide angle diffraction X-ray (WAXRD) measurements, we investigate the process of silicide formation. We also show that the phase transition in the Mo/Si system depends not on annealing temperature, but actually on a minimum amount of silicide formed at the interfaces.

4.3. EXPERIMENTAL

Multilayers of 50 bilayers of Mo and Si with a period thickness of 6.9 nm with a Mo fraction of 0.4 were deposited by electron-beam evaporation onto 25×25 mm^2 super polished silicon substrates. The base pressure during deposition was better than 2×10^{-8} mbar. The deposition system has been described elsewhere [7]. Kr ions were applied after

depositing each Si layer to suppress roughness development within the multilayer. As a result of this, a reflectivity of 69 % is routinely achieved at 13.5 nm at near-normal incidence [8,9,10,11].

The multilayers were successively annealed for 48 h from 20 °C to 400 °C using a halogen lamp in a vacuum chamber (base pressure 10^{-7} mbar) and analyzed by grazing incidence X-ray (GIXR) and wide angle X-ray diffraction (WAXRD) with a Philips X'Pert double crystal X-ray diffractometer using Cu-K_α radiation (0.154 nm). During the WAXRD measurements, the sample was rotated by φ = 20° in the sample plane to suppress the diffraction peak from the mono-crystalline substrate and aligned with the incident beam at a fixed angle of ω = 1° to maximize the illuminated area and thereby the diffracted intensity. A detail analysis of the nano-size crystallites in Mo/Si multilayers is presented in ref 12.

Several multilayers were annealed both in successive runs at temperatures in the range 300 - 350 °C, as well as directly to these temperatures to check if there is any effect of annealing history. No significant difference was observed between the two methods, and only successively annealed samples will be reported on here. Multilayer bi-layer thicknesses were determined from theta-2theta scans using the above X-ray spectrometer. Transmission Electron Microscopy (TEM) was used in bright field mode (Philips CM30T) at 300 kV to indicate the layer structure. Specimens for TEM were prepared by Ar ion milling of multilayer cross sections glued on a copper grid. The SiK_β emission coming from the silicon atoms present in the samples was analysed from X-ray Emission Spectroscopy (XES). This emission corresponds to the 3p-1s transition and describes the occupied valence states having the Si 3p character. The soft X-ray spectrometer with which the measurements are performed was the IRIS apparatus and it is described elsewhere [13]. An InSb (111) crystal was used at the first diffraction order. In these conditions, the spectral resolution E / ΔE is about 2000. The Si 1s core holes, whose binding energy is 1840 eV, are created by an electron beam coming from a Pierce gun. The energy of the incident electrons was set to 7.5 keV. It was verified that this energy is sufficiently low so that the electrons cannot reach the substrate.

4.4. RESULTS AND DISCUSSION

4.4.1. Diffusion through Mo-Si transition zones at enhanced temperatures

The initial thicknesses of the Mo-Si transition zones were determined from TEM measurements. Figure 25 shows a cross-section bright field electron micrograph taken from a Mo/Si multilayer with a Mo fraction of 0.4. From this, it was determined that a 1 nm thick interface is formed at the Mo-on-Si interface, while a thinner interlayer of 0.5 nm is formed at the Si-on-Mo interface. Similar transition zones were previously reported for multilayers deposited by magnetron sputtering [5,14,15]. During thermal treatment in the temperature range 20 – 300 °C, diffusion at Mo-Si interfaces is enhanced and the as-deposited intermixed interfaces gradually expand.

Figure 26 (solid squares) shows the compaction of the multilayer period upon annealing in the temperature range 150 – 300 °C, as determined by GIXR measurements. Also shown are data for T > 300 °C, exhibiting a phase transition, which will be discussed in more detail in section 4.4.2.

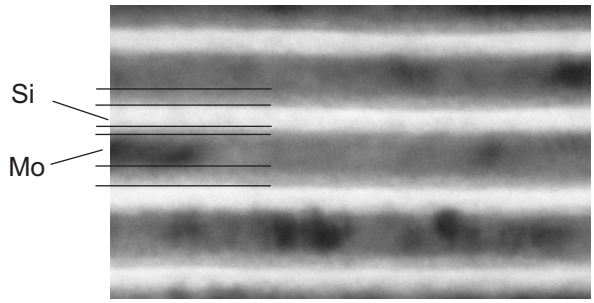

Figure 25. Cross-sectional bright field TEM image of a Mo/Si multilayer, showing 1.0 nm Mo-on-Si and 0.5 nm Si-on-Mo interlayers.

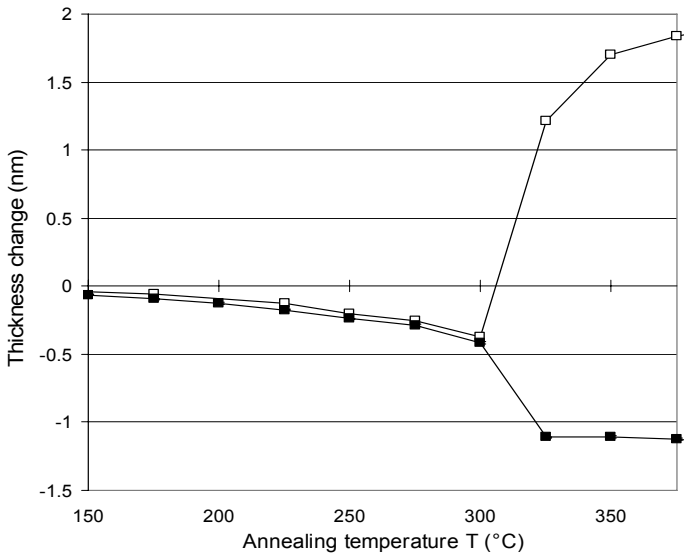

Figure 26. Period compaction (solid squares) and change in transverse crystallite size (open squares) upon annealing. The direct relation between the two curves up to an annealing temperature of 300 °C signifies the formation of additional $MoSi_2$ at the interfaces.

Figure 26 (open squares) also shows the reduction of the Mo crystallite size in the growth direction upon annealing, which is taken to represent the amount of Mo that is consumed into the compound interfaces. Upon this process the interfaces then expand. It is apparent that, below 300 °C, there is a one-to-one correlation between the consumed Mo amount and the reduction in multilayer period. From this, we were able to uniquely determine the type of silicide formed during annealing at Mo-Si interfaces. In Table 7, for all Mo-Si compounds, we calculated the molecular volumes from tabulated density values [16] and we determined the period compaction given for the formation of 1 nm silicide. For example, 0.4 nm Mo and 1 nm Si would be consumed in forming 1 nm of $MoSi_2$, thereby leading to a period compaction of 0.4 nm. Actually, $MoSi_2$ is the only silicide where the period compaction would be equal to the amount of consumed Mo, and therefore equal to the reduction of the Mo crystallite size in the growth direction that is illustrated in Figure 26.

	A [g/mol]	ρ [g/cm^3]	V [cm^3/mol]	V_{Mo} [cm^3/mol]	V_{Si} [cm^3/mol]	V_{Mo}/ $V_{silicide}$	V_{Si}/ $V_{silicide}$	Period compaction: $V_{Mo}+V_{Si}$ -1 [cm^3/mol]
Mo	95.9	10.2	9.40					
Si	28.08	2.3	12.21					
Mo_3Si	315.78	8.97	35.21	28.21	12.21	0.80	0.35	0.15
Mo_5Si_3	563.74	8.2	68.75	47.01	36.63	0.68	0.53	0.22
$MoSi_2$	152.06	6.24	24.37	9.40	24.42	0.39	1.00	0.39

Table 7. Molecular volumes of Mo and Si existing in all Mo_xSi_y compounds divided to the silicides molecular volume are used to calculate the period compaction.

In addition, by comparing TEM pictures before and after annealing at 300 °C, we determined that indeed 1 nm Si was consumed upon formation of 1 nm interface, supporting the previous finding of $MoSi_2$ as the type of interface formed. The TEM analysis performed at samples annealed at 300 °C suggests that the growth of $MoSi_2$ predominantly takes place at the Mo-on-Si interface, which also showed the largest amount of intermixing for the as-deposited multilayer. We suggest similar to the results in ref. [14] collected at room temperature that during annealing the crystallinity of Mo may play a dominant role in determining the growth of the interfaces. During Mo growth, the initial growth of Mo takes place in an amorphous phase, while only after several nanometers a crystalline phase occurs [4,14,15]. Therefore, during annealing in the case of the amorphous Mo, due to a high mobility of the Mo atoms, this interface may be more susceptible to additional silicide formation than the Si-on-crystalline-Mo interface.

To confirm that diffusion takes place preferentially at the Mo-on-Si interface, we treated each as-deposited Si surface with N ions, chosen as an arbitrary example material. This treatment resulted in the formation of a Si_3N_4 interlayer as a diffusion barrier, on the topside of the Si layers. The alternate interface was not treated. Figure 27 shows the period compaction and the Mo crystallite size change for two Mo/Si multilayers with and without Si_3N_4 at the Mo-on-Si interface.

We observe that due to the presence of Si_3N_4 at the Mo-on-Si interface the diffusion rate is significantly reduced during annealing up to 375 °C and the crystallization is absent in this range, confirming that this interface is indeed the most "active" interface during annealing. The remaining compaction is diffusion at Si-on-Mo interface which was not passivated, and possibly at not fully passivated Mo-on-Si interface. In the next section we will discuss the diffusion and crystallization processes for Mo/Si multilayers annealed in the range 300 – 400 °C in more detail.

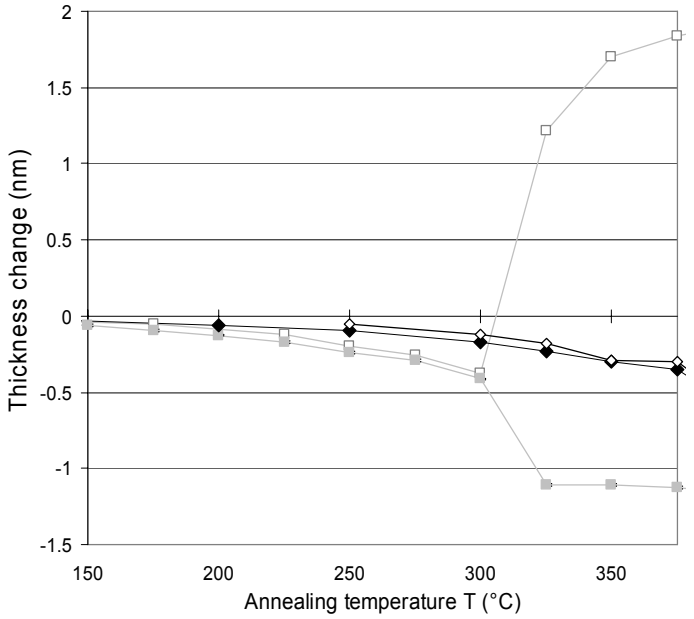

Figure 27. Period compaction (solid circles) and change in transverse crystallite size (open circles) for a Mo/Si multilayer with a Si_3N_4 diffusion barrier. For reference, the period compaction (solid squares) and change in transverse crystallite size (open squares) for a standard Mo/Si multilayer is also shown. The presence of Si_3N_4 significantly reduces diffusion processes, postponing the phase transition to *h*-$MoSi_2$.

4.4.2. Abrupt phase transition to h-$MoSi_2$

At temperatures higher than 300 °C, the "standard" Mo-Si multilayer, composed by the deposition of only Mo and Si materials, suffers an abrupt phase transformation to *h*-$MoSi_2$ [2,3,5] which consumes entirely the available amounts of bulk components [4], as indicated in Figure 26 by the abrupt reduction in period thickness and the sharp increase in crystallite size (actually the $MoSi_2$ crystallite size is measured here, since above 325 °C all bulk Mo is transformed into $MoSi_2$).

The phase transformation of bulk Mo and Si into *h*-$MoSi_2$ is in agreement with XES measurements performed on multilayers annealed at 400 °C. In Figure 28 a clear change is noticed between the Mo-Si multilayer spectrum after deposition and the

multilayer annealed at 400 °C. The Si 3p spectral density of the annealed multilayer at 400 °C shows a close resemblance to the reference spectrum of $MoSi_2$ [17] suggesting a significant evolution in the physical-chemical environment of the silicon atoms between 20 and 400 °C towards $MoSi_2$ formation.

Figure 29 depicts the changes in the Mo-Si multilayer structure during annealing in the range 20 – 400 °C. As discussed before, a 1 nm thick interface is initially formed at the Mo-on-Si interface, which increases to 2 nm after being annealed at 300 °C. It was observed before that in the Mo/Si system, a thickness threshold of 2 nm exists for the abrupt crystallization of Mo, attributed primarily to the interfacial and bulk excess energies of amorphous clusters and secondly to the Si concentration into Mo which should be below the solid solubility limit [15].

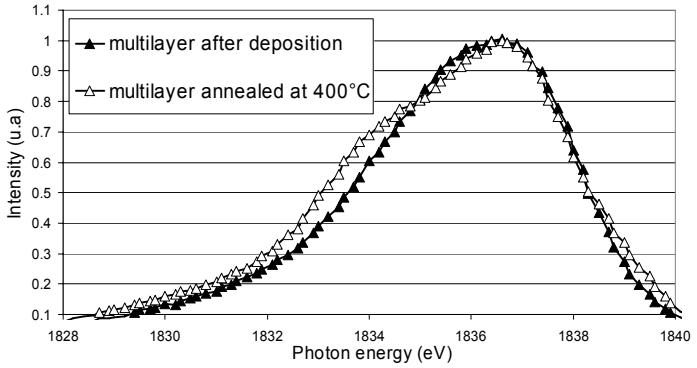

Figure 28. The change in Si 3p spectral densities between the Mo/Si multilayer after deposition (solid triangles) and after annealing at 400 °C (open triangle) suggests the multilayer transformation into $MoSi_2$.

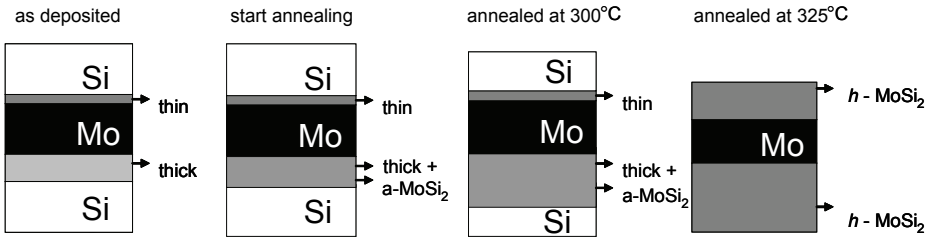

Figure 29. A model of the changes in the structure of a Mo/Si multilayer during thermal treatment is given here, illustrating the gradual formation of amorphous $MoSi_2$ up to a critical thickness of 2 nm, where crystallization of the interface occurs and all available bulk Mo and Si transforms into *h*-$MoSi_2$.

In our case, the multilayer GIXR data could not be modeled considering the composition of the original Mo-Si interface layers formed after deposition as being only $MoSi_2$. Instead, a combination of silicides (Mo_5Si_3 and $MoSi_2$) was used to successfully model the GIXR measurements [18]. Therefore, although the Mo-on-Si interface is initially 1 nm as shown in Figure 25 since it most likely consists of a combination of silicides, more amorphous material has to be formed at this interface during annealing with the Mo:Si ratio of 1:2 which would favor the $MoSi_2$ crystallization [19]. It was shown in section 4.4.1 that for temperatures up to 300 °C, the amorphous material formed at Mo-Si interfaces is $MoSi_2$. At 300 °C, besides the 1 nm silicide combination formed at room temperature, the amorphous environment with the 1:2 Mo:Si ratio formed during annealing is approximately 1.2 nm at Mo-on-Si interface which is sufficient to cause the abrupt interlayer crystallization into *h*-$MoSi_2$ for temperatures higher than 300 °C (a = 4.64 Å, c = 6.53 Å) [19]. We here suggest that the abrupt phase transformation to *h*-$MoSi_2$, evident in Figure 26, is not linked to a threshold value of the annealing temperature but actually to the abrupt crystallization that occurs after a critical thickness of 2 nm Mo-on-Si interlayer is formed. The diffusion rate will increase dramatically [5] along the grain boundaries in the now crystalline Mo-on-Si interface and all bulk available Mo and Si will interact and form *h*-$MoSi_2$. Annealing at temperatures higher than 325 °C, does not change the multilayer formed structure, confirming this intermixing saturation phenomenon.

4.5. Impurities effect on the abrupt phase transformation to h-$MoSi_2$

It was shown in Figure 27 that the diffusion is significantly reduced by passivating the top of each Si layer after deposition with N ions. According to our model, a phase transition to *h*-$MoSi_2$ would still be expected in the entire multilayer when the critical interlayer thickness of 2 nm is reached. However, this could not be reached below 400 °C because of slowed down diffusion through the passivated part of the Si layer. Thus, additional experiments were performed at temperatures higher than 400 °C to verify the existence of a critical crystallisation threshold in systems with a passivated Si surface. We prepared multilayers with different Si_3N_4 thicknesses and the annealing results are summarized in Figure 30.

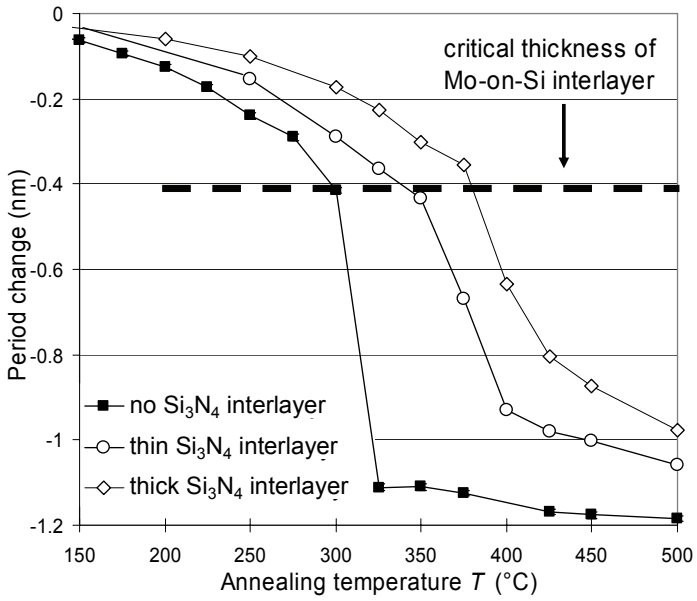

Figure 30. Period compaction during annealing up to 500 °C for multilayers with different Si_3N_4 thicknesses. The same period compaction is observed before the transition, suggesting a critical value for the thickness of the interface before crystallisation takes place.

The curves indicate that the period compaction increases abruptly for the same critical thickness of the Mo-on-Si interface zone, namely 2 nm, consequently confirming our model of the thickness threshold required for silicide crystallization. In Figure 31 we present the WAXRD spectra for the multilayers with thin and thick Si_3N_4 layers deposited on top of each Si layer and the multilayer without Si_3N_4 layer for temperatures corresponding to a Mo-on-Si interlayer thickness equal to 2 nm (before crystallization) and higher than 2 nm (after crystallization). The WAXRD spectra of the *h*-$MoSi_2$ are also shown (black lines). The vertical dotted lines point towards the peak position in these spectra where the presence of a crystalline silicide, *h*-$MoSi_2$, can be identified in the annealed multilayers with a Mo-on-Si interlayer thicker than 2 nm.

Although it is expected that the phase transformation to *h*-$MoSi_2$ occurs in the entire multilayer, the X-ray experimental data show that up to 500 °C (highest temperature applied) the multilayer crystallization does not occur. This might be caused by the lack of Si in the multilayers after Si_3N_4 layers formation by passivating the Si surface. The multilayers studied here consist of 3 nm Mo and 4 nm Si after deposition. To form *h*-$MoSi_2$ over the entire multilayer, all Si should be consumed due to the Mo:Si ratio

of 1:3 in $MoSi_2$. Therefore, in the case of thick (> 2 nm) Si_3N_4 layers, after N treatment, from the original 4 nm Si layer thickness, less than 2 nm remains. This would lead to much less *h*-$MoSi_2$ formation, which is also visible in the crystallographic spectrum.

We attribute this to the presence of N in the system based on previously reported delay effects on crystallization by some materials, like N, O and Ar. Due to the defects created by these elements in the original structure the crystallization is mitigated [20]. This is in agreement with the *h*-$MoSi_2$ formation in multilayers with thick Si_3N_4 layers, where more N is present in the system and consequently, the crystallization into *h*-$MoSi_2$ is less observed in the crystallographic pattern in Figure 31 simultaneously with significantly more crystalline Mo left after crystallization than in the case of thin Si_3N_4 layers or no Si_3N_4 layers.

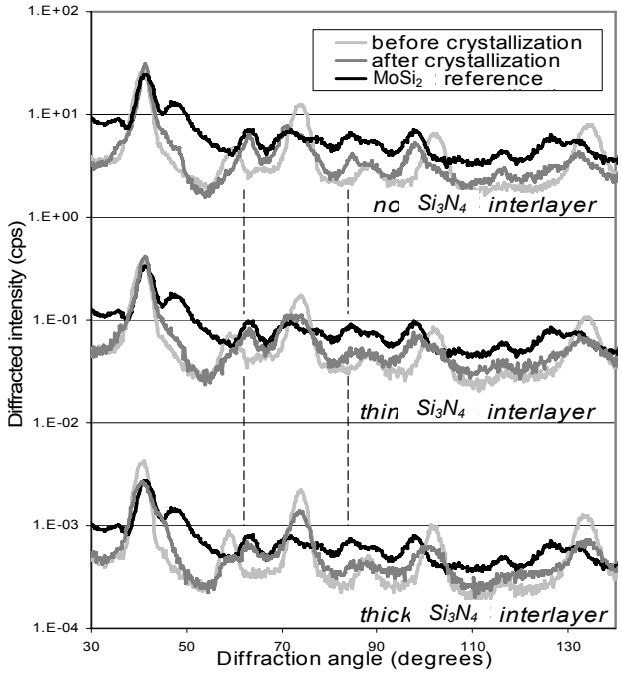

Figure 31. The X-ray diffraction spectra (WAXRD) of annealed Mo/Si multilayers with thin and thick Si_3N_4 layer in top of each Si layer, compared to a Mo/Si without Si_3N_4 layers. The *h*-$MoSi_2$ spectrum (black line) is used to identify in these multilayers the presence of this silicide. The vertical dotted lines point to the *h*-$MoSi_2$ diffraction peaks where the presence of crystalline Mo-on-Si interlayer is visible from the temperature corresponding an interlayer thickness equal to 2 nm (light gray line) to the next successive annealing temperature corresponding an interlayer thickness higher than 2 nm (dark gray line).

4.6. CONCLUSIONS

Mo-Si multilayers, consisting of 50 periods of Mo and Si, were deposited by electron beam evaporation and sequentially annealed up to 500 °C. From TEM, we show that an asymmetry exists between the as-deposited Mo-on-Si (1 nm) and Si-on-Mo (0.5 nm) interface. During thermal treatment, diffusion takes place preferentially through the thick Mo-on-Si interface. We find in this paper that the cause of the higher diffusion rate at this interface is the same before and after annealing, and consists of a different mobility of the Mo atoms linked by either the crystalline structure at the bottom (amorphous intermixture) or the top (polycrystalline film) of the deposited Mo layers.

At enhanced temperatures, the formation of amorphous silicide interfaces continues until a critical thickness of approximately 2 nm is reached, whereupon crystallization of the interface takes place. Diffusion increases along the crystalline grains of the silicide interface and the process of *h*-$MoSi_2$ formation continues until all available Si is consumed, resulting in a sharp phase transformation to *h*-$MoSi_2$ for the multilayer annealed at temperatures higher than 300 °C.

The dependence of the phase transition on a critical thickness, instead of on a critical temperature, was validated by experiments using Si_3N_4 passivation layers of different thickness to reduce diffusion at the Mo-on-Si interface. All systems exhibit the same behaviour, namely an abrupt enhanced diffusion upon annealing at the Mo-on-Si interface, simultaneously with interface crystallization that is linked to its critical thickness.

4.7. ACKNOWLEDGMENTS

The authors wish to thank Frans Tichelaar for the TEM measurements at Delft University of Technology and Philippe Jonnard, Helene Maury and Jean-Michel Andre for the XES measurements at Université Pierre et Marie Curie, Unité Mixte de Recherche du CNRS (UMR 7614, Paris). This work is part of the FOM Industrial Partnership Programme I10 (‘XMO’) which is carried out under contract with Carl Zeiss SMT AG, Oberkochen and the ‘Stichting voor Fundamenteel Onderzoek der Materie (FOM)’, the latter being

financially supported by the 'Nederlandse Organisatie voor Wetenschappelijk Onderzoek (NWO)' and SenterNovem through the 'ACHieVE' and EAGLE programmes co-ordinated by ASML.

4.8. REFERENCES

1 H. Meiling, H. Meijer, V. Banine, R. Moors, R. Groeneveld, H. Voorma, U. Mickan, B. Wolschrijn, B. Mertens, G. van Baars, P. Kürz, N. Harned, "First performance results of the ASML alpha demo tool", Proceedings SPIE Conference, **6151**, 615108-12, Santa Clara, (2006)

2 V. V. Kondratenko, Yu. P. Perschin, O.V. Poltseva, A. I. Fedorenko, E. N. Zubarev, S. A. Yulin, I. V. Kozhevnikov, S. I. Sagitov, V. A. Chirkov, V. E. Levashov, A. V. Vinogradov, "Thermal stability of soft Mo-Si and $MoSi_2$-Si multilayer mirrors", Applied Optics, **32**, no.10, pp. 1811-1816 (1993)

3 J. M. Liang, L. J. Chen, "Interfacial reactions and thermal stability of ultrahigh vacuum deposited multilayered Mo/Si structures", Journal of Applied Physics, **79** (8), pp. 4072-4077 (1996)

4 I. Nedelcu, R. W. E. van de Kruijs, E. Zoethout, E. Louis, A. E. Yakshin, F. Bijkerk, "Temperature dependent micro-crystallinity of Mo/Si multilayers", Phys. Rev. B, accepted for publication

5 R. S. Rosen, D. G. Stearns, M. A. Viliardos, M. E. Kassner, S. P. Vernon, Y. Cheng, "Silicide layer growth rates in Mo/Si multilayers", Applied Optics, **32**, no. 34, pp. 6975-6980 (1993)

6 I. Nedelcu, R. W. E. van de Kruijs, A. E. Yakshin, F. D. Tichelaar, E. Zoethout, E. Louis, H. Enkisch, S. Müllender, F. Bijkerk, "Interface roughness in Mo/Si multilayers", Thin Solid Films **515**, pp. 434-438 (2006)

7 E. Louis, H. –J. Voorma, N.B. Koster, F. Bijkerk, Yu. Ya. Platomov, S. Yu. Zuev, S.S. Andreev, E. A. Shamov, N. N. Salashchenko, "Multilayer coated reflective optics for Extreme UV lithography", Microelectronic Engineering **27** (1-4), pp. 235-238 (1995)

8 R. Stuik, E. Louis, A. E. Yakshin, P. C. Gőrts, E. L. G. Maas, F. Bijkerk, D. Schmitz, F. Scholze, G. Ulm, M. Haidl, "Peak and integrated reflectivity, wavelength and gamma optimization of Mo/Si, and Mo/Be multilayer, multi-element optics for extreme ultraviolet lithography", Journal of Vacuum Science

and Technology B, Microelectronics processing and phenomena, **17** (6), pp. 2998-3002 (1999)

9 E. Louis, H. –J. Voorma, N. B. Koster, L. Shmaenok, F. Bijkerk, R. Schlatmann, J. Verhoeven, Yu. Ya. Platonov, G. E. van Dorssen and H. A. Padmore, "Enhancement of reflectivity of multilayer mirrors for soft x-ray projection lithography by temperature optimization and ion bombardment", Microelectronic Engineering, **23** (1-4), pp. 215-218 (1994)

10 E. Zoethout, G. Sipos, R. van de Kruijs, A. Yakshin, E. Louis, S. Müllender, F. Bijkerk, "Stress mitigation in Mo/Si multilayers for EUV lithography", Proceedings SPIE **5037**-106, Santa Clara (2003)

11 E. Zoethout, P. Suter, R.W.E. van de Kruijs, A.E. Yakshin, E. Louis, F. Bijkerk, H. Enkisch, S. Müllender, "Subatomic accuracy in EUVL multilayer coatings", Proceedings SPIE Conference, **5374**-140, Santa Clara, (2004)

12 R. W. E. van de Kruijs, E. Zoethout, A. E. Yakshin, I. Nedelcu, E. Louis, H. Enkisch, G. Sipos, S. Müllender, F. Bijkerk, "Nano-size crystallites in Mo/Si multilayer optics", Thin Solid Films **515**, pp. 430-433 (2006)

13 C. Bonnelle, F. Vergand, P. Jonnard, J.-M. André, P.-F. Staub, P. Avila, P. Chargelègue, M.-F. Fontaine, D. Laporte, P. Paquier, A. Ringuenet, B. Rodriguez, "Instrument for research on interfaces and surfaces", Review of Scientific Instruments **65** (11), pp. 3466-3471 (1994)

14 S. Yulin, T. Feigl, T. Kuhlmann, N. Kaiser, A.I. Fedorenko, V. V. Kondratenko, O. V. Poltseva, V. A. Sevryukova, A. Yu. Zolotaryov, E. N. Zubarev, "Interlayer transition zones in Mo/Si superlattices", Journal of Applied Physics, **92** (3), pp. 1216-1220 (2002)

15 S. Bajt, D. G. Stearns, P. A. Kearney, "Investigation of the amorphous-to-crystalline transition in Mo/Si multilayers", Journal of Applied Physics, **90**, 2, pp. 1017-1025 (2001)

16 S. P. Murarka, *SILICIDES FOR VLSI APPLICATIONS* (Academic Press, Orlando, 1983)

17 P. Jonnard, I. Jarrige, R. Benbalagh, H. Maury, J.-M. Andre, Z. Dankhazi, G. Rolland, "Physico-chemical and X-ray optical characterizations of a Mo/Si multilayer interferential mirror upon annealing", Surface Science **589**, pp. 164-172 (2005)

18 A.E. Yakshin, E. Louis, P.C. Gőrts, E.L.G. Maas, F. Bijkerk, "Determination of the layered structure in Mo/Si multilayers by grazing incidence X-ray reflectometry", Physica B, **283**, pp. 143-148 (2000)

19 C. Johnson, K. Anderson, A. Gromko, D. Johnson, "Variation of the Nucleation Energy of Molybdenum Silicides as a Function of the Composition of an Amorphous Precursor", Journal of the American Chemical Society **120**, pp. 5226-5232 (1998)

20 E. F. Kennedy, L. Csepregi, J. W. Mayer and T. W. Sigmon, "Influence of 16O, 12C, 14N, and noble gases on the crystallization of amorphous Si layers", Journal of Applied Physics, **48** (10), pp. 4241-4246 (1977)

5. Substrate recovery layers for EUVL optics: effects on multilayer reflectivity and surface roughness

5.1. ABSTRACT

We have investigated the use of separation, or substrate recovery layers (SRL) enabling the re-usage of optics substrates after deposition of multilayer reflective coatings, in particular Mo/Si multilayers as used for Extreme UV lithography. An organic material, a polyimide, was applied, from other work known to reduce the roughness of the substrate [1, 2]. It appeared to be possible to remove the multilayer coating, including the SRL, without any damage or roughening of the substrate surface. The SRL was spin-coated at 1500 - 6000 rpm on different substrate types (Si, quartz, Zerodur) with diameters up to 100 mm. For this range of parameters, the multilayer centroid wavelength value remained unchanged, while its reflectivity loss, upon applying the SRL, was limited to typically 0.7 %. The latter is demonstrated to be caused by a minor increase of the SRL surface roughness in the high spatial frequency domain. The AFM characterized roughness remained constant at 0.2 nm during all stages of the substrate recovery process, independent of the initial substrate roughness.

5.2. INTRODUCTION

Presently, Mo/Si multilayers are intensively employed for development and production of optics for EUVL (Extreme Ultra Violet Lithography) projection systems. This type of optics is needed for the mass production of computer chips in the future when the critical dimensions of line printing have to be in the range of 30 nm and below [3].

During EUV lithography tool operation, the performance of reflective mirrors may deteriorate due to surface chemistry induced contamination in the presence of background gasses [4]. In addition, optics close to the plasma source may suffer from plasma debris. Since replacement of such optics involves manufacturing of expensive, often a-spherically curved substrates, a recovery process for the substrates would be beneficial. Recycling of substrates would also greatly reduce the development costs for iterative deposition processes of reflective multilayer coatings.

Although removal of multilayer coatings from substrates can be achieved by making use of, for instance, wet chemical etching, such methods usually generate a high surface roughness of the substrate (> 0.5 nm) upon multilayer removal. To prevent such roughening, a separation layer can be added between the substrate and the multilayer, as for example described in refs. [5,6]. Although the results of such layers are promising, their use generally still reduces the initial reflectance of the multilayer system deposited on top. Any recovery method should at least meet strict roughness specifications for the optical surface, before and after substrate recovery. A typical value for the high spatial frequency roughness required for a high initial reflectance is in the order of 0.2 nm or below. The method explored here meets this requirement.

The main objective of this paper is to investigate the suitability of using a polyimide layer, known for its ability to reduce initial substrate roughness [2,7], but here explored as a substrate recovery, or separation layer. Our goal was to characterize the processes of repeated deposition and removal of Mo/Si multilayer coatings on single substrates. We present results on the effect on the Mo/Si multilayer surface roughness by comparing the AFM roughness measurements of a reference Mo/Si multilayer on a silicon substrate with the roughness of the probed substrate in all phases of its recovery process. We also present results on EUV reflectivity for multilayers deposited on the substrate with or without using the polyimide, and investigated possible reflectance losses or wavelength shifts measured at 13.5 nm.

5.3. SAMPLE PREPARATION AND ANALYSIS

To determine the feasibility of substrate recovery in the case of the use of polyimide layers, we have employed the scheme presented in Figure 32. Table 8 shows the different steps of the procedure applied. A mono-crystalline Si wafer, surface characterized by atomic force microscopy (AFM), was spin-coated at the Delft University of Technology (DIMES) with a polyimide layer. Using Si wafers, various samples were prepared to investigate the polyimide quality resulting from different rotation speeds and thermal post-treatments. Polyimide was also successfully spin coated on Zerodur substrates. After the polyimide coating was applied, the system was investigated by AFM and then multilayer coated using the FOM coating facilities [8,9] applying a 50 period molybdenum/silicon multilayer. The multilayer period was controlled via an in-situ X-ray reflectometer to allow exact tuning to the centroid wavelength of 13.5 nm. To minimize interfacial roughness during deposition, ion beam polishing was applied after each completed Si layer. More details can be found in refs [8, 9].

After the multilayer coating, AFM surface characterization was repeated and near normal EUV reflectance around 13.5 nm wavelength was measured at the Physikalisch-Technische Bundesanstalt (PTB), using beamline SX700 at storage ring Bessy II, ref. 10**.** Subsequently, the polyimide was removed in a dissolving bath and rinsed, applying a propanol finishing. After recovery, the Si substrate was again surface characterized, and the process of spin-coating the polyimide and electron beam coating the multilayer system was repeated, including the various analysis steps. As a reference, a 50 period Mo/Si multilayer, deposited without SRL onto a Si wafer, was also included in the analysis chain. The measurements of the surface roughness were carried out using an AFM (Digital Instruments) at Carl Zeiss SMT AG in Oberkochen. The high spatial frequency surface roughness was extracted from 1x1 μm^2 scans at three positions on the wafers, one in the center and two points at 6 mm distance from the center. In addition to AFM measurements, specular and off-specular X-ray measurements (rocking curves) were performed with a Philips X'Pert double crystal X-ray diffractometer using Cu-K_α radiation (0.154 nm).

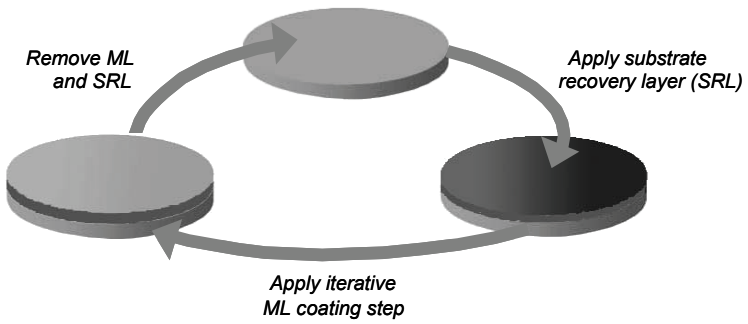

Figure 32. Schematic representation of the substrate recovery process. The substrate recovery layer (SRL) is deposited on the substrate, followed by deposition of the multilayer (ML). By removing the SRL and the multilayer the original substrate is recovered.

Sample stage	Process step
a. Substrate	Spin coating of SRL
b. Substrate + SRL	Coating of Mo/Si multilayer
c. Substrate + SRL +multilayer	SRL and multilayer removal
d. Substrate	Repeated spin coating of SRL
e. Cleaned substrate + SRL	Repeated coating of Mo/Si multilayer
f. Cleaned substrate+SRL+multilayer	

Table 8. Process steps applied to the EUV mirror substrates.

5.4. RESULTS AND DISCUSSION

5.4.1. AFM analysis

Figure 33a shows the atomic force micrographs on selected stages in the substrate recovery cycle described in Table 8. The gray scale for the height, between 0 (black) and 2 nm (white), is the same for all figures. The rms roughness σ was calculated from

$$\sigma^2 = \frac{1}{m \cdot n} \sum_{i=0}^{m} \sum_{j=0}^{n} z_{i,j}^2 - \left(\frac{1}{m \cdot n} \sum_{i=0}^{m} \sum_{j=0}^{n} z_{i,j} \right)^2, \qquad (7)$$

where z_{ij} is the height of each scan point with indices i and j, and m and n the maximum values of i and j. The experimental roughness values calculated are thus averaged over the probed area and are depicted in Figure 33a.

From Figure 33a we conclude that the AFM characterized surface roughness of the Mo/Si multilayers on polyimide coated silicon substrates remained unchanged during the entire cycle of multilayer deposition, removal and subsequent deposition on polyimide coated substrates. In addition, the surface roughness did not differ significantly (within 0.01 nm) from a reference multilayer, deposited without SRL. This suggests that the application and removal of this type of SRL and multilayer does not influence the substrate quality in the high special frequency roughness regime (HSFR), as probed by AFM.

Additionally, this 0.2 nm roughness was achieved independent of the initial substrate roughness, on all probed substrates. This result shows, at least within the limited process window probed here, that the HSFR value, as determined by AFM, is independent of the investigated spin coating parameters (rotation speed, sample size, annealing treatment). The presence of a 0.2 nm limit in all cases is well above the resolution limit of the AFM, suggesting that this limit is caused by the polymerization of the polyimide during drying, i.e. independent of the initial substrate conditions. Smoothening of rough substrates by polyimide was also reported in ref [7].

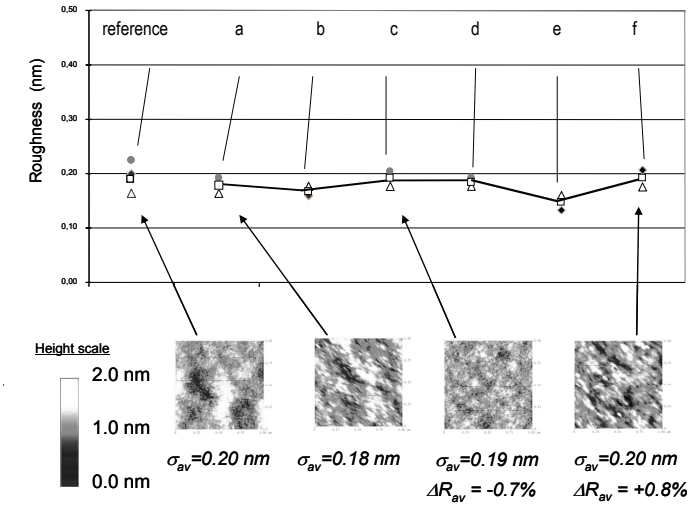

Figure 33a. AFM surface roughness measurements. The gray scale corresponds to roughness and ranges between 0 (black) and 2 nm (white), being the same range for all figures. AFM images are also displayed for the reference sample, consisting of a multilayer on a silicon substrate, including stages a, c and f as defined in Table 8. In addition to the three measurements of the roughness per sample (circle, triangle and rhomb), also the mean roughness of all three points per sample is measured and displayed (solid line).

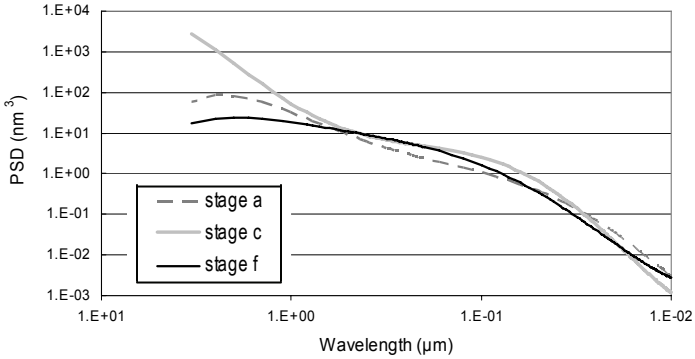

Figure 33b. Power spectral densities of samples in stages a. and f. showing a slightly higher roughness of stage f in the frequency range from 0.01 to 1 µm.

Further analysis of the area-averaged AFM measurement data by differentiating over the frequency range of the roughness did indicate minor differences between the roughness of a bare substrate and SRL treated samples. To this end we have calculated the Power Spectral Density (PSD) curves from the AFM data (Fig. 33b). As compared to

a bare, untreated sample, the PSDs show a higher roughness in parts of the HSF domain (i.e. 0.03 - 3.3 μm) of a sample on a mono-crystalline Si substrate at stage c (SRL spin coated and multilayer coated), and a slightly lower value in the range above 1 μm and below 0.1 μm of the sample at stage f. (i.e. SRL spin coated and multilayer coated upon removal of the first SRL and multilayer). These PSD curves suggest that the SRL does increase the roughness in the HSF domain while after cleaning the SRL and multilayer and again recoating the SRL and multilayer, a comparable roughness as the bare substrate is obtained. The small multilayer roughness decrease at stage f is in agreement with the small reflectivity increase observed (Figure 33a). Obviously, the area-averaged AFM data do not reveal differences in different roughness regimes, though the frequency dependence of the roughness smoothening of the process remains to be investigated.

5.4.2. Hard X-ray scattering

Besides having a high throughput of the optical system, EUV projection lithography systems also require low flare. In addition to at-wavelength measurements of these quantities, indications for such quantities can readily be obtained from specular and diffuse scattering experiments at hard-x ray facilities [11].

From the unchanged modulation of the Bragg peaks intensity in the specular reflectivity experiments (not shown here), we determined that the layered structure of the multilayer did not change significantly when applying a substrate recovery layer, independent of the investigated spin-coating parameters (i.e. rotation speed and temperature treatment). However, a small decrease of the reflected intensity at the high order Bragg peaks suggested that the multilayer total roughness slightly increased when polyimide was applied.

For roughness quantification over an extended range of frequencies, we have done diffuse scattering measurements on a reference sample without SRL and for 3 samples with SRL's using different rotation speeds and temperature treatments during polyimide spin-coating (Figure 34).

By way of obtaining a first indication of the parameter dependence of the process, we have selected a rotation speed for sample 2 and 3 which was twice the value used for sample 1. Also, the temperature of the post-annealing treatment for sample 2 was half compared to the other two samples. The increase of the diffuse scattering around the specular peak indicated the presence of a high-spatial frequency component of the multilayer roughness, induced by the polyimide layer under the multilayer. This is in

agreement with the PSD spectrum in the high-spatial frequency domain presented in the previous section. It is noted from these measurements that X-ray diffuse scattering was found to be more sensitive in determining the HSFR of the multilayer structure compared to the AFM analysis. This could be caused by the fact that the AFM tip probes only the relatively smooth SiO_2 top layer of the multilayer, not the underlying interfaces.

Although the differences between the various preparation procedures were small, a slight dependence on rotation speed and treatment temperature could be identified. For higher temperatures, and higher rotation speeds, the amount of diffuse scattering went down, indicating a lower roughness in the high spatial frequencies. This is in agreement with findings regarding homogeneity of a spin coated fluid [12].

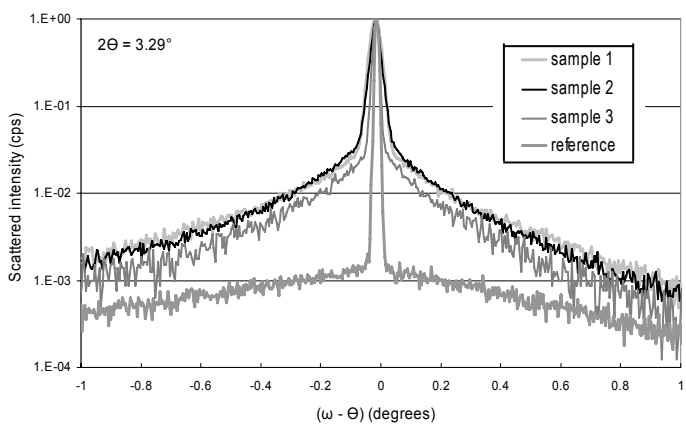

Figure 34. Diffuse reflectivity at the Cu-K wavelength versus (ω - θ) around the 5th order Bragg peak where ω is the incident angle and θ = 1.645° the detection angle. The data of each sample are normalized to the Bragg peak intensities. The 5th Bragg peak order is chosen to obtain a reasonable rocking range at sufficient signal-to-noise ratio. The rotation speed of sample 2 and 3 was doubled compared to sample 1. The temperature of the post-annealing treatment of sample 2 was almost half compared to the other two samples.

5.4.3. EUV reflectivity

Figure 35(a) shows the difference in multilayer period between a Mo/Si multilayer deposited on a substrate without SRL, and the period of Mo/Si multilayers deposited on SRL's using the same rotation speeds and thermal post-treatments as in the previous section. For all cases, the addition of an SRL did not significantly change the period thickness of the added multilayer to within an accuracy of 2 pm. This is a critical requirement for using SRL's in iterative coatings for the optimization of multilayer coatings. The small variations are thought to be caused by tolerances in the deposition and alignment steps of these samples.

Figure 35(b) shows the reflectivity loss for the same samples with respect to the reference multilayer deposited directly on the substrate. The mean reflectivity of the multilayers coated on an SRL coated substrate was 0.7 % lower than that of a reference sample without SRL. This reduced reflectivity could be explained by the increased high spatial frequency surface roughness, as found by PSD curves and diffuse scatter measurements (Sect. 5.4.1 and 5.4.2). Furthermore, no significant effect on reflectivity was found for the different polyimide spin-coating parameters (i.e. rotation speed, thermal treatment temperature).

After cleaning the silicon substrates, spin coating with polyimide and again depositing a multilayer, the reflectivity did not decrease any further, indicating that no further roughening of the substrate occurred during the cleaning procedure. This is confirmed by the AFM analysis presented in section 5.4.1.

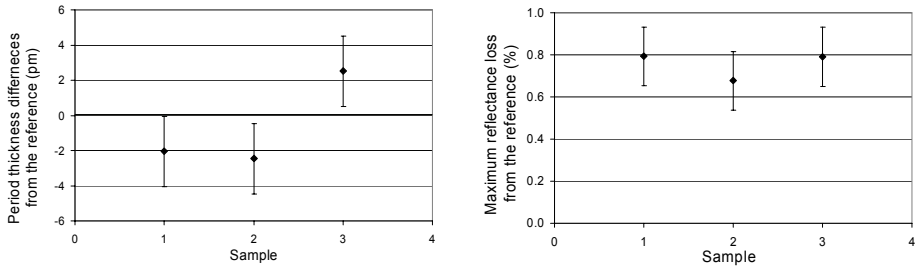

Figure 35. The period thickness change with respect to a non-SRL reference sample is displayed (a) for three multilayers deposited on polyimide spin coated samples with different rotation speeds and temperatures during post thermal treatment. The reflectivity loss for these samples with respect to the reference multilayer deposited directly on the substrate is illustrated in (b).

Reflectivity measurements were also performed on multilayers deposited on polyimide spin-coated Zerodur substrates. The reflectivity loss due to the presence of an SRL layer was found to be similar to the loss using silicon substrates (< 1 %). This is again explained by the increase in high-spatial frequency surface roughness, as discussed in section 5.4.2. Although spin coating with polyimide worked, the process of removing the SRL from Zerodur so far resulted in an increased substrate roughness (0.5 nm – 1 nm). Other cleaning methods are therefore still under investigation.

5.5. SUMMARY AND CONCLUSIONS

The feasibility of applying a polyimide separation, or substrate recovery layer for the purpose of applying EUV optics substrate recovery was investigated using AFM, hard X-ray scattering and at-wavelength reflectometry. On Si wafers, the processes of depositing a multilayer on an SRL layer, cleaning the substrate, and re-depositing the SRL and multilayer resulted in a constant 0.2 nm, AFM characterized roughness. Hard X-ray diffuse scatter measurements and PSD curves show that the roughness in the high spatial frequency range did increase when applying an SRL, resulting in a 0.7 % reflectivity loss observed using at-wavelength reflectometry. The cleaning and re-coating of SRL and multilayer did not decrease the reflectivity any further, nor did the centroid wavelength of the multilayer coating change to within 2 pm. This demonstrates the usefulness of the process for substrate recovery or sample re-usage.

On Zerodur substrates, the same small reflectivity loss was observed when applying an SRL, again attributed to the same kind of increase in high-spatial frequency surface roughness that was observed after spin coating silicon substrates, using X-ray scattering. In addition, the AFM characterized high spatial frequency roughness, after applying the substrate recovery layer, was 0.2 nm, the same result as obtained after spin coating silicon wafers. Proper recovery of Zerodur substrates still requires study of a wider range of parameters as investigated here.

5.6. ACKNOWLEDGMENTS

The authors thank Bernard Rousseeuw (DIMES, Delft) for all polyimide spin coatings performed at the Dimes clean room facilities at Delft and to Hartmut E. Enkisch from Carl Zeiss SMT AG, Oberkochen for providing the AFM scans. This work is part of the FOM Industrial Partnership Programme I10 ('XMO') which is carried out under contract with Carl Zeiss SMT AG, Oberkochen and the 'Stichting voor Fundamenteel Onderzoek der Materie (FOM)', the latter being financially supported by the 'Nederlandse Organisatie voor Wetenschappelijk Onderzoek (NWO)', and SenterNovem through the EAGLE/ACHieVE project carried out in collaboration with ASML and Carl Zeiss SMT AG.

5.7. REFERENCES

1. P. B. Mirkarimi, S. L. Baker, C. Montcalm, J. A. Folta, " Recovery of multilayer-coated Zerodur and ULE optics for extreme-ultraviolet lithography by recoating, reactive-ion etching, and wet-chemical processes", Applied Optics **40** (1), pp. 62-70 (2001)

2. R. Soufli, "Polyimide smooths surface of EUV aspheric condenser", Laser Focus World **41** (2), (2005)

3. M. van den Brink, www.sematech.org/meetings/archives.htm, International EUVL Symposium, Barcelona (2006)

4. B. Mertens, Weiss M, Meiling H, Klein R, Louis E, Kurt R, Wedowski M, Trenkler H, Wolschrijn B, Jansen R, van de Runstraat A, Moors R, Spee K, Plőger S, van de Kruijs R, "Progress in EUV optics lifetime expectations", Microelectronic Engineering **73-74,** pp. 16-22 (2004)

5. D. P. Gaines, N. M. Ceglio, S. P. Vernon, M. Krumrey, and P. Muller, "Repair of high performance multilayer coatings", in *Multilayer Optics for Advanced X-Ray Applications*, N.M. Ceglio, ed. Proceedings SPIE **1547**, pp. 228-238 (1991)

6. K. Early, D. L. Windt, W. K. Waskiewicz, O. R. Wood II, and D. M. Tennant, "Repair of soft x-ray optical elements by stripping and re-deposition of Mo/Si

reflective coatings", Journal of Vacuum Science and Technologies **B 11**, pp. 2926-2929 (1993)

7. R. Soufli, E. Spiller, M.A. Schmidt, J. C. Robinson, S. L. Baker, S. Ratti, M. A. Johnson, E. M. Gullikson, "Smoothing of diamond-turned substrates for extreme ultraviolet illuminators", Optical Engineering **43** (12), pp. 3089-3095 (2004)

8. E. Louis, H.J. Voorma, N.B. Koster, L. Shmaenok, F. Bijkerk, R. Schlatmann, J. Verhoeven, Yu.Ya. Platonov, G.E. van Dorssen and H.A. Padmore, "Enhancement of reflectivity of multilayer mirrors for soft x-ray projection lithography by temperature optimization and ion bombardment", Proceedings Microcircuit Engineering (ME93), Maastricht, pp. 27-29 (1993)

9. A. E. Yakshin, E. Louis, P.C. Gőrts, E.L.G. Maas and F. Bijkerk, "Determination of the layered structure in Mo/Si multilayers by grazing incidence X-ray reflectometry", Physica B, **283**, pp. 134-148 (2000)

10. J. Tümmler, F. Scholze, G. Brandt, B. Meyer, F. Scholz, K. Vogel, G. Ulm, M. Poier, U. Klein, W. Diete, "New PTB reflectometer for the characterization of large optics for the extreme ultraviolet spectral region", Proceedings SPIE **4688**, pp. 338-347 (2002)

11. D. E. Savage, J. Kleiner, N. Schimke, Y.-H. Phang, T. Jankowski, J. Jacobs, R. Kariotis and M.G. Lagally, "Determination of roughness correlations in multilayer films for x-ray mirrors", Journal of Applied Physics, **69**, 3, pp. 1411-1424 (1991)

12. B. D Washo, "Rheology and Modeling of the Spin Coating Process", IBM Journal of Research and Development **21** (2), pp. 190-198, (1977)

6. Microstructure of Mo/Si multilayers with B_4C as barrier layers

6.1. ABSTRACT

The growth behaviour of B_4C interlayers deposited at interfaces in Mo/Si multilayers has been investigated using X-ray photoemission spectroscopy, X-ray reflectivity and X-ray diffraction measurements. We report for the first time an asymmetry in B_4C formation, where for B_4C-on-Mo the correct stoichiometry is formed, while for B_4C-on-Si the XPS depth profile suggests C-diffusion out from the B_4C interfaces into the multilayer. As a result, a discrepancy is found in the optical response at 13.5 nm wavelength, where B_4C-on-Mo behaves according to model simulations, while B_4C-on-Si does not. The as-deposited off-stoichiometric B_4C-on-Si interface also explains the thermal treatment results, where B_4C-on-Si shows poor barrier quality against temperature induced interdiffusion.

We explain the formation of B_4C with different stoichiometries at Mo-Si interfaces by the different structure of the layer onto which B_4C is grown. Due to enhanced diffusion into the amorphous Si surface, deposited boron and carbon atoms would be able to form Si_XB_Y and Si_XC_Y compounds. The low formation enthalpy of Si_XC_Y ensures C-depletion of any formed B_XC_Y interlayer. Only after a saturated interfacial layer is formed, further deposition of boron and carbon atoms results in actual B_4C formation. In contrast to off-stoichiometric B_4C growth on top of Si, the limited diffusion into the (poly)-crystalline Mo surface, as well as higher formation enthalpies for Mo_XB_Y and Mo_XC_Y formation, result in stoichiometric B_4C growth on top of Mo.

6.2. INTRODUCTION

The commercial viability of extreme ultraviolet projection lithography is closely linked to the quality of the optics used to collect and project 13.5 nm radiation. Such optics typically consist of substrates, coated with a Mo/Si multilayer, which theoretically reflect up to 74 % of the (near normal) incident radiation. In reality, the reflectivity at λ = 13.5 nm is reduced to below 70 % [1] due to the development of roughness during multilayer deposition and due to reduced optical contrast as a result of silicide formation at Mo-Si interfaces [2]. Silicide formation will continue at enhanced temperatures [3] that are expected during high photon flux illumination, further lowering the optics throughput, and ultimately threatening optics lifetime [2].

To limit intermixing at the Mo-Si interfaces, the naturally formed Mo_xSi_y interlayers can be replaced by ultra-thin artificial diffusion barriers [4, 5]. For example, 0.2 - 0.3 nm C and B_4C barrier layers were successfully used to limit interdiffusion, thereby increasing the multilayer reflectivity above 70 % [5]. In addition to achieving higher reflectivity values, thick (> 1 nm) C and B_4C have also proven successful in enhancing the multilayer resistance against thermally induced intermixing at the interfaces [4].

The successful application of barrier layers in EUVL multilayer coatings strongly depends on understanding and optimizing the multilayer reflectance and thermal stability with respect to diffusion barrier thicknesses. We present here a study of B_4C thin film growth properties, when applied as barrier layers for Mo/Si multilayer coatings. Surface roughness and layer stoichiometry as a function of barrier thickness have been investigated using X-ray scattering and X-ray photoemission spectroscopy. The observed discrepancies in EUV reflectance and barrier quality against thermal treatment are shown to be related to initially C-depleted (B_4C) barrier layer growth at the Mo-on-Si interfaces.

6.3. EXPERIMENTAL

Multilayers consisting of 50 bilayers of Mo and Si with thin B_4C interlayers on Mo or on Si were deposited by electron-beam evaporation onto 25×25 mm^2 super polished silicon substrates. Deposition flux masking [6] was used during B_4C layer growth to obtain a gradient in the interlayer thickness of 0.3 nm – 2 nm, values that are

typical for barrier layer thicknesses expected to enhance reflectivity and/or provide thermal stability. The base pressure during deposition was better than 2×10^{-8} mbar. To suppress surface roughness development through the multilayer during deposition, the surface of each completed Si layer was smoothened using low energy Kr ions. The deposition setup has been described in more detail in ref [7].

The optical response of the multilayer to incident radiation around 13.5 nm was measured near normal incidence at the Physikalisch-Technische Bundesanstalt (PTB) [8,9] at the BESSY II storage ring in Berlin. X-ray photoelectron spectroscopy (XPS) was used to determine the in-depth layered structure, as well as to obtain chemical information on the nature of the compounds (B_xC_y, Mo_xSi_y) formed in the multilayer system.

To test B_4C barrier layer quality, multilayers were successively annealed for 48h from 20 °C to 450 °C in a vacuum chamber (10^{-8} mbar base pressure, 10^{-7} mbar during annealing) using a halogen lamp. Before and after each annealing treatment, the samples were characterized by grazing incidence X-ray reflectometry (GIXR), diffuse scattering (rocking curves) and wide angle X-ray diffraction (WAXRD), using a Philips X'Pert double crystal X-ray diffractometer (Cu-K_α radiation, 0.154 nm). During the WAXRD measurements, the sample was rotated by φ = 20° in the sample plane to suppress the diffraction peak from the mono-crystalline substrate and aligned with the incident beam at a fixed angle of ω = 1° to maximize the illuminated area and thereby the diffracted intensity. Mo/Si multilayers without B_4C interlayers, as well as with thick (2 nm) B_4C interlayers, were prepared as reference coatings and subjected to the same analysis and thermal treatment. These multilayers have also been annealed directly to 300 °C (plain multilayer) and 600 °C (2 nm B_4C) to rule out any uncertainty on the thermal history of the samples. X-ray measurements on both reference coatings showed no differences between successive and direct annealing, and as a result we limit ourselves here to results obtained from successively annealed multilayers.

6.4. RESULTS AND DISCUSSION

6.4.1. Optical response

Figure 36 shows multilayer peak reflectivity, obtained near λ = 13.5 nm, for multilayers with B_4C interlayers that have B_4C thicknesses in the range 0.3 - 1.8 nm. The light grey symbols represent multilayers with B_4C deposited on Mo (further denoted as Mo/B_4C/Si), whereas the dark grey symbols represent multilayers with B_4C deposited on Si (further denoted as Mo/Si/B_4C). Also shown (dashed lines) are corresponding IMD simulations [10] of the reflectivity for Mo/Si/B_4C (dark grey) and Mo/B_4C/Si (light grey) multilayers. The simulated reflectivities have been normalized to the experimental data to facilitate data analysis.

From Figure 36, it is clear that the measured reflectivity on the Mo/B_4C/Si multilayer can be quite well reproduced by model simulations. To obtain a good quality fit, the simulated reflectivity values were reduced by approximately 4 %. This reduction is partially caused by the reduced optical contrast that is still present at the interface that was not blocked. Also, the multilayer roughness that is replicated during growth may be influenced by the presence of B_4C and affect the reflectivity values.

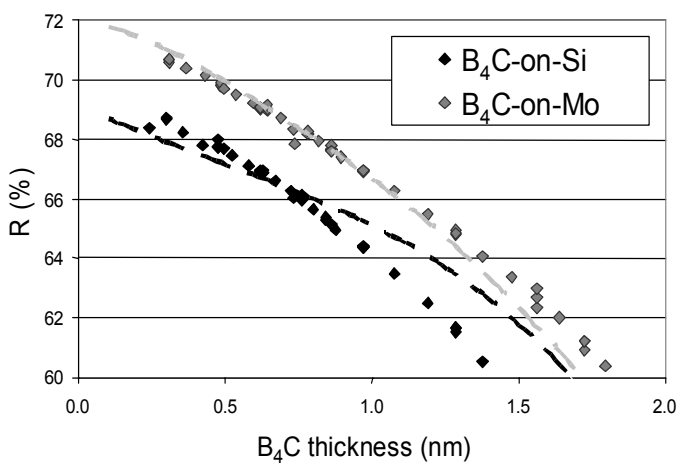

Figure 36. Multilayer peak reflectivity as a function of the B_4C thickness applied on Mo (light grey symbols) and on Si (dark grey symbols). The calculated reflectivities (dashed lines) of these multilayer structures have been normalized to facilitate data analysis.

In contrast to the case for Mo/B_4C/Si, the model simulations for Mo/Si/B_4C do *not* agree with experimental results. There is a pronounced discrepancy in the absolute reflectance, which is approximately 6 % lower than expected, larger than for the case of Mo/B_4C/Si. More important, the decrease in peak reflectance as a function of B_4C thickness is also larger than expected from the theoretical model.

A possible change in surface roughness, which could explain the observed discrepancy in reflectivities, was investigated using diffuse X-ray scattering. To compare the surface roughness of multilayers with and without B_4C at Mo-Si interfaces, we measured diffuse scattering around the 5th order Bragg peak. Figure 37 shows rocking curves obtained from Mo/Si (black curve), Mo/B_4C/Si (dark grey curve) and Mo/Si/B_4C multilayers (light grey curve). The diffuse scattering does not increase in the presence of B_4C, thereby ruling out any significant increase of multilayer roughness. The cause for the reported discrepancy in reflectivities must then be found elsewhere, e.g. layer density, stoichiometry, etc.

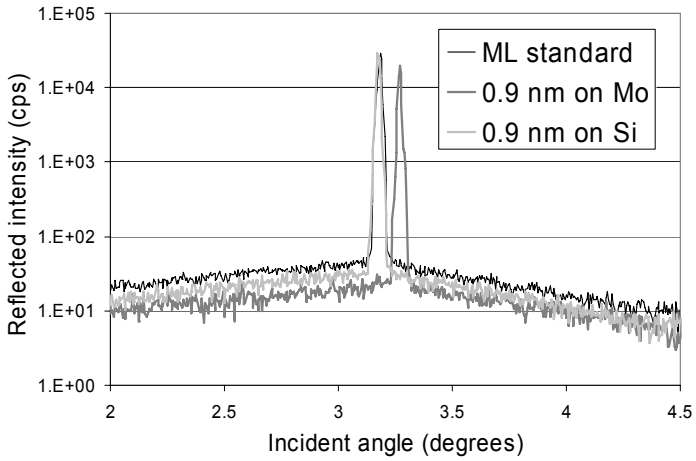

Figure 37. Diffuse scattering as a function of the X-ray angle of incidence around the 5th order Bragg peak. This Bragg peak order is chosen to obtain a reasonable rocking range at sufficient signal-to-noise ratio and in the same time to have the same peak intensity height for all investigated samples. The Mo/Si multilayer (black line) is a reference in comparing the diffuse reflectivity of Mo/Si multilayer with 0.9 nm of B_4C on Mo (dark grey line) and 0.9 nm of B_4C on Si (light grey line). The multilayers containing B_4C present lower reflected intensity than the reference, indicating lower multilayer roughness.

6.4.2. Layered structure

To analyze the depth-distribution of elements present in the multilayer, XPS measurements were performed on multilayers with B_4C on Mo, presented in Figure 38 (a), and on multilayers with B_4C on Si, presented in Figure 38 (b). In both multilayers, the periodic structure is evident from the modulation of the contribution from elemental Mo and Si. The main difference between these multilayers becomes evident when the B and C depth profiles are considered. Both multilayers show the modulation in boron that is expected for a B_4C interlayer localized at the Mo/Si interfaces. However, only in Figure 38(a) carbon is localized. In Figure 38(b) carbon is present in the entire stack, suggesting that B_4C is not formed in the 4:1 stoichiometry, when deposited on Si. The formation of C-depleted B_4C on Si was observed not only using thermal evaporation deposition sources, but also in multilayers deposited using physical sputtering of particles (magnetron sources), ruling out artifacts that may have to do with deposited particle energies, background pressure, deposition speed, etc.

Figure 39 shows the ratio of boron to carbon at the Mo/Si interfaces, obtained using XPS, for a range of B_4C thicknesses between 0.3 nm and 1.8 nm. The results show that stoichiometric growth of B_4C on Mo takes place in the entire investigated thickness range. In contrast, B_4C does not grow stoichiometrically on top of Si at low barrier layer thicknesses. Initially, a carbon depleted $B_{>4}C$ barrier is formed, which saturates after approximately 1 nm thickness, with subsequent B_4C layer growth exhibiting correct stoichiometry.

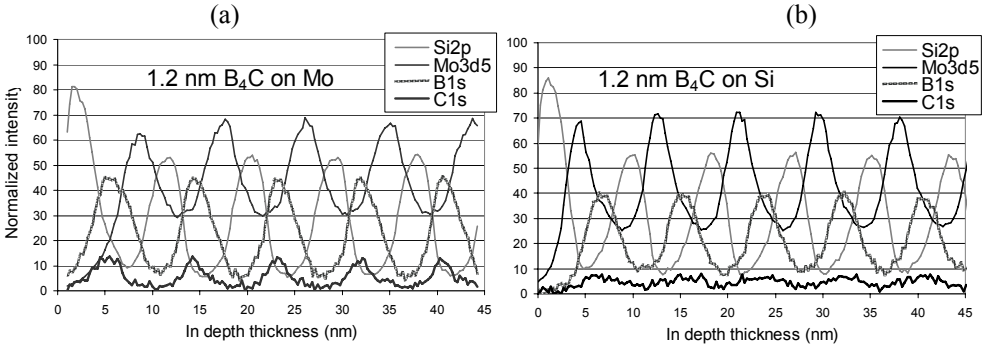

Figure 38. XPS in depth profile for multilayers with 1.2 nm B_4C on Mo (a) and 1.2 nm B_4C on Si (b).

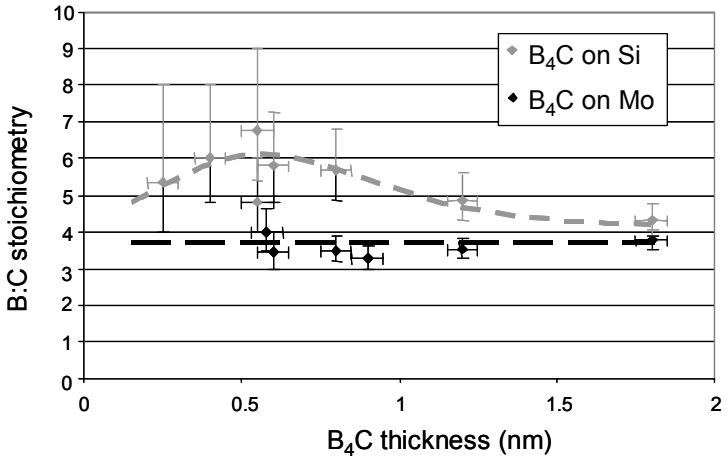

Figure 39. B:C stoichiometry determined from XPS in depth profile, as a function of the B_4C thickness, as deposited on quartz, when B_4C was deposited on Mo (black line) and on Si (grey line). The stoichiometry is 4:1 when B_4C is deposited on Mo, independent of its thickness. The stoichiometry is 6:1 when B_4C is deposited on Si for B_4C thickness lower than 1.0 nm, and 4:1 for B_4C thickness higher than 1.5 nm.

We propose here that the formation of a depleted B_4C layer can be understood from the physical properties of the underlying layer onto which B_4C has been deposited, as well as from differences in formation enthalpies. Figure 40 shows a detailed XPS sputter depth profile for a Si/B_4C/Mo multilayer. To exclude artifacts introduced during XPS depth profiling, the depth profiles were taken using two different ion sputtering energies, 250 eV and 500 eV with no apparent differences visible. The asymmetric shape of the Si atomic depth profile suggests increased diffusion at the B_4C-on-Si interfaces. This could be explained by the diffusion of Si towards the surface during B_4C deposition, caused by the low Si surface free energy [11]. In addition, asymmetric intermixing regions may form due to the crystalline nature of the layers: in ref [3] it was shown that different intermixing regions form when depositing Mo adatoms onto amorphous Si, compared to when depositing Si adatoms onto polycrystalline Mo [12].

When the C atomic depth profile in Fig 38 is compared to the B atomic depth profile, a shift is noticed, suggesting that during B_4C growth C diffuses into Si, while B remains at the surface. Due to a favourable formation enthalpy [13], the excess amount of boron may actually form MoB.

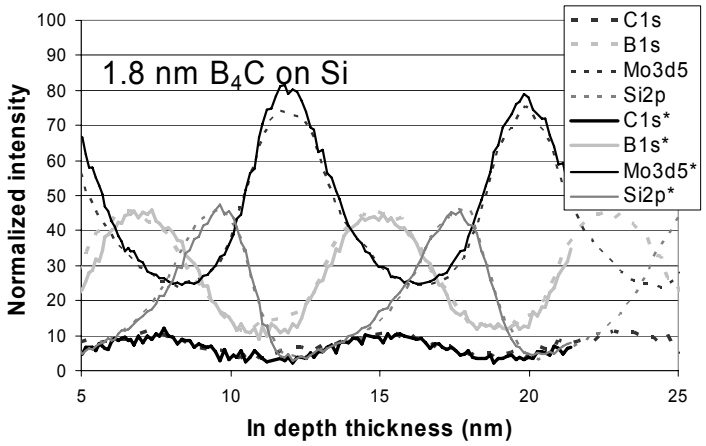

Figure 40. XPS in depth profile for one multilayer with 1.8 nm B_4C on Si when the ion sputtering energy is 500 eV (dashed lines) and 250 eV (continues lines). The same in depth profile obtained for different ion sputtering energies proves that the ions do not influence the diffusion at thin layer interfaces.

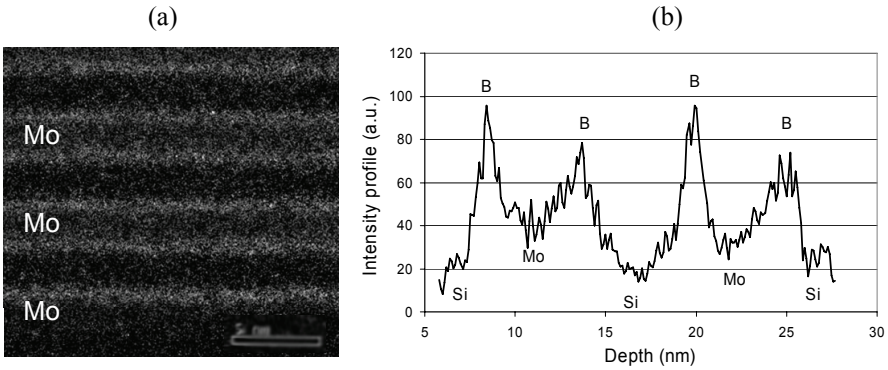

Figure 41. Energy-filtered TEM image using the energy of B K-edge (a) and the derived intensity profile (b) of a $Mo/B_4C/Si/B_4C$ multilayer. The intensity profile (b) presents an asymmetry at the Mo-on-B_4C interface which suggests more intermixing at this interface.

Figure 41(a) shows an energy filtered TEM intensity profile of a $Mo/B_4C/Si/B_4C$ multilayer using energies that correspond to the B K-edge. The intensity profile exhibits a larger intermixing zone for B_4C on Si. In addition, a larger intermixing of Mo and B (B_4C) might be recognized in the intensity profile, close to the Mo/B_4C interface. The exact composition of the highlighted interfaces in Figure 41(a) is not possible to determine since no clear compound formation (shoulder) is present in the intensity

profile. Therefore although the identification of the highlighted interfaces is not possible the appearance of intensity asymmetry only at one interface (on Si) supports the XPS results regarding B_4C depletion.

6.4.3. B_4C barrier quality against thermal diffusion

Upon thermal treatment, Mo/Si multilayers without diffusion barriers exhibit a reduction in multilayer period that is caused by compaction at the interfaces due to additional silicide formed from Mo and Si. At temperatures higher than 300 °C, a full multilayer recrystallization into *h*-$MoSi_2$ occurs [14,15,16]. Diffusion barriers like B_4C are expected to slow down diffusion along the interfaces and postpone the recrystallization towards higher temperatures.

For multilayers deposited by magnetron sputtering upon annealing at 400 °C when B_4C is deposited on Si, Bottger et al [17] proved experimentally that the multilayer period compaction is significantly higher than when B_4C is deposited on Mo. We found the same results on multilayers deposited by electron beam evaporation and magnetron sputtering. This is in agreement with the reflectivity findings from section 6.4.1.

However, Mo/Si multilayers generally exhibit diffusion along the interfaces, at temperatures well below those where phase transformations are reported in these systems. Diffusion along interfaces, and subsequent additional Mo_xSi_y compound formation at the interfaces, results in the compaction that can be observed in Figure 42 (and is emphasized for clarity) just before the phase transformation. Due to the reported differences in diffusion along Mo-on-Si and Si-on-Mo [18] interfaces, it is expected that by using diffusion barriers, there should be a noticeable difference in compaction resulting from diffusion along the unblocked interface.

In Figure 42 the period compaction is plotted as a function of the annealing temperature for multilayers with B_4C on Mo and B_4C on Si, as well as for a reference Mo/Si multilayer without B_4C at the interfaces. The data clearly shows that the rapid reduction of the multilayer period due to Mo_XSi_Y formation is postponed from 300°C to 325 °C due to the presence of B_4C at the interfaces, but the compaction is similar in both cases. This suggests that either diffusion in case of an unblocked Si-on-Mo interface is much larger than expected, or diffusion along a blocked Mo-on-Si interface is much larger than expected. In light of the results presented in the previous section, the latter explanation is the more plausible. The off-stoichiometric growth of B_4C on Si clearly hampers its functioning as a barrier against diffusion.

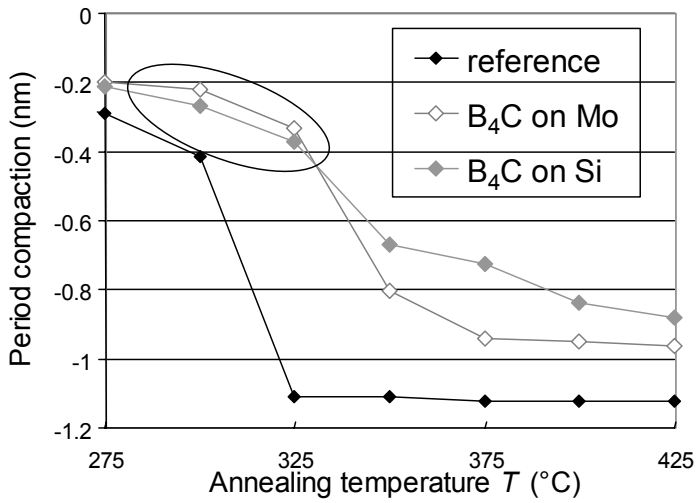

Figure 42. Period compaction as a function of the multilayer temperature for the Mo/Si multilayer (black diamonds) used as a reference in comparing the Mo/Si multilayers with 0.9 nm of B_4C on Mo empty diamonds) and 0.9 nm of B_4C on Si (grey diamonds). Similar period compaction is noticed for the both multilayers containing B_4C before the multilayer re-crystallization into *h*-$MoSi_2$, which occurs 25 °C later than in the reference case.

To investigate the link between the layered and the crystallographic structure, XRD experiments were carried out on multilayers with and without B_4C barriers. Figure 43 shows the crystallite size X along the growth direction, obtained using Scherrer's formula:

$$X = \frac{0.94\lambda}{L\cos(\theta)} \quad , \qquad (4)$$

where $\lambda = 0.154$ nm, L is the full width at half maximum determined for every peak in the spectrum, and 2θ is the diffraction angle between the source and the detector. Since the diffracting planes giving rise to the (110) peak are oriented like the film plane (offset by 20°), the crystallite size in the film growth direction can be easily calculated by correcting for this offset angle. The reference multilayer clearly exhibits a sudden increase in crystallite size due to recrystallization to *h*-MoSi2, which occurs at the same temperature where the multilayer period showed a sudden decrease (Figure 42).

Figure 43 shows that the process of multilayer crystallization is clearly affected by using B_4C as a diffusion barrier. In the case of B_4C on Mo, the recrystallization is delayed by 25 degrees, in agreement with the delayed onset of rapid period compaction that is observed in Figure 42. A B_4C barrier on Mo clearly reduces diffusion across the interface, but does not significantly impede the formation of *h*-$MoSi_2$. A dramatically different behaviour is noticed in the case of B_4C used as barrier on top of Si. The reported off-stoichiometric B_4C growth on Si not only allows diffusion to continue, it also affects the crystalline state at high temperatures.

When B_4C is deposited on Si, the recrystallization into *h*-$MoSi_2$ is not observed in the investigated temperature range (20 °C - 425 °C). The constant decrease of crystallite size suggests a continuous Mo consumption due to formation of amorphous Mo_XSi_Y. The presence of carbon throughout the multilayer (see also Figure 38b) clearly prevents nucleation of Mo_XSi_Y [19].

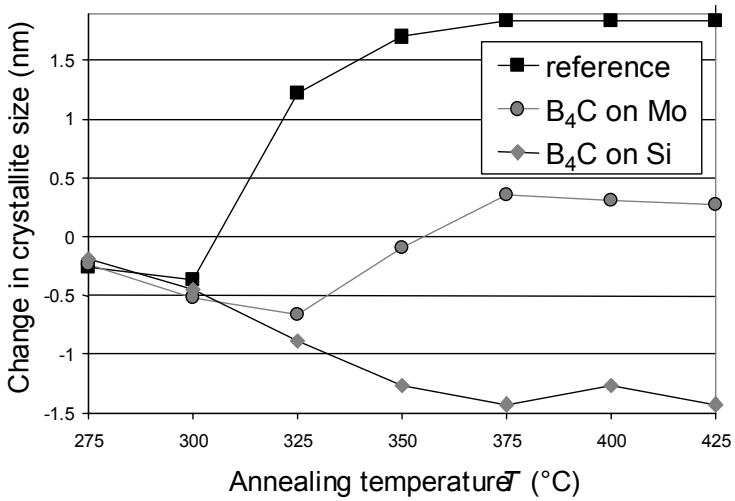

Figure 43. The crystallite size change as a function of the annealing temperature for multilayer without B_4C (reference) (black squared) and multilayers with B_4C on Mo (grey circles) and B_4C on Si (grey diamonds). The re-crystallization to *h*-$MoSi_2$ observed in the reference multilayer case for temperatures higher than 300 °C, also occurs for the multilayer with B_4C on Mo for temperatures higher than 325 °C. When B_4C is deposited on Si, no re-crystallization occurs in the investigated temperatures range (20 – 425 °C).

6.5. SUMMARY AND CONCLUSIONS

An asymmetry in B_4C formation at Mo/Si interfaces is reported here for the first time. From XPS analysis, stoichiometric B_4C growth was observed on top of Mo, while off-stoichiometric B_4C growth was observed on top of Si. A 1 nm carbon depleted B_4C layer is initially formed on top of Si, further followed by stoichiometric B_4C growth. The off-stoichiometric growth on top of Si results in a 2 % reduction of multilayer peak reflectance at 13.5 nm. The formation of a carbon depleted B_4C interlayer on top of Si is explained from a higher diffusion rate of adatoms into the amorphous Si.

The off-stoichiometric B_4C-on-Si interface also exhibits poor quality as a barrier against diffusion. Based on the much higher diffusion rates reported along Mo-on-Si interfaces, compared to those reported along Si-on-Mo interfaces, B_4C barriers should have a much larger effect on the thermal stability when applied on top of Si. In reality, no increased stability was observed, compared to the case where B_4C was deposited on Mo.

Finally, recrystallization to *h*-$MoSi_2$ at enhanced temperatures, present in plain Mo/Si multilayers, as well as multilayers with B_4C deposited on top of Mo, does not occur in cases where B_4C is deposited on Si. We suggest that carbon, present throughout the entire stack, prevents nucleation of Mo_XSi_Y.

6.6. ACKNOWLEDGMENTS

This work is part of the FOM Industrial Partnership Programme I10 (‘XMO’) which is carried out under contract with Carl Zeiss SMT AG, Oberkochen and the ‘Stichting voor Fundamenteel Onderzoek der Materie (FOM)’, the latter being financially supported by the ‘Nederlandse Organisatie voor Wetenschappelijk Onderzoek (NWO)’.

6.7. REFERENCES

1. E. Louis, A. E. Yakshin, P. C. Gőrts, S. Oestreich, R. Stuik, E. L. Maas, M. J. Kessels, F. Bijkerk, M. Haidl, S. Müllender, M. Mertin, D. Schmitz, F. Scholze, G. Ulm, "Progress in Mo/Si multilayer coating technology for EUVL optics" SPIE **3997,** art. No. 406 (Micro Lithography), Santa Clara (2000)
2. D. Atwood, *Soft x-rays and extreme ultraviolet radiation, Principles and Applications*, Cambridge, University Press (1999)
3. I. Nedelcu, R. W. E. van de Kruijs, A. E. Yakshin and F. Bijkerk, "Thermally enhanced interdiffusion in Mo/Si multilayers", submitted to Journal of Applied Physics
4. S. Bajt, J. Alameda, T. Barbee, W.M. Clift, J.A. Folta, B. Kaufmann, E. Spiller, "Improved Reflectance and Stability of Mo/Si Multilayers", Optical Engineering **41** (8), pp. 1797-1804 (2002)
5. S. Braun, H. Mai, M. Moss, R. Scolz, A. Leson, "Mo/Si Multilayers with Different Barrier Layers for Applications as Extreme Ultraviolet Mirrors", Japanese Journal of Applied Physics, **41**, pp. 4074-4081 (2002)
6. R. W. E. van de Kruijs, E. Louis, A. E. Yakshin, P. Suter, E. Zoethout, F. Bijkerk, S. Müllender, H. Enkisch, H. Trenkler, M. Wedowski, M. Weiss, B. Mertens, B. Wolschrijn, R. Jansen, A. Duisterwinkel, A. van de Runstraat, R. Klein, S. Plőger and F. Scholze, "Optimization of protective capping layers for EUVL optics", Poster **122**, Proceedings of the 2nd International EUV Lithography Symposium, Antwerp, (2003)
7. E. Louis, H. –J. Voorma, N.B. Koster, F. Bijkerk, Yu. Ya. Platomov, S. Yu. Zuev, S.S. Andreev, E. A. Shamov, N. N. Salashchenko, "Multilayer coated reflective optics for Extreme UV lithography", Microelectronic Engineering **27** (1-4)**,** pp. 235-238 (1995)
8. J. Tümmler, H. Blume, G. Brandt, J. Eden, B. Meyer, H. Scherr, F. Scholz, G. Ulm, „Characterization of the PTB EUV reflectometry facility for large EUVL optical components", Proceedings SPIE **5037**-265 (2003)
9. A. Gottwald, U. Kroth, M. Letz, H. Schoeppe, M. Richter, „High-accuracy VUV reflectometry at selectable sample temperatures", Proceedings SPIE **5538**-157 (2004)
10. IMD, version 4.1.1, written by David L. Windt (2000)

11. F. R. de Boer, R. Boom, W.C.M. Mattens, A.R. Miedema, and A.K. Niessen, *Cohesion in Metals: Transition metal alloys* (North-Holland Physics Publishing, Amsterdam, 1988)
12. R. W. E. van de Kruijs, E. Zoethout, A.E. Yakshin, I. Nedelcu, E. Louis, F. Tichelaar, H. Enkisch, G. Sipos, S. Müllender, F. Bijkerk, "Nano-size crystallites in Mo/Si multilayers optics", Thin Solid Films **515** (2), pp. 430-433 (2005)
13. *Handbook of chemistry and Physics*, 55th edition, CRC (1974-1975)
14. S. Yulin, T. Feigl, T. Kuhlmann, N. Kaiser, A.I. Fedorenko, V. V. Kondratenko, O. V. Poltseva, V. A. Sevryukova, A. Yu. Zolotaryov, E. N. Zubarev, "Interlayer transition zones in Mo/Si superlattices", Journal of Applied Physics, **92** (3), pp. 1216-1220 (2002)
15. V. V. Kondratenko, Yu. P. Perschin, O.V. Poltseva, A. I. Fedorenko, E. N. Zubarev, S. A. Yulin, I. V. Kozhevnikov, S. I. Sagitov, V. A. Chirkov, V. E. Levashov, A. V. Vinogradov, "Thermal stability of soft Mo-Si and $MoSi_2$-Si multilayer mirrors", Applied Optics, **32**, no.10, pp. 1811-1816 (1993)
16. R. S. Rosen, D. G. Stearns, M. A. Viliardos, M. E. Kassner, S. P. Vernon, Y. Cheng, "Silicide layer growth rates in Mo/Si multilayers", Applied Optics, **32**, no. 34, pp. 6975-6980 (1993)
17. T. Bottger, D. C. Meyer, S. Braun, M. Moss, H. Mai, E. Beyer, "Thermal stability of Mo/Si multilayers with boron carbide interlayers", Thin Solid Films **444**, pp. 165-173 (2003)
18. K. Holloway, K. B. Do, R. Sinclair, "Interfacial reactions on annealing molybdenum-silicon multilayers", Journal of Applied Physics, **65** (2), pp. 474-480 (1989)
19. V. N. Patel, J. L. Conarroe, "Amorphous switching device with residual crystallization retardation", Patent number 4433342, Appl. No. 06/251,106, Filed:Feb.21,(1984)

7. SUMMARY

This thesis refers to the design, fabrication and characterization of Mo/Si multilayers mainly used as optics in EUV lithography. At Mo-Si interfaces, sub-nanometer interlayers are formed which influence microscopic (density, crystallinity) as well as macroscopic (reflectivity, stress) multilayer properties. The composition of the sub-nanometer interlayers formed at Mo/Si interfaces is not possible to determine directly with the standard techniques. This thesis focuses on the structural analysis of the Mo and Si layers and the interdiffusion along Mo/Si interfaces during and after ion bombardment and thermal treatment. The structural and chemical changes were analyzed by soft and hard X-ray measurements, in combination with TEM, XPS, XES, and AFM analysis.

The structure of Mo/Si multilayers changes as a function of the Mo fraction of a multilayer period. For multilayers having low and high Mo fractions, applicable to plasma diagnostics or stress compensation, a two layer system is formed, consisting of Mo/Mo_XSi_Y or Si/Mo_XSi_Y, depending on Mo fraction. For intermediate Mo fractions, used in EUV reflective multilayer mirrors, a four layer system is formed, containing pure Mo and Si layers, as well as Mo_XSi_Y interlayers. This thesis presents a detailed study of Mo/Si multilayers for a wide range of Mo fractions, directly after deposition, as well as after thermal treatment.

In this thesis, chapter 2 presents a detailed study of the multilayer roughness development as a function of ion bombardment energy and Mo fraction. We found that ion smoothening during layer deposition works efficiently when applied at low energies and during the latter part of the layer deposition. Under high ion energy bombardment, more intermixing takes place and the Si-on-Mo interface stoichiometry changes from Mo_3Si to $MoSi_2$.

The diffusion at Mo-Si interfaces, already occurring naturally during multilayer deposition, is enhanced under EUV radiation. To analyze the changes that may be expected in the multilayer structure during years of lithography tool operation, many experimental studies on the thermal behaviour of Mo/Si multilayer have been performed. These studies showed that at enhanced temperature different silicides can form as a

function of the annealing temperature. However, so far no general theory has existed to predict silicide formation upon annealing. Chapter 3 of this thesis presents a model, based on minimization of the total energy of the system, that predicts the final silicide stoichiometry formed in Mo/Si multilayers as a function of the as deposited Mo fraction.

An asymmetry in diffusion speeds at Mo-on-Si and Si-on-Mo interfaces has previously been reported in literature. However, no model was suggested so far to explain this asymmetry. The understanding of diffusion in ultra-thin Mo and Si films is important not only for application in EUV lithography but also from fundamental point of view. In chapter 4 we consider a model that explains the asymmetry in Mo-Si interface formation at room temperature. We extend this model to higher temperatures and we propose a new model to explain the sudden transformation to a crystalline silicide upon annealing. This transformation is shown to be triggered by a threshold thickness for the amount of silicide interface formed, in contrast to the so far reported dependence on the annealing temperature.

To produce mirrors for EUV lithography, many deposition parameters have to be optimized in iterations which require many expensive substrates. Many substrate recovery methods are available to reduce the manufacturing costs, but the challenge is to obtain the original low roughness on the substrate. In chapter 5 we propose the use of a polyimide, known to reduce substrate roughness, as a substrate recovery layer. We demonstrate that the high special frequency roughness in all stages of the recovery process remains unchanged and consequently no significant multilayer reflectivity loss is registered after recoating the recovered substrate. After successful demonstration of substrate recovery on small substrates, the process is currently being implemented in an industrial process on large, aspheric substrates.

Finally, to increase the multilayer reflectivity and thermal stability in EUV lithography, the use of other materials such as carbon and B_4C has been explored as diffusion barriers at Mo-Si interfaces. In chapter 6 we present a fundamental study of B_4C layer growth on Mo and Si surfaces. We discover an inconsistency in multilayer reflectivity and thermal stability when applying B_4C on top of Si. We propose an explanatory model on these experimental observations. These results can be explained by an in-depth XPS analysis of the multilayer structure.

8. SAMENVATTING

Dit proefschrift beschrijft ontwerp, productie, en karakterisatie van Mo/Si multilagen voor toepassing in EUV lithografie. Aan de Mo-Si interfaces vormen zich tussenlagen van enkele Angstroms dik, die de microscopische eigenschappen (dichtheid, kristallisatie) zowel als macroscopische eigenschappen (reflectiviteit en stress) van de multilagen beïnvloeden. Dit proefschrift focusseert zich op de structurele analyze van de Mo en Si lagen en de interdiffusie door Mo/Si interfaces onder invloed van ionen en thermische behandelingen. De structurele en chemische veranderingen in de multilaag werden geanalyseerd met behulp van X-ray metingen, gecombineerd met TEM, XPS, XES en AFM analyse.

De structuur van Mo/Si multilagen veranderd als functie van de Mo fractie in de multilaag periode. Voor multilagen met lage zowel als hoge Mo fracties, toepasbaar in plasma diagnostieken of stress compensatie, vormt zich een twee-laags systeem bestaande uit Mo/Mo_XSi_Y of Si/Mo_XSi_Y, afhankelijk van de Mo fractie. Voor tussenliggende Mo fracties, gebruikt in EUV reflecterende multilaag spiegels, vormt zich een vier-laags systeem dat bestaat uit pure Mo en Si lagen zowel als Mo/Si tussenlagen. Dit proefschrift beschrijft een gedetailleerd onderzoek aan Mo/Si multilagen met verschillende Mo fracties, direct na depositie zowel als na thermische behandeling.

In hoofdstuk 2 van dit proefschrift wordt een gedetailleerde beschrijving gegeven van de ontwikkeling van ruwheid in Mo/Si multilagen, als functie van de ionen energie en van de Mo fractie. Ionen polijsten tijdens Si laaggroei werkt het meest efficiënt wanneer toegepast met lage ionen energieën en tijdens het laatste deel van de laaggroei. Bij hogere ionen energieën vind er intermixing plaats en verandert de interface stoichiometrie van $MoSi_3$ naar $MoSi_2$.

De diffusie aan Mo-Si interfaces, die al plaatsvindt tijdens multilaag depositie, wordt versneld onder EUV bestraling. Om de veranderingen te analyseren die verwacht kunnen worden in de multilaag structuur tijdens jarenlang gebruik van lithografie machines, zijn er vele experimentele studies gedaan om het thermisch gedrag van Mo/Si multilagen te bestuderen. Deze studies hebben laten zien dat bij verhoogde temperaturen er verschillende silicides kunnen vormen als functie van de temperatuur. Er is zover echter geen algemene verklaring voor de vorming van specifieke silicides bij bepaalde temperaturen. In hoofdstuk 3 wordt een model gepresenteerd dat gebaseerd is op

minimalisatie van de totale energie van het multilaag systeem, wat de stoichiometrie van de gevormde silicides verklaard.

Een asymmetrie in diffusie snelheden aan Mo-op-Si en Si-op-Mo interfaces is eerder al gerapporteerd in literatuur. Er is zover nog geen model gepresenteerd dat deze asymmetrie kan verklaren. Het begrijpen van diffusie processen in ultra-dunne Mo en Si lagen is belangrijk voor toepassing in EUV lithografie zowel als uit fundamenteel oogpunt. In hoofdstuk 4 beschouwen we een model dat de asymmetrie in Mo-Si interface formatie verklaard bij kamertemperatuur. We breiden dit model uit naar hogere temperaturen en stellen een nieuw model voor dat de plotselinge transformatie naar een kristallijn silicide verklaard tijdens verhitting. Deze transformatie wordt geïnitieerd door een minimale dikte voor het gevormde silicide interface, in contrast tot de tot nu toe gerapporteerde temperatuursafhankelijkheid van de transformatie.

Om multilaag spiegels te produceren voor EUV lithografie, moeten er veel depositie parameters geoptimaliseerd worden tijdens vele iteraties op dure substraten. Er zijn vele substraat herwinning methodes beschikbaar om de productiekosten de reduceren., maar de uitdaging is om de originele ruwheid te herstellen. In hoofdstuk 5 stellen we een polyimide voor als substraat herwinningslaag, bekent voor het verlagen van substraatruwheid. We demonstreren hier dat de hoge frequentie ruwheid in all stages van het herwinningsproces onveranderd blijft, en als resultaat hiervan zijn er geen belangrijke reflectiviteitsverliezen na het opnieuw deponeren van een multilaag op het herwonnen substraat. Na de succesvolle demonstratie van het volledige substraat herwinningsproces op kleine substraten, wordt het proces momenteel geïmplementeerd in de industrie op grote, a-sferische substraten.

Ten slotte, om de multilaag reflectiviteit en de thermische stabiliteit te verhogen voor EUV lithografie, zijn materialen als koolstof en B_4C voorgesteld als barrières aan Mo/Si interfaces. In hoofdstuk 6 presenteren we een fundamenteel onderzoek naar de laag aangroei van B_4C op Mo en Si oppervlaktes. We hebben een inconsistentheid gevonden in de multilaag reflectiviteit en thermische stabiliteit wanneer B_4C op Si gedeponeerd wordt. Deze resultaten kunnen verklaard worden uit een diepgaande XPS analyse van de multilaag structuur.

9. REZUMAT

Aceasta teza de doctorat se refera la design-ul, fabricarea si caracterizarea multistratului compus din straturi alternative de Mo si Si. Aceste multistraturi sunt folosite preponderent in procesul de litografie cu radiatie din regimul extrem ultraviolet. La contactul dintre straturile de Mo si Si se formeaza in mod natural dupa depunerea acestor materiale, straturi extrem de subtiri (sub un nanometru) care influenteaza in egala masura atat proprietatile microscopice ale intregului multistrat (ex. densitate, cristalinitate), cat si proprietatile macroscopice (ex. reflectivitate, stres). Din cauza dimensiunii sub-nanometrice, compozitia acestor straturi nu poate fi determinata folosind tehnicile standard. In consecinta, aceasta teza se focalizeaza pe analiza structurii straturilor de Mo si Si si a procesului de difuzie la interfetele dintre aceste materiale in urma bombardamentului cu ioni in timpul si dupa depunerea straturilor de Si, si a tratamentului termic. Variatiile structurale si chimice ale acestor multistraturi au fost analizate prin masuratori de raze X in combinatie cu alte tehnici: TEM, XPS, XES si AFM.

Multistratul de Mo/Si consista din 50 de perioade identice, fiecare perioada fiind compusa dintr-un strat de Mo si altul de Si. Structura multistratului se modifica in functie de raportul Mo:Si dintr-o perioada. Multistraturile cu un procentaj foarte mare de Mo intr-o perioada se folosesc la compensarea stresului, cel cele cu procentaj foarte mic de Mo, ca si diagostice ale surselor de plasma. Aceste multistraturi dupa depunerea straturilor alternative de Mo si Si, se transforma in sisteme compuse din doua straturi: Mo/Mo_XSi_Y sau Si/Mo_XSi_Y in functie de procentajul de Mo dintr-o perioada. Pentru procentaje intermediare de Mo, multistraturile folosite ca oglinzi pentru radiatia ultravioleta, se constituie intr-un sistem de patru straturi: doua straturi pure de Mo si Si, si doua straturi la interfetele dintre aceste materiale. Aceasta teza prezinta un studiu amanuntit al multistraturilor de Mo/Si pentru o varietate larga de valori a procentajului de

Mo intr-o perioada, indata dupa depunere la temperatura camerei si dupa tratament termic efectuat intr-o gama larga de temperaturi.

In aceasta teza, capitolul 1 prezinta un studiu detaliat asupra evolutiei rugozitatii in multistraturi in functie de energia ionilor folositi in bombardamentul straturilor de Si si in functie de procentajul de Mo intr-o perioada.

Difuzia la interfetele dintre Mo si Si in timpul depunerii multistratului este amplificata de radiatia din domeniul extrem ultraviolet. Pentru a studia transformarile in structura multistraturilor ce ar corespunde functionarii lor neintrerupte ca oglinzi pentru radiatia ultravioleta, in domeniul experimental se analizeaza influenta tratamentului termic asupra multistraturilor de Mo/Si. In urma tratamentului termic, s-a observat formarea a diferite tipuri de silicide - compusi ai Si - in functie de temperatura. Totusi, pana in acest moment, dovezile experimentale nu si-au gasit suportul intr-o teorie care sa prezica tipul de compus ce se formeaza in functie de temperatura. Capitolul 2 din aceasta teza prezinta un model teoretic, bazat pe minimizarea energiei totale a sistemului care prezice stoichiometria compusului format in starea stabila finala a multistratului in functie de procentajul de Mo dintr-o perioada.

Existenta unei asimetrii in viteza de difuzie la interfata Mo-pe-Si si Si-pe-Mo a fost raportata in literatura de specialitate, insa nici un model care sa explice aceste rezultate nu a fost emis. Intelegerea difuziei la interfata dintre straturile ultrasubtiri de Mo si Si este extrem de importanta nu numai pentru aplicatia tehnica a acestor multistraturi in litografia extrem ultravioleta, dar mai ales din punct de vedere al intelegerii fundamentale a proceselor fizice care au loc. In capitolul 4, noi folosim un model care explica formarea asimetrica a straturilor sub-nanometrice la interfetele Mo-Si la temperatura camerei, pe care il extindem pentru temperaturi mai ridicate. Totodata, noi propunem un nou model care explica transformarea brusca a intregii multistructuri intr-un compus cristalin al Si in timpul tratamentului termic. Modelul propus arata ca aceasta transformare brusca in cristalinitatea si compozitia multistratului depinde de marimea compusului de Si format, si nu de temperatura la care are loc tratamentul termic, dupa cum se sugereaza in literatura de specialitate.

Pentru producerea de oglinzi functionale in litografia cu radiatie din domeniu ultraviolet, optimizarea diversilor parametri de depunere a multistraturilor solicita un numar mare de iteratii pe substrati extrem de costisitori. Pentru a reduce costul productiei de oglinzi s-au incercat multe tehnici de recuperare a acestor substrati costisitori, insa dificultatea principala ramane obtinerea rugozitatii originale, foarte redusa, a substratului. In capitolul 5, noi propunem un material nou pentru procesul de recuperare al substraturilor, si anume un polimid, cunoscut din literatura pentru proprietatea de a

reduce rugozitatea suprafetei pe care este depus. Astfel, rugozitatea suprafetei in toate etapele procesului de recuperare ramane neschimbata. Demonstrarea recuperarii cu succes a substratilor pentru probe cu diametru redus este urmata in prezent de implementarea metodei la scara industriala pentru probe cu diametru mult mai mare.

In final, pentru a imbunatati atat reflectivitatea cat si stabilitatea termica a ogllinzilor folosite in litografia extrem ultravioleta, se impune folosirea altor materiale ca si bariere de difuzie la interfetele de Mo-Si. Capitolul 6 prezinta un studiu detaliat asupra cresterii stratului de B_4C depus pe straturi subtiri de Mo si Si. Noi am descoperit o inconsistenta in reflectivitatea si stabilitatea termica a multistraturilor atunci cand B_4C este depus pe Si. Aceste rezultate experimentale pot fi explicate prin analiza XPS a structurii multistraturilor, pentru a carei intelegere noi propunem un model explicativ.

10. ACKNOWLEDGMENTS

I am grateful to many people, who helped me in my work during my doctoral research, who encouraged me to overcome problems and who made pleasant my stay at Rijnhuizen. I'm very thankful to my department head and promotor Prof. Bijkerk, who gave me the opportunity to start my PhD in the nanolayer Surfaces and Interfaces department, under his supervision. He taught me that the power of a message is in its simplicity and its clarity. He corrected very careful everything that I wrote during my PhD period and he contributed to the writing of my articles with intelligent advice and very useful comments. I wish to thank Andrey Yakshin, leader of the Thin Films and Multilayers group, for all the interesting discussions about the interpretation of my experimental results, where his brilliant ideas were more than welcome. He also gave great moral support in the moments when experiments were unsuccessful, he encouraged instead of pushing. His personal example of hard work was an inspiration for me and it was the driving force for me to continue when big problems seemed unsolvable. I wish to thank Robbert van de Kruijs for his guidance as direct supervisor, for his patience, hard work, seriousness at work and for all the fun outside work. I greatly value his corrections and comments to my thesis and all the help regarding the use and the work in the world of X-ray diffraction. I am thankful to Eric Louis and Erwin Zoethout for all their help, ideas and comments especially regarding the papers on polyimide (chapter 5) and on B_4C growth (chapter 6).

My work was mainly experimental and I wouldn't have managed without the help of the very good technicians from my group. I want to acknowledge Michel ten Have who built and maintained the annealing system that I used extensively. I wish to thank Arend-Jan van Calcar who was always ready to help with all the problems regarding the annealing system and the Cu-K reflectometer.

Chapter 10: Acknowledgments

I also wish to thank Pascal Suter and Thomas Norskov Nielsen, brilliant students who during their short stay at Rijnhuizen contributed to my work with fresh and intelligent ideas. I wish to thank to Maria Grigore, Elena Toma and Mariana Tomozeiu from whom I learned a lot in the beginning of my PhD period. I am thankful to all the PhD students who came after me, Tim Tsarfati, Veronique Lohmann and Saskia Bruijn, for interesting discussions and great company. My department grew bigger and bigger during my stay in these almost 5 years, so I will address a big THANK YOU! to all my colleagues. I learned a lot from each of them. Here I met Robbert and I'm very happy that he became my partner in life. This makes that I don't feel like leaving Rijnhuizen or my colleagues, because I'll hear of you all every day even if I'll work somewhere else.

Finally, I wish to thank my family and friends in Romanian: Draga mama, fara ajutorul moral de zi cu zi n-as fi reusit sa termin acest doctorat. Stiu ca ti-ai dorit sa reusesc, pentru mine e mare lucru si imi doresc sa fii intotdeuana mandra de mine. Mihai si Cristina desi departe, m-am bucurat intotdeauna sa citesc mesajele cu vesti sau cu incurajari. Catalin si Mirela, de cand am venit in Olanda la interviu, voi ati fost vesnic aproape de mine si de sufletul meu. M-am simtit inteleasa si incurajata de cei in aceiasi situatie ca si mine.

By coming to work at FOM, I met a new society, a new culture and a new mentality. I got the opportunity to follow courses about Dutch culture, society and language. It was a great opportunity to learn in these almost 5 years more than if I would have lived 10 years in Romania. Dus, ik moet zeggen aan iedereen in FOM: Dank jullie wel, FOM!

11. CURRICULUM VITAE

Ileana Nedelcu was born on 26 April 1974 in Sibiu, Romania. She followed secondary school and the Theoretical High School "Gheorghe Lazar" in Sibiu. In 1992 she graduated the baccalaureate in 5 majors with 9.82, in the first 10 of the Sibiu department. She followed the Physics Faculty at "Babes-Bolyai" University in Cluj-Napoca, Romania. She graduated in 1996 with the final report in "Permanent magnets" and she followed a one-year Master in Solid Physics. During the Master year, she benefited from a Tempus scholarship for a three month study at the laboratory Paris-Orsay, France, in the group of Prof. H. Jerome where she completed the Master report "Tunnel spectroscopy in organic superconductors". She taught physics in secondary school in Sibiu (1997-1999) as teacher and at "Lucian Blaga" University, Sibiu (1999-2002) as Assistant Professor. On 15 September 2002 she started as a PhD student at FOM-Rijnhuizen in the group of Prof. F. Bijkerk. The results of this work are presented in this manuscript. The work was supervised by promotor Prof. Bijkerk, under daily guidance of both Dr. A. Yakshin and Dr. R van de Kruijs.